UNIVERSITY OF CALIFORNIA

SANTA CRUZ

ELECTROCHEMICAL DOPING AND THE OPTICAL PROPERTIES OF LIGHT-EMITTING POLYMER MATERIALS AND DEVICES

A dissertation submitted in partial satisfaction
of the requirements for the degree of

DOCTOR OF PHILOSOPHY

in

PHYSICS

by

Janelle Maureen Leger

June 2005

The Dissertation of Janelle Maureen Leger
is approved:

_____
Professor Sue Carter, Chair

_____
Professor David Belanger

_____
Professor Jin Zhang

_____
Robert C. Miller
Vice Chancellor for Research and
Dean of Graduate Studies

TABLE OF CONTENTS

LIST OF FIGURES

CHAPTER 1: POLYMERIC SEMICONDUCTORS

LIST OF TABLES

ABSTRACT

ELECTROCHEMICAL DOPING AND THE OPTICAL PROPERTIES OF LIGHT-EMITTING POLYMER MATERIALS AND DEVICES

Janelle Leger

The discovery in 1990 by Bradley et. al. that organic polymers with a conjugated backbone display semiconducting properties began an intensive research effort to understand the fundamental physics underlying these materials, to synthesize materials with certain desired properties, and to develop potential applications. Specifically, semiconducting polymers have been used in a wide range of device applications including light-emitting devices, transistors, photovoltaics, memory devices, and actuators, among others. The promising characteristics of polymer semiconductors include low-cost, easy processing, tailored synthesis, and potential for use in large-area and flexible devices.

In this dissertation I introduce the field of semiconducting polymers and present my studies of electrochemical doping and the optical properties of light-emitting polymers in the context of improving functionality in a range of solid-state device applications. While great strides have been made toward the practical realization of a range of polymer-based optoelectronic and electronic applications,

there is still much to learn about the fundamental processes affecting their optical properties. Specifically, detailed studies of the electrochemical doping of light-emitting polymers are lacking despite the emergence of a range of technologies such as polymer light-emitting electrochemical cells that depend heavily on the process of *in situ* electrochemical doping. In addition, the factors affecting the optical properties of light-emitting polymers and polymer-based devices have been limited in scope.

The first three chapters of this dissertation serve as an introduction to the field of light-emitting polymers and polymer-based devices including materials, device construction, and measurement techniques. In chapter one I discuss the physical models necessary to understand semiconductivity in conjugated polymers. Chapter two reviews the device physics of several important applications. In chapter three I introduce the experimental techniques used in the following studies.

Two well established light-emitting polymer devices include the polymer LED and the polymer LEC. The LEC uses electrochemical doping to achieve the charge injection necessary for light emission, while the LED injects charge directly from contact electrodes. I use a technique employing simulations of interference effects in multilayered device structures, matching experimental device spectra to simulation in order to gain insight into the location of light emission within the device. In chapter four I use this technique to explore the thickness dependence of PLEDs. In chapter five I combine simulations of interference effects in LECs with

studies of planar geometry devices, thereby providing information about the fundamental operating mechanism of these devices.

Several polymer-based applications include light-emitting electrochemical cells (LEC), electrochromic devices (ECD), and actuators, for which the operating mechanism depends heavily on electrochemical doping. Unfortunately, the doping of light-emitting polymers is not well understood. In chapter six I study the basic electrochemical doping reactions of one common light-emitting polymer, MEH-PPV. I explore factors affecting the fundamental doping reaction through cyclic voltammetry. Further, I investigate the optical properties of doped films in order to gain insight into the structural changes and changes in the energy band structure induced by doping.

Finally, I explore some unique functionalities of MEH-PPV, specifically electrochromic and thermochromic effects. Chapter seven presents a MEH-PPV based electrochromic device with a layered polymer/gel electrolyte structure that displays sharp contrast and high reversibility when biased at low operating voltages. In chapter eight I study the reversible, high-contrast thermochromic behavior of MEH-PPV gel films, occurring in a practically relevant temperature range and without phase or volume changes.

ACKNOWLEDGEMENTS

My name appearing alone on the first page of this work does not reflect the enormous contributions of the following individuals, both directly and indirectly, to the very existence of this manuscript. Most important is the thanks I owe to Sue Carter, whose teaching, support, and encouragement I struggled to deserve until the end. Amanda Holt and Beat Ruhstaller have contributed to a great extent directly to the studies presented here and have been an absolute pleasure to work with. Invaluable help has also come from other sources in the form of materials and other assistance, in particular Luisa Bozano and Campbell Scott at IBM, who helped with several measurements that were central to the work.

The text of this dissertation includes reprints of the following previously published material: "Solid-state electrochromic devices based on poly (phenylene vinylene) polymers", Appl. Phys. Lett. **86** (2005) and "Thickness-dependent changes in the optical properties of PPV- and PF- based polymer light-emitting diodes", Phys. Rev. B **68** (2003). Professor Sue Carter directed and supervised the research which forms the basis for the dissertation.

Last but not least there are the people in my life who have supported me endlessly. For friendship and camaraderie throughout my time at UCSC I want to thank in particular Melissa Kreger and Yuko Nakazawa. I want to thank my father for advice and support, and my mother for saving my sanity both as a graduate

student and as a mother. Most of all, I dedicate this work to Eric, who has given me love, unwavering support, and Kaia.

INTRODUCTION

The field of semiconducting polymers was born in 1977 when it was discovered that polyacetylene, when chemically doped, exhibited a several orders of magnitude increase in its electrical conductivity (Shirakawa et. al. 1977). By 1979, Su, Schrieffer, and Heeger had proposed a theoretical model describing conductivity in doped conjugated polymers (Su et. al. 1979), and a collection of new polymers had been synthesized, including the luminescent polymer poly (p-phenylene) (PPP) (Ivory et. al. 1979). Additionally, in 1979 it was discovered that these materials could also be electrochemically doped to achieve a conductive state, and that this process was reversible (Nigrey et. al. 1979).

In the 1980's and 1990's research focus tended to be on demonstrating the usefulness of semiconducting and conducting polymers in a broad range of applications. Organic field-effect transistors (Burroughes et. al. 1988), electrochromic devices, actuators, and several other applications based on conjugated polymers all made their appearance in the late 1980's (MacDiarmid and Zheng 1997). In 1990, electroluminescence from a light-emitting diode based on the luminescent polymer poly (phenylenevinylene) (PPV) was demonstrated (Burroughes et. al. 1990). One year later, a polymer light-emitting diode was fabricated by spin-casting a polymer film from the soluble PPV derivative, poly [2-methoxy-5-(2-ethylhexyloxy)-1,4-phenylenevinylene)] (MEH-PPV) (Braun and Heeger 1991). In

the mid-1990's the polymer photovoltaic cell (Yu et. al. 1994, Brabec et. al. 2001) and the polymer light-emitting electrochemical cell (Pei et. al. 1995) were reported.

The heavy research effort and exploding application development in the field of polymer semiconductor materials and devices in the past 28 years is indicative of the potential of these materials in a wide range of applications (Epstein 1997). For example, their synthetic process allows for easy tunability of their optical and electronic properties. In comparison with traditional crystalline semiconductors, the ease of processing of conjugated polymers is vastly improved, promising significant cost advantages over current technologies. Perhaps the most significant benefit, however, comes from the liquid processing capabilities of polymers. This opens up the possibility of making large area, mechanically flexible devices on a wide range of substrates including plastic, paper, or even textiles (Forrest 2004). In addition, film deposition can be accomplished by cheap, efficient processes such as ink-jet printing, screen-printing, and others that will allow roll-to-roll production of technologies such as all-polymer displays.

Currently the field of organic electronic devices has reached the performance and stability necessary to achieve commercial production for a few applications. The introduction of organic devices into commercial production has shifted research focus somewhat from reaching certain performance and stability requirements to tuning material and device properties to certain specific applications. For example, multicolored displays fabricated using PLEDs will require a detailed understanding of

how the spectral properties of a device are affected by device construction and operating parameters. In this work I explore how the optical properties of LEPs are affected by such parameters as temperature and electrochemical doping for thin films, and device thickness and operating voltage, among others, through the study of optical interference effects in solid-state device applications.

Despite meeting the basic requirements for limited commercial production, several problems of short- and long-term efficiency continue to limit polymer device fabrication. In particular, stability is a major limitation of polymer device lifetimes. The polymers themselves are particularly sensitive to exposure to oxygen, moisture, and UV radiation. Further, some polymer device applications require the use of reactive high work function electrodes. These environmental instabilities of polymer devices demand highly effective encapsulation techniques for long-term device operation, reducing ease of production and low-cost benefits.

The issue of contact degradation in air has been overcome in part through the development of the polymer light-emitting electrochemical cell. In general, the requirement of a high work function top electrode has been shown to be overcome through carefully controlled chemical or electrochemical doping of the polymer layer(s), which reduces the energetic barrier to charge injection and therefore the sensitivity to top electrode work function. Technologies based on electrochemical doping of light-emitting polymers therefore have become a subject of great interest in the research community.

Surprisingly, a decade after the initial report of the LEC in the literature, little has been studied about the fundamental process of electrochemical doping in soluble LEPs and its impact on the optical and electrical properties of the material in thin films and solid-state devices. I present a detailed study of electrochemical doping in MEH-PPV, the most commonly studied soluble light-emitting polymer, and use the findings to better understand the underlying operating mechanism of the light-emitting electrochemical cell. A more thorough understanding of electrochemical doping in LEPs will allow better control in a variety of applications including LECs, electrochromic devices, polymer actuators, sensors, and perhaps frozen-junction diodes and photovoltaics.

CHAPTER 1

POLYMERIC SEMICONDUCTORS

1.1 Origins of semiconductivity in conjugated polymers

In an inorganic solid, semiconductivity is described by the band theory of solids (Ashcroft and Mermin 1976). Within this theory the energetic structure of the material is defined primarily by the lattice structure of the solid. In a crystalline solid, rather than having discrete electron energies, the available energy states form bands. Semiconductors are then materials for which the top of the highest occupied, or valence band is separated from the bottom of the lowest unoccupied, or conduction band by an energy of ~1-4eV (see figure 1.1).

Because the band theory of solids is defined only for highly ordered crystalline materials, it is insufficient for describing the behavior of polymers, quasi-1 dimensional materials which are intrinsically disordered in the solid state (Saricifti 1997). Despite the fundamental differences in the formalism required to describe the origin of semiconductivity in crystalline inorganics and polymers, significant analogies exist in their fundamental behavior. Specifically, the basic picture shown in figure 1.1 remains appropriate for disordered semiconductors if one replaces the bands with dense discrete energy levels. The terms valence and conduction are still

occasionally encountered in discussion of semiconducting polymers to describe the upper filled and lower unfilled energy levels, respectively.

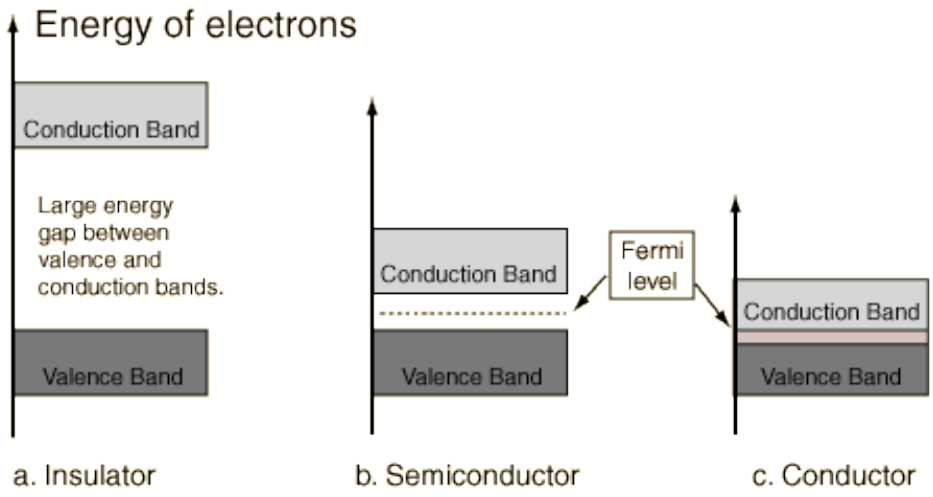

Figure 1.1 Energy bands in an insulator, semiconductor, and conductor.

In order to understand the origin of semiconductivity in conjugated polymers, it is necessary to build from a basic understanding of carbon bonding (Atkins 1990). The electronic configuration of a carbon atom is $1s^2 2s^2 2p^2$. Due to Hund's rule, this can be written $1s(\uparrow\downarrow)2s(\uparrow\downarrow)2p(\uparrow\uparrow)$. Carbon will then prefer 4 bonds to attain a 'filled octet'. Valence bond theory, which provides a description of covalent bonding in terms of atomic orbitals, tells us that a single bond gives a σ-bond (parallel to the internuclear axis) while a double bond gives a σ-bond and a π-bond (perpendicular to

the internuclear axis). The carbon atoms in the backbone of polyacetylene, for example, form alternating single and double bonds with an additional bond to a hydrogen atom. Hybrid orbital theory then describes this electronic configuration as $1s(\uparrow\downarrow)2p(\uparrow)sp^2(\uparrow\uparrow\uparrow)$. In general, the backbone of a conjugated polymer contains carbon atoms with sp^2 hybridized orbitals bonding with other carbon atoms in a linear or aromatic structure, an sp^2 bond with a hydrogen atom, and an additional unhybridized off-axis p_z orbital.

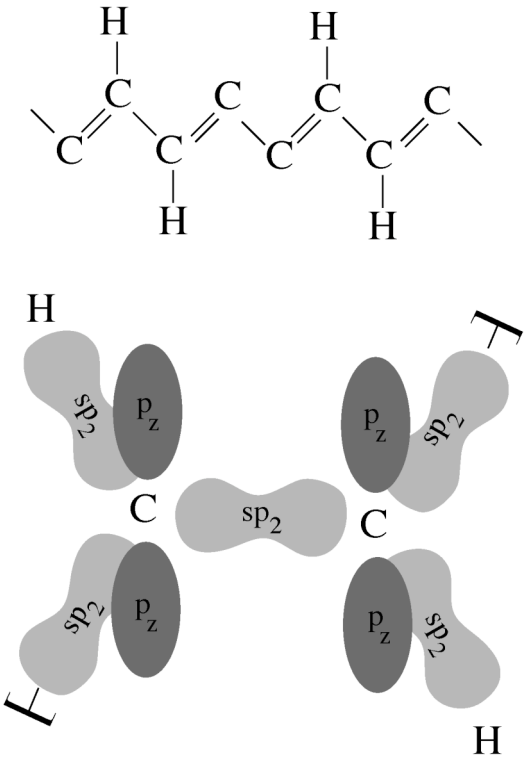

Figure 1.2 The molecular structure and molecular orbitals of polyacetylene.

An illustration of the orbitals of polyacetylene is shown in figure 1.2. In reality, the p hybrid orbitals form π-molecular orbitals that are delocalized along the polymer backbone and provide a conductive pathway along the chain (Roth 1995). Using methods of molecular orbital theory we are able to draw the energy levels of electrons in these materials as they arise from the combination of individual atomic levels (figure 1.3). In general the energy gap is ultimately defined by the energy level splitting between the bonding and antibonding orbitals created between neighboring carbon p_z orbitals. Because they are necessarily off-axis, they are then π and π^* levels (Kagan 1993). The terms HOMO (highest occupied molecular orbital) and LUMO (lowest unoccupied molecular orbital) are introduced here and become analogous to the top of the valence band and the bottom of the conduction band, respectively.

Another factor that influences the energy levels of electrons in a polymer and thus the ultimate bandgap energy is the conjugation length. The conjugation length refers to the distance along the polymer chain with uninterrupted delocalization of molecular orbitals. The levels of the delocalized segments are adjusted due to quantum mechanical particle-in-a-box type effects, in which energy levels are inversely proportional to the square of the conjugation length. In general, then, a shorter conjugation length will result in a larger bandgap and blueshifted absorption and emission.

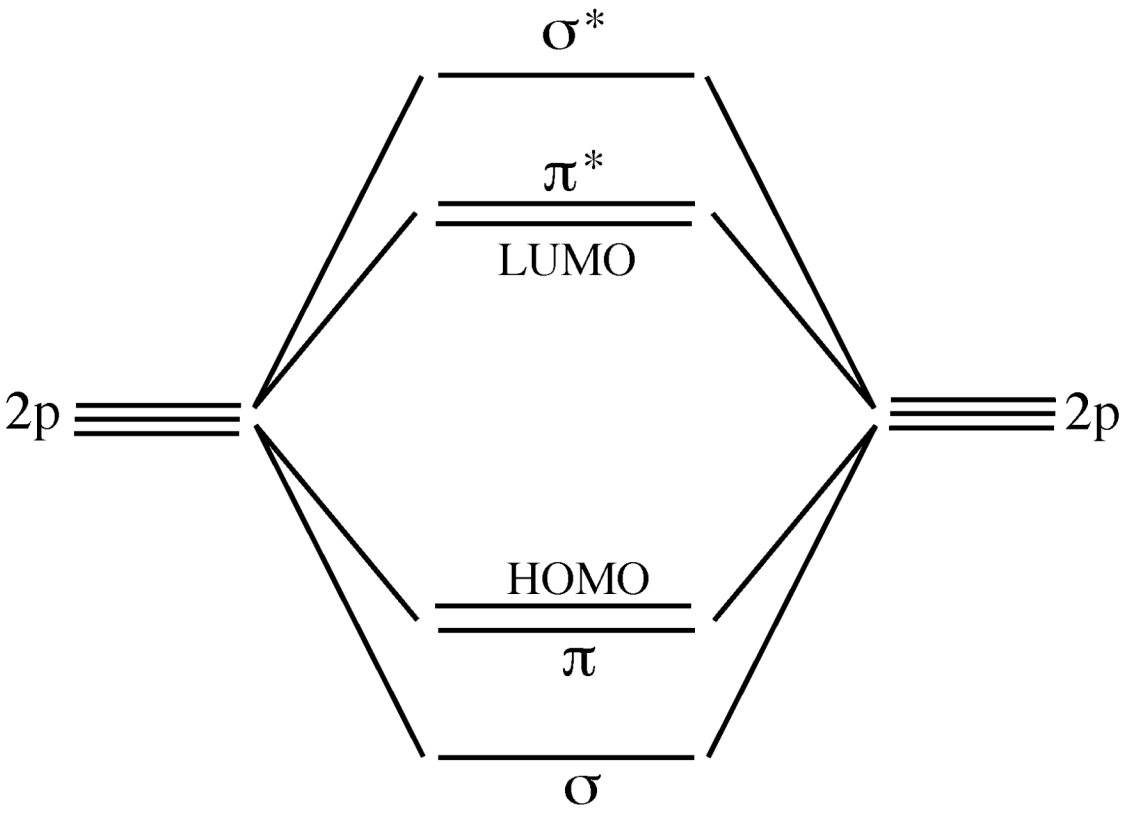

Figure 1.3 Energy level splitting of orbitals in a conjugated polymer according to molecular orbital theory.

1.2 Absorption and emission processes

The presence of an energy gap of between 1 eV and 4 eV allows for the absorption and emission of photons in the visible wavelength range. The potential energy curves as a function of internuclear distance for a diatomic molecule are shown in figure 1.4, and are assumed to be a good approximation to the chromophores in a conjugated polymer (Rohatgi-Mukherjee 1978). At room

temperature, electrons can be found in the lowest vibrational levels of the ground electronic state. In general, therefore, an absorbed photon with an energy greater than the bandgap excites an electron from the lowest vibrational level in the ground electronic state to a vibrational level in the excited electronic state. The excited electron quickly undergoes vibrational transitions until it reaches the lowest level of the excited electronic state. Typically the timescale of a vibrational transition is much faster than that of fluorescence or phosphorescence and therefore the relaxation of an excited electron to the ground electronic state always occurs from the lowest vibrational level of the excited electronic state.

Upon examination of the features of figure 1.4 one can see that the absorption of the material will be blue-shifted from the emission for any material with a non-zero horizontal separation between the excited and ground state potential minima. The band shapes also determine to some extent the spectral overlap between the absorption and emission spectra. The wavelength separation between the peak of absorption and emission of a material is known as its Stokes shift. An example is shown in figure 1.5. The Stokes shift and spectral overlap are important in determining the energy loss through heating of an excited electron upon emission as well as the probability of an emitted photon to be reabsorbed, in a sense dictating the usefulness of a material for various applications. In most cases, a small Stokes shift with little spectral overlap is desired.

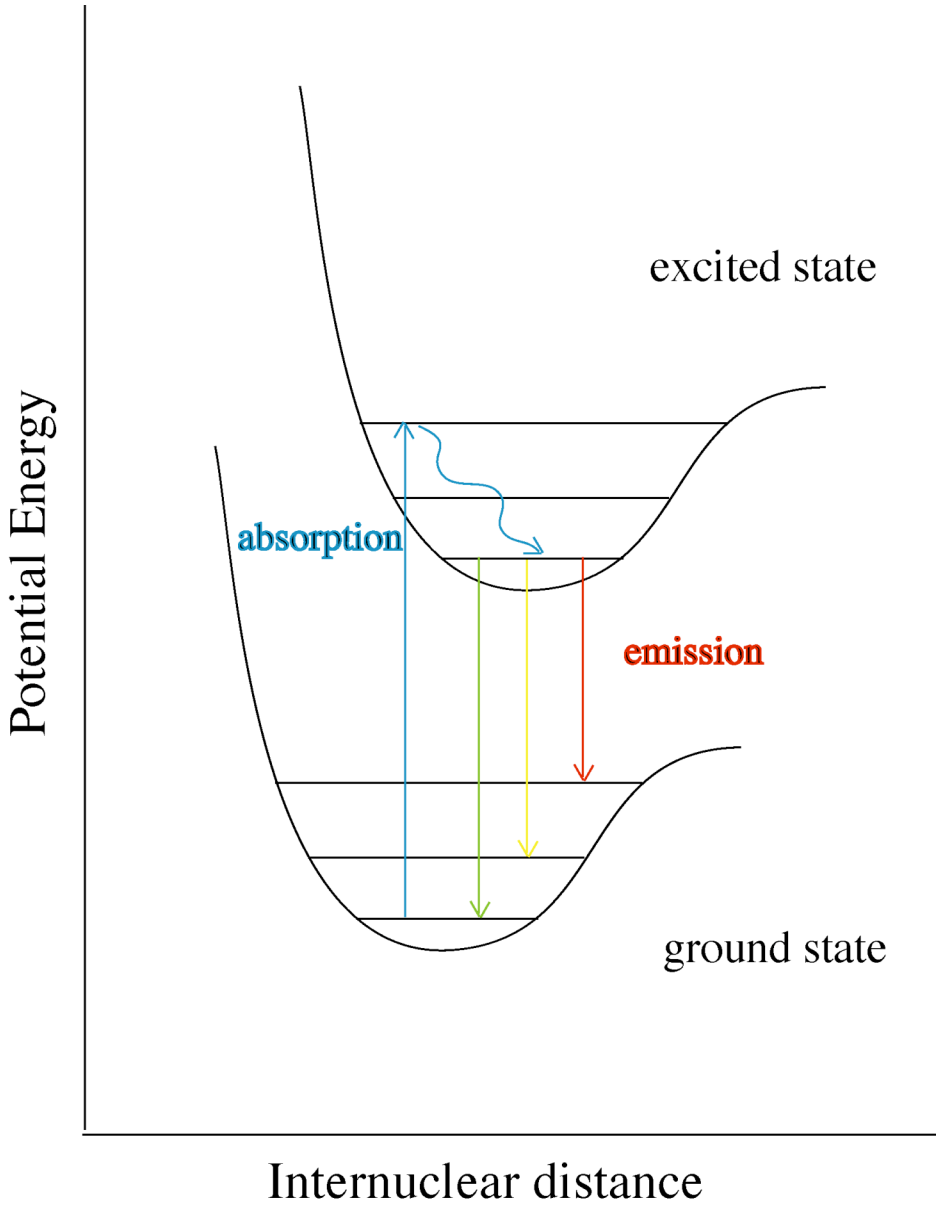

Figure 1.4 Potential energy as a function of internuclear distance for the ground and first excited states of a diatomic molecule. Absorption occurs from the lowest vibronic level of the ground state and emission occurs from the lowest vibronic level of the excited state.

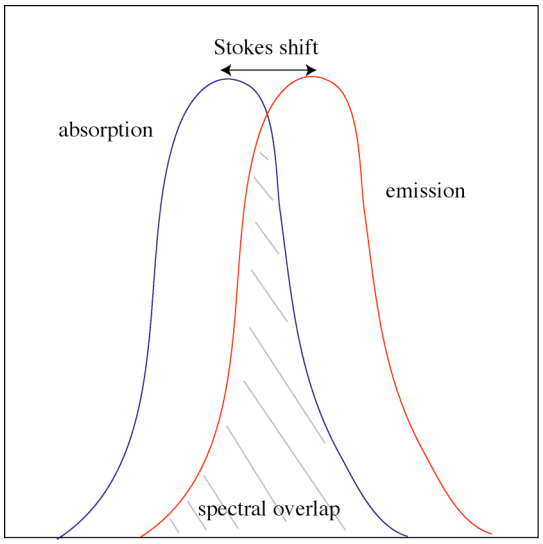

Figure 1.5 Example absorption and emission spectra, Stokes shift, and spectral overlap.

Excited carriers can be generated through photoexcitation or through the injection of an electron and a hole into the LUMO and HOMO, respectively (Kagan 1993). These processes are depicted in figure 1.6. Upon photoexcitation, an electron is promoted from a ground state singlet to what is known as a singlet exciton. Because fluorescence is a singlet-singlet transition, the theoretical maximum internal quantum efficiency for photoluminescence is 100%. With injected carriers, however, the injected electron and hole can form either a singlet or triplet state. Assuming an equal probability of each reduces the maximum internal quantum efficiency for electroluminescence to 25% (Helfrich and Schneider 1966). Recently, however,

studies have suggested that the long assumed maximum efficiency of 25% may not hold, although the subject is a matter of intense debate (Reufer et. al. 2005).

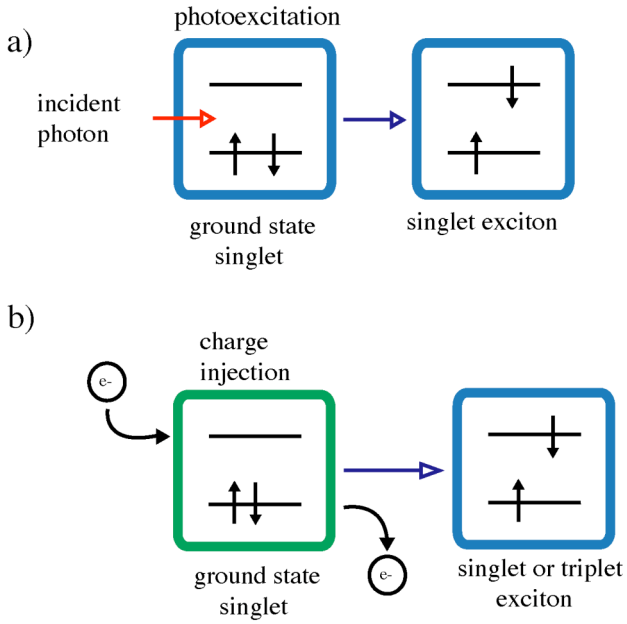

Figure 1.6 Exciton formation from a) photoexcitation and b) injected carriers.

The various pathways for recombination of a singlet exciton are shown in figure 1.7. The excited exciton can decay non-radiatively (in the form of heat) or radiatively (fluorescence) directly to the ground state. Alternatively, the exciton can undergo a singlet-triplet intersystem crossing. The energy of the triplet states are below that of the excited state, therefore a triplet exciton must undergo a non-radiative or radiative (phosphorescence) triplet-singlet intersystem crossing to return to the ground state (Kagan 1993).

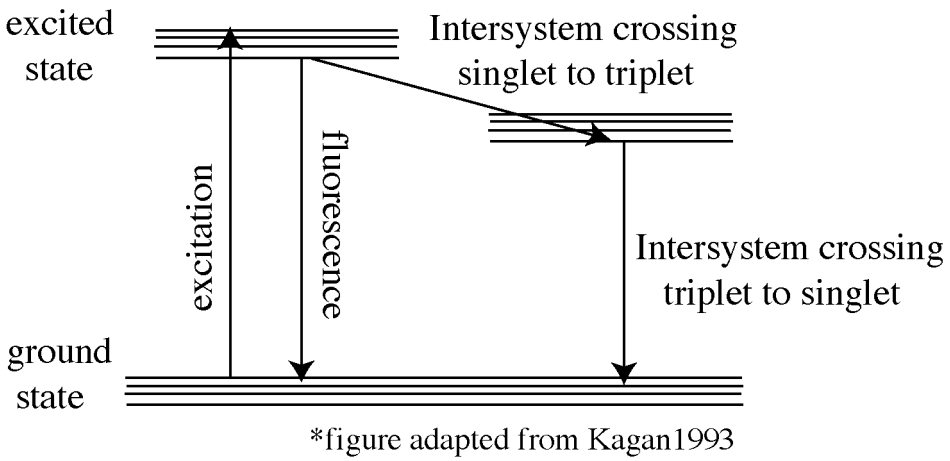

Figure 1.7 Pathways for recombination of a singlet exciton in a conjugated polymer.

The nature of the excited carriers themselves have been a subject of debate in recent years (Jenekhe and Osaheni 1994). It is generally accepted that the primary excitation in conjugated polymers is the singlet exciton. The singlet exciton consists of an electron in the LUMO and a hole in the HOMO bound by Coulomb attraction. The binding energy of a singlet exciton is typically 0.1eV- 0.5eV and accounts for the difference between the 'electrochemical bandgap' (defined by the low energy onset of absorption) and the 'optical bandgap', defined by the absorption maximum.

Evidence suggests, however, that the singlet excitons alone can not account fully for the observed properties of the excitations in conjugated polymer films. Because the polymer chains in thin film are randomly distributed and amorphous (figure 1.8), the possibility exists for the delocalized π-orbitals in one conjugation

segment of the polymer to overlap with another conjugation segment on the same chain or on a neighboring chain. Such excitations are referred to as excimers, exciplexes, and aggregate states, and generally result in a broad red-shifted feature in the polymer emission (Jenekhe and Osaheni 1994).

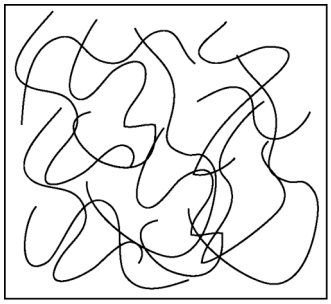

Figure 1.8 Amorphous polymer in thin film form.

1.3 Doping of semiconducting polymers

Much of the earlier work done attempting to understand the fundamental effects of chemical or electrochemical doping in semiconducting polymers has focused on exploring structural differences in doped and non-doped poly(phenylenevinylene) (PPV). Bradley et. al. 1987 did a study of the infrared and optical absorption spectra for both non-doped and electrochemically p-doped PPV. Their results showed that electrochemically p-doped PPV demonstrated additional energy levels within the bandgap as evidenced by the appearance of new peaks in the

optical absorption spectra of the doped sample. They suggested that the energy levels were consistent with the formation of bipolaron defects in the doped polymer film. In addition they showed that p-doping created additional peaks in the IR absorption spectra that appeared to be independent of dopant type. Lefrant et. al. 1989 then presented a complementary study which looked at the IR and Raman scattering from non-doped and chemically doped PPV. Modeling of experimental results suggested that the polymer is structurally modified along the backbone by these polaron defects from a benzoid to a quinoid form as a direct result of doping (figure 1.9).

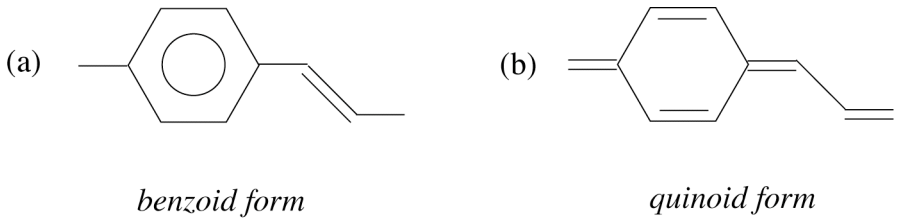

Figure 1.9 Molecular structure of the PPV repeat unit in (a) benzoid (non-doped) and (b) quinoid (doped) form.

Both theoretical and experimental work has since been extended to more thoroughly understand the structural changes of doping in PPV and the resulting change in the properties of the material but the general picture has not changed. Tian et. al. 1991 used the theory of the effective conjugation coordinate (ECC) to further support the concept of a doping-induced quinoid structure in PPV, Orion et. al. 1998

looked at chemically n-doped PPV and found that the fundamental changes in structure are essentially the same as seen in the p-doped material, and Tzolov et. al. 2000 presented similar results using photothermal deflection spectroscopy. The general understanding of the fundamental effects of doping in PPV is that doping does not significantly alter the original energy levels of the material but instead inserts levels within the bandgap through structural modifications (figure 1.10). Doping does not simply add charges to the conduction band or take them away from the valence band. This is because the strong coupling between the electrons and phonons characterizing the polaron and bipolaron tends to cause distortions in the polymer backbone. Furthermore this effect does not appear to be dependent on dopant type or whether the polymer was doped chemically or electrochemically.

Another consequence of the existence of polarons or bipolarons in the doped polymer material is that as the doping level is increased, the additional mid-gap energy levels begin to form a polaron band, partially filled and thus electrically conducting (Epstein 1997). However, because of the disordered nature of the polymer materials, the charge carriers tend to be highly spatially localized. Therefore charge transport occurs primarily through hopping (Monroe 1985). Arkhipov et. al. 2003 have shown that the dependence of charge carrier mobility on charge carrier density is dominated by the generation of a random Coulomb field by dopant ions which broadens the DOS distribution and decreases mobilities for low dopant concentrations, and by the filling of deep traps which facilitates hopping and increases mobilities at higher dopant concentrations.

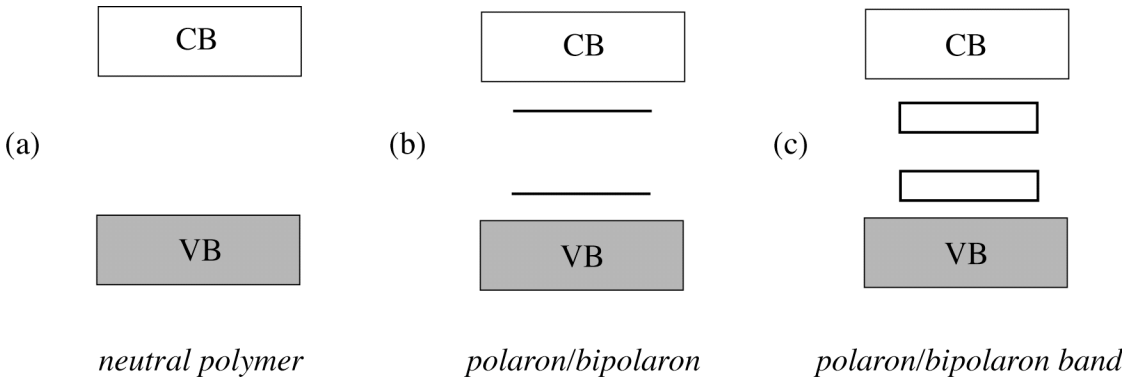

Figure 1.10 Energy levels of a conjugated polymer in (a) neutral form, with conduction and valence bands only, (b) lightly doped, with the addition of a single bipolaron energy level, and (c) more heavily doped, with a broad bipolaron band.

Despite the unanimous assignment of doping-induced structural changes in conjugated polymers to polaronic-type defects, considerable disagreement exists about whether these defects in the polymer film appear as polarons, bipolarons, or both depending on conditions. A simple depiction of the formation of polarons and bipolarons is shown in figure 1.11. An intermediate state, loosely termed the 'nuetral polaron', is formed in which an electron is shifted to a dangling p orbital, leaving a radical cation and forcing a rearrangement of carbon bonds from the previously mentioned benzoid to quinoid form. Because a single defect introduces an energetically unfavorable domain wall, the system prefers to form two.

If an electron is added (reduction) or removed (oxidation) to one of the dangling p orbitals the resulting defect is termed a negative or positive polaron. If this occurs at both defect sites, this is termed a bipolaron. The primary difference

between the polaron and bipolaron is in the allowed electronic transitions. The energetic structure and allowed transitions for polarons and bipolarons are shown in figure 1.12.

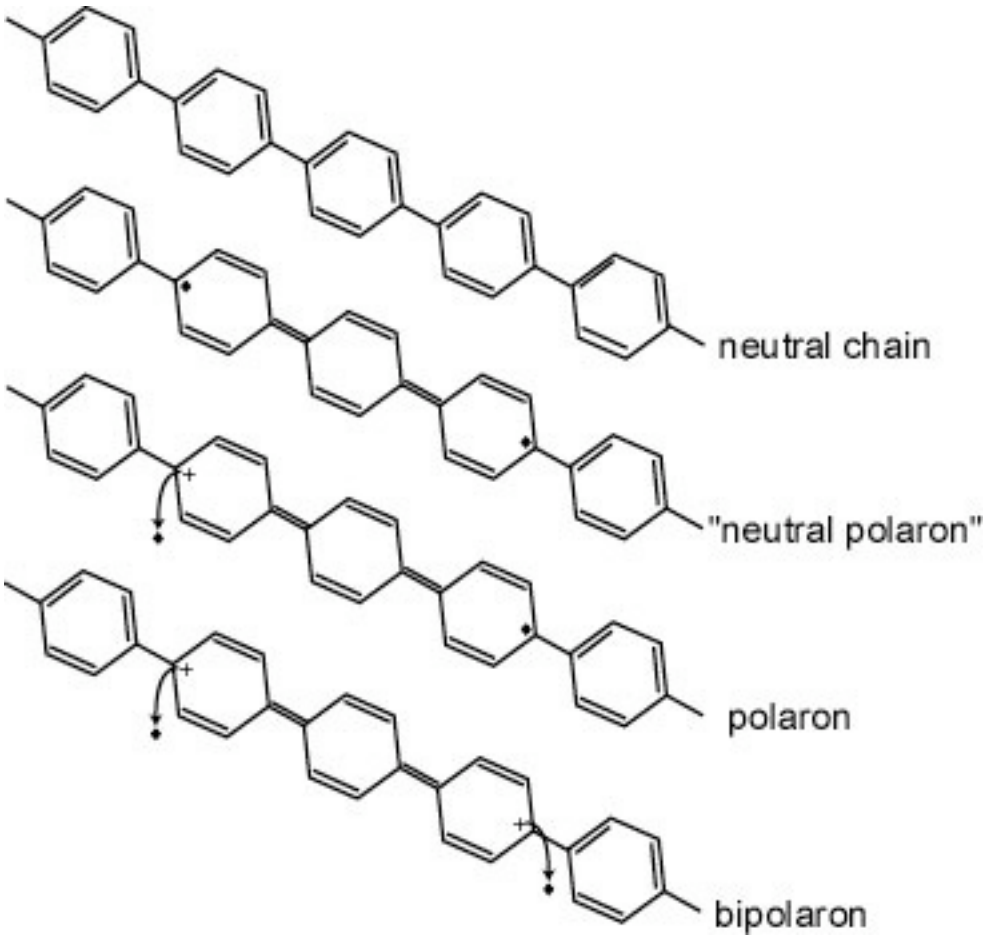

Figure 1.11 The formation of polaron and bipolaron defects in a conjugated polymer.

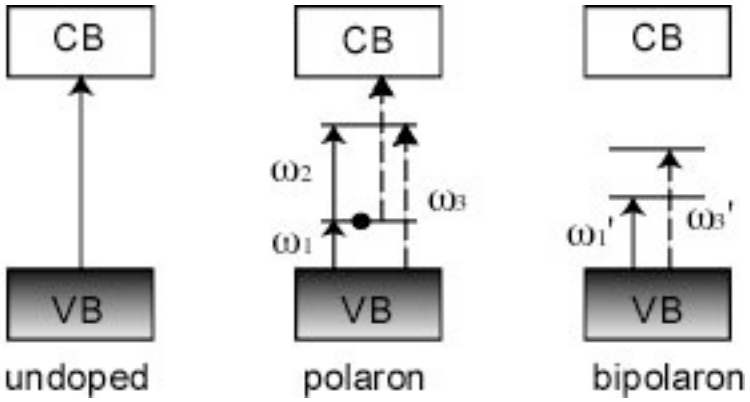

Figure 1.12 Energetic structure of a material with polaron and bipolaron defects and allowed electronic transitions

The most favorable defect with doping and its depiction in ESR, Raman and absorption data is currently in debate. Theoretically, models using the Su-Schrieffer-Heeger model Hamiltonian (Su et. al. 1980, Shimoi and Abe 1994), find bipolarons to be more energetically favorable due to the greater lattice relaxation while others (Bredas et. al. 1984), which consider electron-electron interactions, find that because of Coulomb interactions, polarons are energetically more stable until high doping levels are reached where bipolarons are formed. Many initial experimental investigations concluded that polarons were present in lightly doped systems followed by bipolaron formation with greater doping confirmed by observed optical transitions and ESR studies (Bredas et. al. 1984, Patil et. al. 1997). The intensities of the optical transitions though did not agree with the intensity relationships proposed by the FBC model.

More recently, Furukawa reassigned observed transitions to remedy the intensity anomaly argued that polarons are the primary doping species in non-degenerate polymers and the ESR results are due to polaron-polaron interactions (Furukawa 1996). However, the energy transition reassignments do not add up to the interband transition. Others using vibrational spectroscopy have come to the conclusion that polarons and bipolarons are both present in thermal equilibrium at high doping levels (Baitoul et. al. 1997, Baitoul et. al. 2000). Still others suggest that two transitions correspond to polarons and one transition corresponds to bipolarons and that previous doping levels were not high enough to detect the single transitions associated with bipolarons (Apperloo et. al. 1999).

While much of the fundamental research on doping in light-emitting polymers has focused on PPV, studies have also been done on the electrochemistry of some of the PPV derivatives, mainly in an effort to understand how the addition of various sidechains affects the properties of the material. Eckhardt et. al. 1989 studied a variety of PPV and poly(thienylene vinylene) derivatives, comparing the non-doped optical absorption spectra and using electrochemical measurements to compare the bandgap in each material. In a similar study, Li et. al. 1999 compared 10 PPV derivatives, focusing on the doping potentials for thin films as well as in an LEC configuration. They concluded that the presence of electron donating sidegroups tends to lower p-doping potentials, while electron accepting sidegroups tend to make the p-doping and n-doping potentials more electronegative.

CHAPTER 2

OPTOELECTRONIC POLYMER DEVICES

2.1 Light-emitting diodes

The first inorganic LED's came into commercial production in the 1960's. Slowly, technology improved to include a wider variety of colors and higher efficiencies, but it wasn't until 1990 that the ability to create a diode using conjugated polymer was reported (Burroughes et. al. 1990). In 1991, Braun and Heeger reported light emission from PLED's made with the soluble semiconducting polymer MEH-PPV (Braun and Heeger 1991). Since then, the field of PLED's has grown tremendously with the development of a wide range of colors and the appearance of some of the first commercially viable polymer based displays.

The state-of-the-art LED is based on doped crystalline semiconductors. A basic sketch of a p-type and n-type semiconductor and its corresponding energy diagram is shown in figure 2.1 a) and b), respectively. In p-type doping, a molecule from the lattice is replaced by an acceptor molecule; that is, one that requires an additional electron to complete a bond. Acceptors introduce an energy level close to the semiconductor's valence band. At room temperature, electrons in the valence band have enough energy to move into the new energy level, allowing for the movement of a free hole through the material. Similarly, in n-type doping, a donor

molecule is introduced that adds an energy level close to that of the semiconductor's conduction band, and a free electron is introduced to the material.

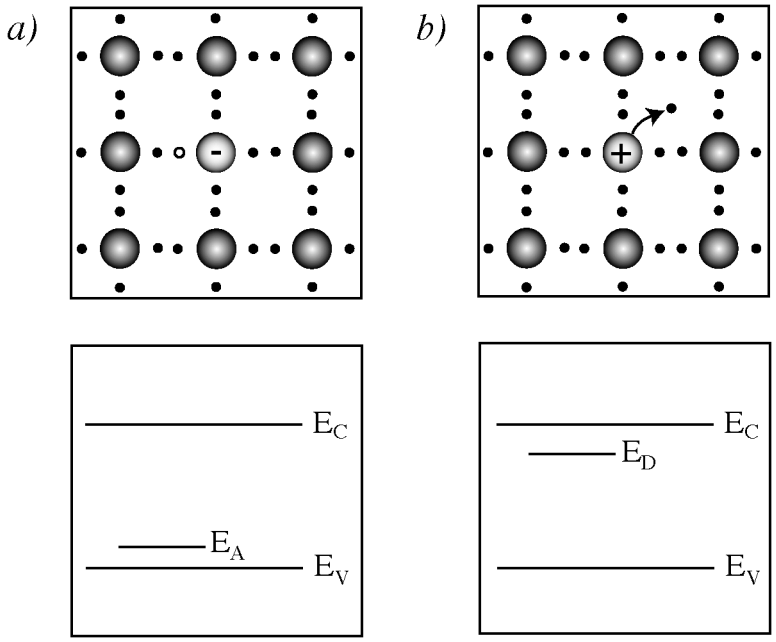

Figure 2.1 Lattice structure and energy band diagram for (a) p-type and (b) n-type crystalline semiconductor.

A p-n junction is formed by making contact between a p-type and an n-type semiconductor. This process is illustrated in figure 2.2. Prior to the junction formation, we have a neutral piece of p-type and n-type semiconductor, with energy bands and Fermi levels as shown in figure 2.2(a). After contact is made, the free electrons at the n side of the junction fall into the free holes on the p side, leaving a region on the p side of the junction with a net negative charge and vice versa for the p

side. This sets up a region known as the depletion zone with a non-zero electric field and no free charge carriers. Upon junction formation, the Fermi levels of the two sides match up and the conduction and valence bands on either side of the junction bend in response to the built-in electric field. Clearly after the junction has been established, it becomes energetically unfavorable for free charge carriers to wander into the depletion zone in the absence of an external electric field. By forward-biasing this system, charge injection is initiated. A typical LED is then a forward-biased p-n junction constructed using suitably chosen materials.

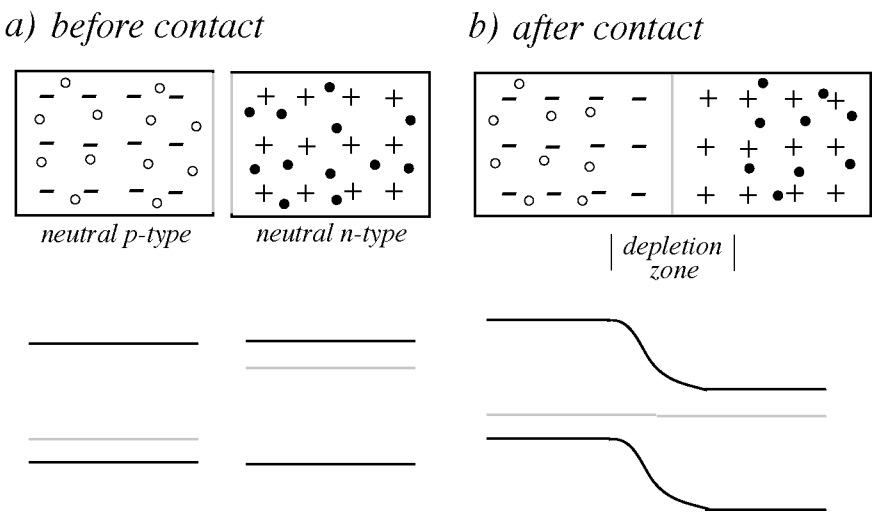

Figure 2.2 Formation of a p-n junction.

The mechanism governing the operation of a polymer LED (PLED) is quite different from that of a crystalline semiconductor based LED. The origin of the semiconducting nature of these polymers itself, as described in section 1b, must be described using molecular orbital theory rather than semiconductor band theory, in contrast with the materials described above. In addition, the optimal configuration for a PLED could be described as a metal-insulator-metal diode (MIM), with the central layer being the non-doped semiconducting polymer, instead of the previously described p-n junction configuration.

The PLED's described in this work are constructed using a sandwich structure as shown in figure 2.3. Using the experimental methods described in section 4a, a layer of PEDOT-PSS (Bayer corp.) is spin cast onto an ITO patterned glass substrate (Thin Film Devices Inc.) to function as the device's anode. The polymer layer is then spin cast above, and finally a layer of calcium followed by aluminum is thermally evaporated to serve as the cathode. The function of the PEDOT-PSS is twofold; it assists in hole injection into the device and creates a smooth even surface on which to spin the polymer film. The calcium functions as the effective cathode of the device; an evaporated layer of aluminum is added to the process to help barrier the calcium against oxidation. A typical energy level/ work function diagram for such a device is given in figure 2.4.

Figure 2.3 Polymer LED device structure with Ca/Al cathode and PEDOT-PSS/ITO anode.

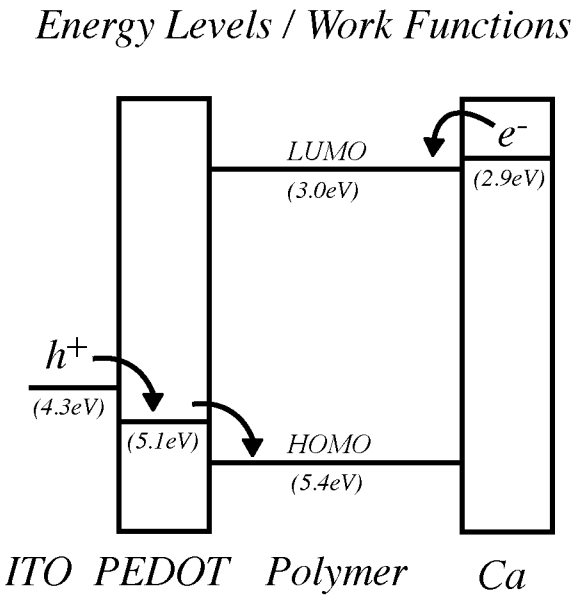

Figure 2.4 An example energy level/ work function diagram for a PLED. The HOMO/LUMO levels for the polymer shown are that of MEH-PPV (Campbell et. al. 1996, Bozano et. al. 1999). In this example, no barrier exists for electron injection.

A schematic diagram of this type of device structure in forward bias is illustrated in figure 2.5. Electrons from the cathode are injected into the LUMO of the polymer on one end of the device, and holes are injected from the anode into the polymer HOMO on the other. The charge carriers recombine within the polymer layer and emit light. Therefore, the three main processes affecting the operation of the device are charge injection, charge transport, and recombination.

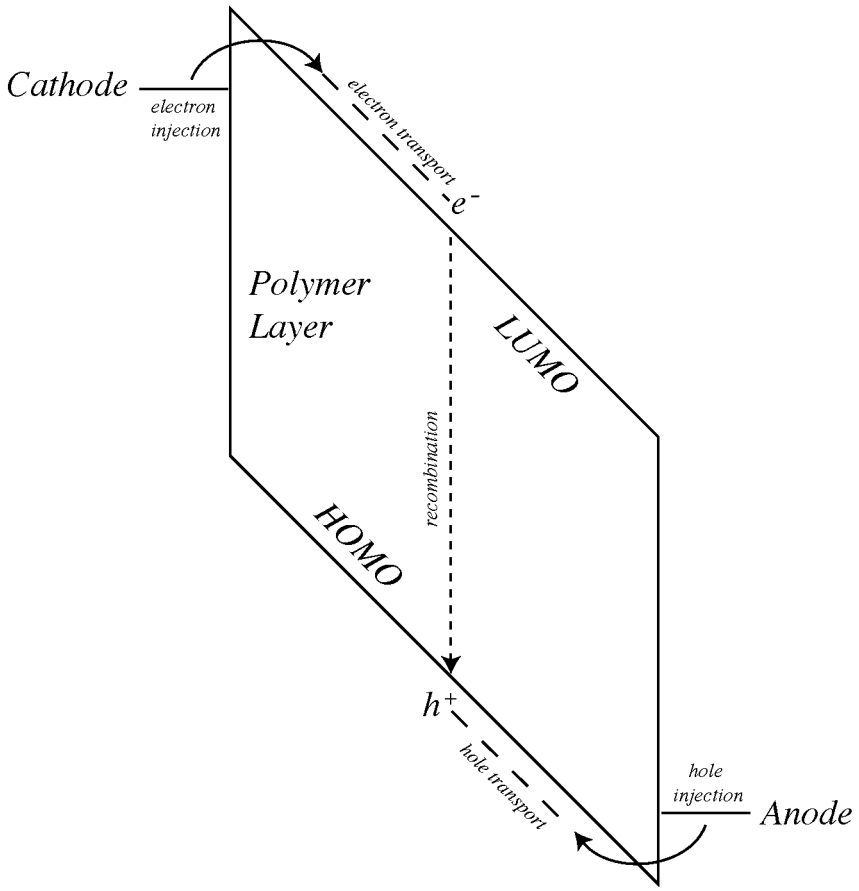

Figure 2.5 Schematic diagram of a PLED in forward bias illustrating the charge injection, transport, and recombination processes.

Charge injection is characterized primarily by the difference between the electrode work function and the polymer HOMO/LUMO levels. The two primary mechanisms for charge injection into a polymer diode with an energetic barrier to charge injection are referred to as Fowler-Nordheim tunneling (Fowler and Nordheim 1928) and thermionic injection, shown schematically in figure 2.6 a) and b), respectively. Both types of charge injection reduce to Ohmic behavior in the limit of zero barrier height, the condition which provides optimal charge injection. Parker proposed a model for the behavior of a polymer LED that is dominated by Fowler-Nordheim tunneling (Parker 1994). However, Davids showed that for low barrier height, thermionic emission actually dominates over F-N tunneling (Davids et. al. 1997).

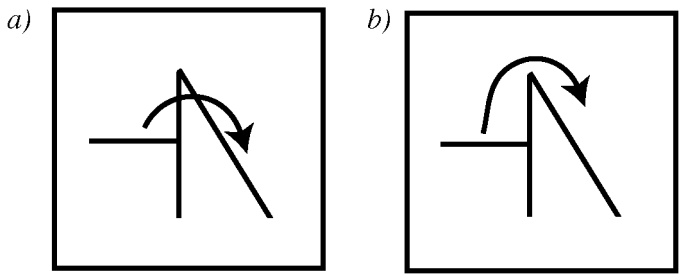

Figure 2.6 Two proposed methods for charge injection in a PLED include a) Fowler-Nordheim tunneling and b) thermionic injection.

While injection plays a major role in the operation of a PLED, in many cases it is charge transport that dominates the device characteristics. For large energy barriers the device is injection limited, while for lower energy barriers, the current is space-charge limited (Davids et. al. 1997). Blom found that in PPV-based PLED's, the hole-current tends to be space-charge limited while the electron-current tends to be trap limited (Blom et. al. 1997). Malliaras and Scott show that the recombination profile depends heavily on the ratio of electron and hole mobilities and less so on choice of contacts (Malliaras and Scott 1998).

The mechanism for charge recombination in PLED's has been shown to follow the theoretical Langevin process (Blom and de Jong 1998). In this model, the charges undergo a random walk, and those that come within Coulomb's radius of each other will recombine (Langevin 1903), where the Coulomb radius is defined as the distance at which the thermal energy equals the electron-hole binding energy.

2.2 Light-emitting electrochemical cells

The light-emitting electrochemical cell (LEC) first appeared in the literature in 1995 (Pei et. al. 1995). This device type is similar in construction to the polymer light-emitting diode, but operates using a very different mechanism. The emitting layer in an LEC incorporates a salt and a solid electrolyte into the light-emitting polymer layer. The exact role of the ions in the operation of the LEC is under some debate (see below). The primary practical differences between the two are that the

LEC is operationally independent of the electrode work functions, which allows moving away from the highly reactive cathode materials commonly used in PLED fabrication, and that it has the ability to emit light in both forward and reverse bias. Because of these promising features, the LEC has been pursued extensively for application. However much of the physics involved in the operation of this device type has yet to be fully explored.

The LEC's described in this work are constructed using a relatively simple device design as shown in figure 2.1. The LEC ink is a mixture of light emitting polymer, a polymeric ion transporter (solid electrolyte) such as polyethylene oxide (PEO), and a salt, such as Li or Ca triflate or tetrabutylammonium tetrafluoroborate. The ink is spin cast on the ITO glass substrate and a cathode, typically Al, is thermally evaporated on top, following the experimental methods described in section 3.2. The PEO forms a network after thermal annealing that assists in the conduction of ions through the polymer film.

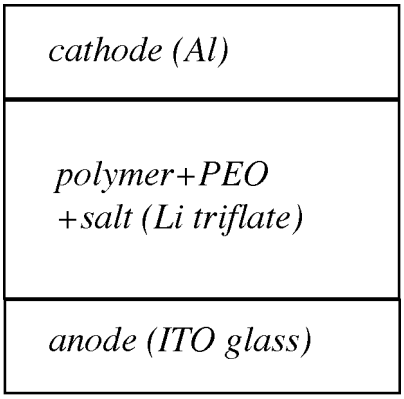

Figure 2.7 A typical LEC device structure.

The initial report on the operation of LEC's, as well as much of the subsequent follow-up research, was published by Alan Heeger's group at UNIAX Corp. (Pei et. al. 1995, Yang and Pei 1996, Pei et. al. 1996). According to this group, the LEC operates as follows: The salt dissociates to form free ions within the polymer film. Under the applied electric field, the ions move, assisted by the admixed electrolyte, toward the electrodes (see figure 2.2.). The ions then electrochemically dope the polymer under the applied electric field, p-type near the anode and n-type near the cathode, to form a p-n type junction in the bulk of the emitting layer (Pei et. al. 1995). Because the doped polymer film is conductive (see section 1.e.), contact between the film and the electrode becomes Ohmic, and therefore charge injection no longer depends on the work function of the electrodes as it does for the PLED. In addition, due to the reversibility of doping in conjugated polymers, the junction formed is reversible and light emission becomes possible under reverse bias.

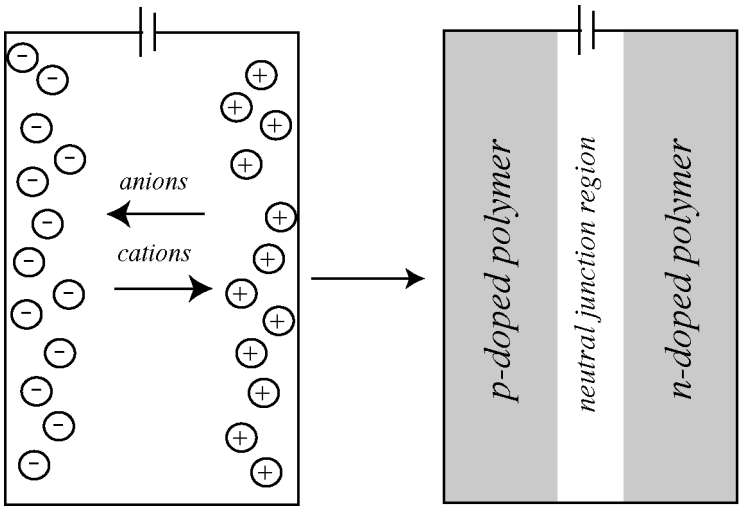

Figure 2.8 Proposed operating mechanism for an LEC. Under external bias, the ions move to opposite sides of the device. With a high enough voltage, the ions electrochemically dope the polymer to form a p-n type junction within the device.

Following this initial publication describing the operating mechanism of an LEC, attempts were made to further explore these devices by theoretically modeling their I-V characteristics (Smith 1997, Riess and Cahen 1997). While Riess and Cahen were able to model an LEC using the assumption of the formation of a pn-junction in an LEC, Smith showed that the nature of the junction formed in an LEC is quite different in nature than a standard pn-junction. Both models assume p-type doping near the device anode and n-type doping near the device cathode.

In 1998, however, an alternate operating mechanism was proposed by R. Friend's group (deMello et. al. 1998). According to this group, the ions play the central role in the operation of an LEC, but no doping takes place. Instead, the ions that accumulate near the electrodes create a region with high ionic space charge,

resulting in a large electric field at the polymer-electrode interface that reduced the barrier to charge injection (deMello et. al. 1998). This results in a very low electric field in the bulk of the polymer, with charge movement within the film being dominated by diffusion (figure 2.3). This proposed theory is also capable of explaining the observed behavior of LEC's (Ohmic contacts and reversible light emission).

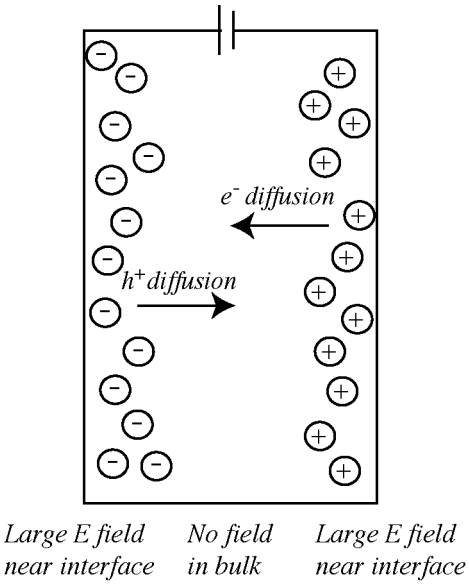

Figure 2.9 Alternate proposed mechanism for LEC operation. Ion accumulation creates a large electric field at the electrode-polymer interface, reducing the barrier to charge injection. Charge movement through the low electric field in the bulk of the film occurs primarily through diffusion.

Although the disagreement over the fundamental operating mechanism of the LEC has not been satisfactorily resolved, the progress toward improving the LEC and better understanding its basic characteristics has not been hindered. Early on, it was

demonstrated that the addition of a surfactant-like additive (octylcyanoacetate) improved the polymer/electrolyte network and therefore the operation of an LEC (Cao et. al. 1996), and two-color emission was achieved by forward- or reverse-biasing a bilayer LEC (Yang and Pei 1996). More recently, mutilayered polymer/electrolyte devices were reported to improve the LEC (Lee et. al. 2002), and a change in EL spectrum in forward- vs. reverse- bias was reported, giving clues to the location of light emission in an LEC.

2.3 Electrochromic devices

Electrochromism is defined as an electrochemically induced color change. In particular, it is the change in optical absorption bands brought on by an electrochemical redox reaction in a material. A discussion of electrochromism first appeared in the literature in the early 1960's (Platt 1961). Since then electrochromism has been demonstrated in a variety of materials, both inorganic and organic, and has been utilized to develop contrast-based display and various other technologies (Monk 1995).

A solid-state device that changes color upon application of an external bias is called an electrochromic device (ECD). Such devices can be assembled into a display. Electrochromic displays are passive; that is, they require external lighting to view. Therefore the primary competing technology is liquid crystal displays

(LCD's). The advantages of ECD's for display application are the persistent image with little or no additional power input, the ability to make large area displays, and the ability to use polyelectrochromic materials for multiple colors per pixel. Currently commercial applications for ECD's include darkening rear-view mirrors (Baucke 1987) and limited display applications.

Several organic materials have been established as displaying promising electrochromic behavior. In particular, bipyridilium has been pursued extensively. Several organic polymer systems display well-known electrochromic behavior including polyaniline (Kobayashi et. al. 1984), polypyrrole and polythiophene (Garnier et. al. 1983). Currently, there is limited understanding of electrochromism in light-emitting conjugated polymers. An exception is a study on the electrochromic behavior of MEH-PPV by Santos et. al. that demonstrates a near-reversible color change upon electrochemical oxidation (Santos et. al. 2002).

The electrochromic devices presented in this work are constructed using the sandwich structure illustrated in figure 2.1. A polymer layer is spin-cast on one piece of ITO glass and a gel electrolyte layer is spin-cast on another, as described in section 4a. The two are then pressed together and dried overnight. The use of a second ITO glass electrode rather than an evaporated metal electrode facilitates transmission measurements. In this device structure the top ITO layer is commonly referred to as the working electrode because it is the electrode at which the redox reaction takes place, and the lower ITO layer is referred to as the counter electrode because it is the

electrode that completes the circuit, following the conventions established in two-electrode electrochemistry experiments. The device is operated with the working electrode biased as the anode and the counter electrode as the cathode. Upon application of the external voltage, the anions in the electrolyte diffuse into the polymer layer and oxidize it near the working electrode.

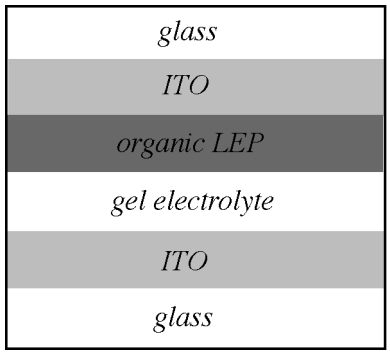

Figure 2.10 A typical ECD device structure.

The analysis of an ECD typically consists of measuring the change in the absorption of the polymer layer in the non-doped and the doped state. Properties of interest of an ECD determined in this way include Δ%T, or the change in percent transmission, and the write-erase efficiency, expressed as a ratio absorbance changes of the non-doped state after repeated cycles. Measuring the current and time of voltage application also allows the characterization of the response time and the

coloration efficiency, measured as the change in absorption coefficient divided by the charge transferred per unit area.

2.4 Interference in multilayered device structures

Two distinct types of interference effects are present in a typical polymer light-emitting device structure with one highly reflective cathode (such as gold or aluminum) and an ITO anode (a highly transparent but slightly reflective metal). The first is wide-angle interference (Fig. 2.11.a) in which light emitted from within the device toward the rear electrode reflects off of the reflective cathode and interferes with the light directly emitted toward the viewing side. Wide-angle interference tends to pick out wavelengths $\lambda = 4nl$, where n is an integer and l is the distance from the location of light emission to the reflective cathode.

The second type of interference present in such structures is multiple-beam interference (Fig. 2.11.b). In this type of interference light emitted within the device reflects between the ITO and reflective top electrode multiple times, resulting in the selection of wavelengths correlating with the resonant mode of the cavity. In general for device thickness less than half the wavelength of light the multiple-beam interference results in a blue-shift. Because the reflectivity of the ITO is generally low, wide-angle interference tends to be the dominant process in polymer light-emitting devices.

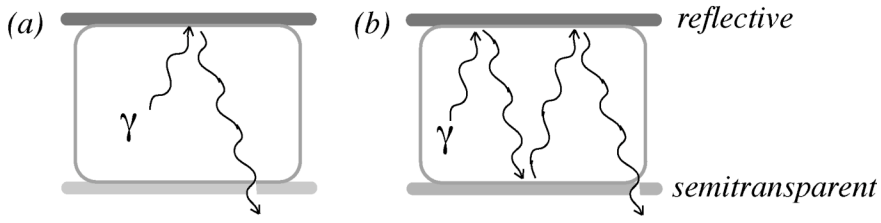

Figure 2.11 (a) Wide-angle and (b) multiple-beam interference effects in polymer light-emitting devices.

Because organic light-emitting devices consist of multiple layers with varying refractive indices and typically one highly reflective electrode, optical interference effects can be critically important in determining the spectrum and intensity of emitted light (Leger et. al. 2003). The parameters that are necessary for the simulation of interference effects in multilayered devices include the thickness and wavelength-dependent complex refractive indices of each layer, the photoluminescence spectra of the polymer material, and the location and profile of light emission within the active layer.

In the absence of a light source, one can write the solution to the one-dimensional Helmholtz equation $d^2\psi/dz^2 + k^2\psi = 0$ as the superposition of a right and left traveling plane wave $\psi = \psi^+ e^{ikz} + \psi^- e^{-ikz}$. In layered media, the continuity conditions at layer boundaries can be written in matrix form (Lekner 1987, Bjork et. al. 1991). For instance, the boundary transfer matrix relating the amplitudes ψ^+ and ψ^- of the adjacent layers *l* and *l+1* for *S*-polarization reads

$$\begin{pmatrix}\psi_l^+\\ \psi_l^-\end{pmatrix}=\frac{1}{2}\begin{pmatrix}1+\frac{k_{l+1}}{k_l} & 1-\frac{k_{l+1}}{k_l}\\ 1-\frac{k_{l+1}}{k_l} & 1+\frac{k_{l+1}}{k_l}\end{pmatrix}\begin{pmatrix}\psi_{l+1}^+\\ \psi_{l+1}^-\end{pmatrix}, \tag{1}$$

where the wavenumber $k=2\pi n/\lambda$ depends on the wavelength λ and the refractive index *n*, which becomes complex in the case of absorptive media. In addition, the propagation transfer matrix for plane wave propagation in a layer of thickness Δz reads

$$\begin{pmatrix}\psi_l^+\\ \psi_l^-\end{pmatrix}=\begin{pmatrix}\exp(jk\Delta z) & 0\\ 0 & \exp(-jk\Delta z)\end{pmatrix}\begin{pmatrix}\psi_{l+1}^+\\ \psi_{l+1}^-\end{pmatrix}. \tag{2}$$

Thus, by multiplication of layer and boundary transfer matrices from multiple layers an effective matrix relating the wave amplitudes at different locations in the multilayer structure is obtained, from which the reflection and transmission Fresnel coefficients *r* and *t* are derived.

For the simulation of light emission in a layered medium the inhomogeneous Helmholtz equation with a source consisting of an oscillating point dipole needs to be solved (Crawford 1988, Lukosz 1981, Neyts 1998). Dipole methods have previously been used successfully to model organic LED emission (Burns et. al. 1996, Kim et. al. 2000). Such simulations in general require the distinction of parallel and vertical dipole orientations as well as *S* and *P*-polarization. However, for emission in the normal direction the expression for the emitted power density simplifies to

$$P\sim\frac{\left|1+r_l^-\exp\left(2ik_lz^-\right)\right|^2}{\left|1-r_l^-r_l^+\exp\left(2ik_ld_l\right)\right|^2}\cdot\left|t_l^+\right|^2, \tag{3}$$

(Neyts et. al. 1998) where r_l^+, r_l^-, and t_l^+ are the Fresnel coefficients for light originating in layer *n*, and z^- is the distance of the dipole from the lower boundary of layer *n* whose thickness is d_l. In expression (3) the denominator accounts for layer thickness dependent multiple beam interference while the nominator depends on the dipole position within this layer.

CHAPTER 3

EXPERIMENTAL TECHNIQUES

3.1 Cyclic voltammetry

The experimental technique known as cyclic voltammetry (CV) is a versatile tool which allows the electrochemical characterization of a wide variety of materials. The fundamental process of doping in semiconducting polymers can be most directly explored using this technique. Cyclic voltammetry primarily provides information about the onset voltage and reversibility of doping in a material. In addition, the experimental setup can be used to generate doped samples for additional study. A main component of this research involves using cyclic voltammetry data for a study of light-emitting polymer materials, allowing a study of the electrochemical doping of MEH-PPV (chapter 6) as well as the temperature dependence of the HOMO/LUMO levels of two related materials (chapter 8).

The core of the experimental setup used in cyclic voltammetry is the typical 3-electrode electrochemical cell pictured in figure 3.1. The components of this setup include a working electrode, an auxiliary, or counter, electrode, and a reference electrode all submerged in electrolyte solution. The working electrode is the electrode at which the electrochemical redox reaction takes place. The reference electrode is used to measure the potential at the working electrode, and is typically

one whose electrochemical potential is well known and constant in the absence of current flow. The auxiliary electrode is an inert conductor which completes the circuit. In cyclic voltammetry, the potential between the working and reference electrodes is cycled between fixed values. Ions from the electrolyte solution dope the sample at the working electrode, creating a cell current through the circuit. This current is measured and provides information about the doping of the sample.

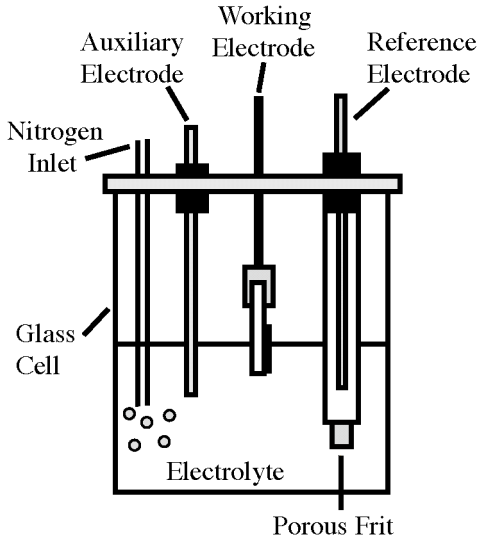

Figure 3.1 Typical 3-electrode electrochemical cell (with film sample) used in cyclic voltammetry experiments.

In the experiments described in this work, the working electrode consists of polymer spin-coated onto an indium tin oxide (ITO) coated glass substrate. The ITO substrate is highly conductive and largely transparent, allowing for the subsequent study of the optical properties of the polymer films, such as the optical absorption and

photoluminescence spectra. Electrical contact is established with a platinum wire secured to the ITO substrate just above the polymer film. The auxiliary electrode is a simple platinum wire. Our reference electrode is 3 M Ag/AgCl with a reference voltage of ~.207 V. The typical electrolyte solution used is .01 M tetrabutylammonium tetrafluoroborate (TBABF4) in acetonitrile (AN). A nitrogen inlet is included, and the entire cell is flushed with nitrogen gas prior to running the experiment, as the setup is sensitive to the presence of air in the cell.

The potential between the working and the reference electrode is controlled with the use of a potentiostat. In cyclic voltammetry, the potentiostat cycles the cell potential linearly using a triangular waveform (figure 3.2). The circuit is completed between the working electrode and the auxiliary electrode to avoid current flow through the reference electrode. Therefore the potential between the working electrode and the reference electrode is measured and controlled using a feedback loop (figure 3.3). The cell potential and cell current are then measured by the potentiostat and read into the computer (figure 3.4). The potentiostat used in the experiments reported in this work is an EG+G Model 362 scanning potentiostat. Two Keithley multimeters, 2000 and 2010, are used to measure the voltage and current from the potentiostat. A Labview script was constructed to measure the output of the multimeters into data files.

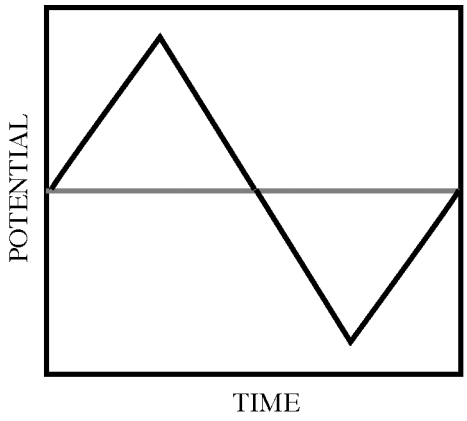

Figure 3.2 Triangular waveform generated by the potentiostat in a typical cyclic voltammetry experiment.

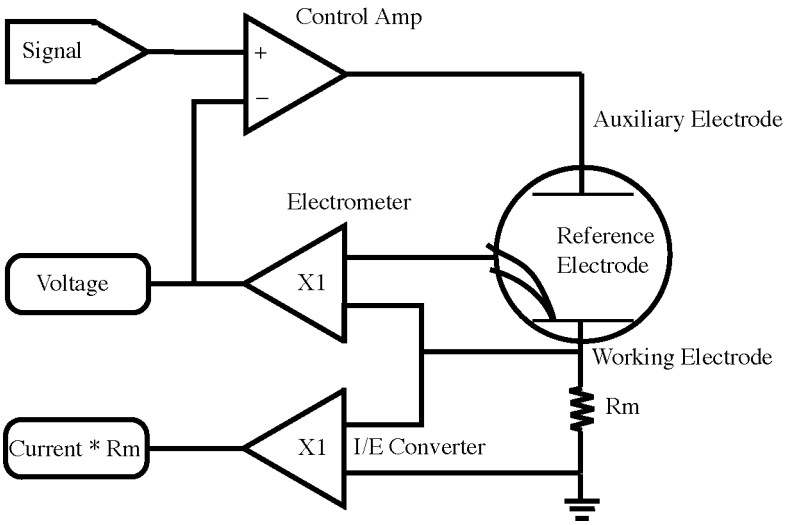

Figure 3.3 Basic potentiostat layout.

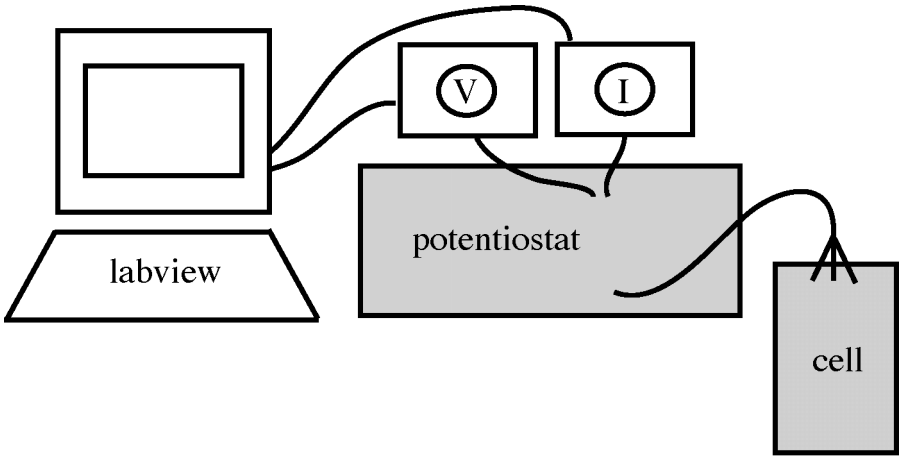

Figure 3.4 Experimental setup for cyclic voltammetry. Voltage and current are monitored with multimeters that are external to the potentiostat.

The current-voltage data taken in a cyclic voltammetry experiment is referred to as a voltammogram. An example of a voltammogram for an ideal system is given in figure 3.5. In the forward scan, we start the system at point A and start increasing the voltage according to figure 3.2. The oxidation reaction begins shortly and peaks at point B. Eventually the material becomes completely doped, and the current through the circuit stabilizes. At point C, the voltage peaks and reverses. The doping in the material begins to reverse, resulting in a negative current which peaks at point D. Again this current subsides and stabilizes at point E.

The critical parameters of such a voltammogram are E_{pc}, E_{pa}, I_{pc}, and I_{pa}. In this notation, p refers to the fact that we are in the forward, or oxidizing, scan (p-doping). The cathodic values are then pc and the anodic values are pa. These values give information about doping potentials and the reversibility of doping in a given material. In an ideal, reversible system with a one-electrode reaction, $I_{pc} \approx I_{pa}$, and

the peak separation $E_{pc} - E_{pa} = 58mV$. The dependence on scan rate is seen in the peak height, as $I \propto \sqrt{\nu}$, where ν = scan rate, and E_{pc} and E_{pa} are independent of scan rate. The increase in peak height as a function of scan rate can be understood by considering that the number of reactions and therefore the total charge transferred must be the same for all scan rates. While for faster scan rates the time step is shorter, the integral of current as a function of time must remain constant and thus the current is higher at the end of each step.

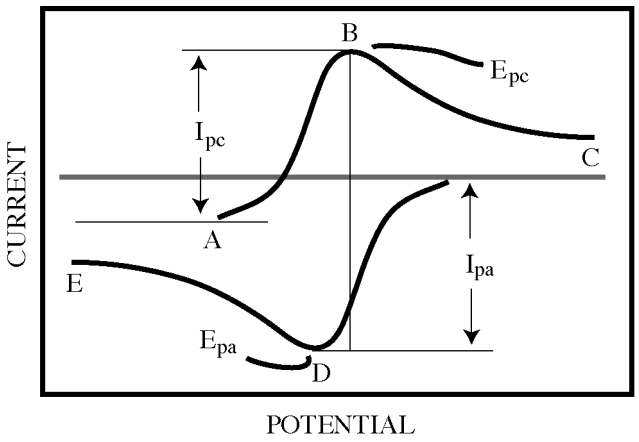

Figure 3.5 A voltammogram of an ideal system in forward scan.

For so-called quasi-reversible reactions, however, the peak separation will always be larger than for the ideal case. Quasi-reversible behavior can be inherent to the reaction studied in the case of slow reaction kinetics, or can arise from such factors as limited ion mobility through the sample, contamination of the system by oxygen or water, material loss, or a number of other factors. The peak position for a

quasi-reversible system increases as a function of scan rate, as the voltage step occurs prior to the establishment of equilibrium in the sample. All reactions in this work display quasi-reversible properties.

3.2 Device construction

All of the types of polymer devices described in chapter 2 have the same basic architectures and methods of construction with the exception of the planar light-emitting electrochemical cells, though the details of the polymer solutions and cathode metals vary from one device type to another. In this section I describe the broad details of device construction as they apply to all of the sandwich structure devices studied in this work. The more detailed information about any particular device will be given as the particular study is outlined. Some of the polymer materials used in the study were obtained through academic collaborations and others are commercially produced. The polymer materials are dissolved in various organic solvents (typically chlorobenzene or toluene) and are stirred and often heated to encourage the solids into solution.

The devices are made using glass substrates with patterned indium tin oxide (ITO) as the transparent electrode (manufactured by Thin Film Devices, Inc.). The ITO is deposited using RF sputtering, using a mask to achieve the desired pattern. The substrate with ITO pattern is illustrated in figure 3.6. The ITO surface itself is

1500 Å thick with a surface roughness of ≤10 Å and a resistivity of 20 Ω/sq. The substrates are cleaned with ethanol prior to use.

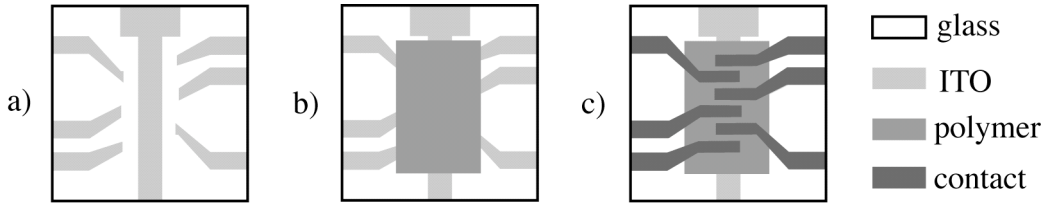

Figure 3.6 Device geometry at various stages of construction. a) ITO patterned substrate. b) substrate with polymer layer covering active device area. c) substrate with polymer layer and evaporated contacts.

The polymer layer(s) are formed by spin-casting the liquid polymer solution on the ITO substrate. Spin casting involves placing the substrate on a vacuum stage that holds the device in place as it spins rapidly (typically between 800-3500 rpm) for 30-40 seconds. The viscosity of the polymer solution and the spin speed determine the final layer thickness and uniformity. Layer thickness is measured using an atomic force microscope (see section 3.4). After the spin casting, the edges of the substrate are wiped with solvent to expose the ITO contact pads (see figure 3.6). Often the device is made with more than one polymer layer, as is the case for most LED's which include a layer of PEDOT-PSS (manufactured by Bayer Corp.) to even the ITO surface and aid in hole transport (Carter et. al. 1997). In the case of a layered structure, the first layer is spin cast on the substrate, and the solvent is then removed from the layer before the next layer is spin cast on top. To ensure that the first layer

does not dissolve upon the addition of the second layer, the first material cannot be soluble in the solvent of the second solution, which can prove to be a significant limitation of layered structures.

In the work presented here, all device contacts are made using thermal evaporation. The devices are placed in masks forming the contact geometry (shown in figure 3.6) and placed in a vacuum chamber. A current is forced through a tungsten boat containing the metal being used, which is then evaporated slowly (approximately 1-3 Å/s) onto the device. The vacuum system used is an LH Turbovac 150 turbo pump backed by an LH Trivac roughing pump and reaches pressures $\sim 10^{-6}$ torr. Contact evaporation is monitored using an LH Inficon deposition monitor.

3.3 Measurement of photoluminescence and absorption spectra

The optical processes of absorption and photoluminescence discussed in section 1.2 are of primary importance in that they essentially define the optical properties of a given material. Measuring the absorption and photoluminescence spectra of a material is a fairly straightforward experimental process. The absorption and photoluminescence spectra of the specific materials used in this work are shown in later chapters.

The absorption spectra for the various materials studied in this work were obtained on various specific instruments as specified for each study. A brief

schematic for these instruments in transmission measurement mode is shown in figure 3.7. The absorption of a film of material is obtained by measuring the fraction of light transmitted over the range of wavelengths of interest. The absorption is then obtained using $A(\lambda) = 1 - T(\lambda)$, where $T(\lambda)$ is percent transmission. To be precise, this method ignores the fraction of reflected light $R(\lambda)$. Typically, however, $R(\lambda)$ is a small value for the materials used. In addition, the measurement of $R(\lambda)$ returns both the reflected light as well as a significant contribution from photoluminescence, thus lessening the accuracy of the measurement. We therefore approximate the absorption spectra of our materials using the method described.

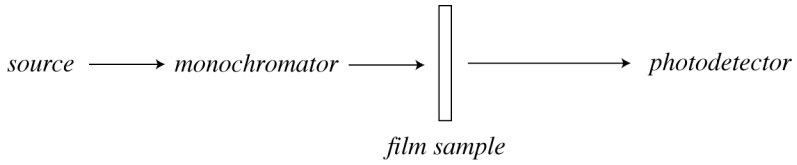

Figure 3.7 Brief schematic of the instrument used to measure the fraction of light transmitted through a film sample.

Films are made for absorption measurement by spin casting a polymer film onto a transparent or nearly transparent substrate. Quartz substrates are used whenever possible, however some studies reported in this work required the use of ITO coated glass substrates for absorption measurements, in particular the samples generated using cyclic voltammetry.

The photoluminescence data used in this work was taken on either a Perkin Elmer LS 50B or LS 45 luminescence spectrophotometer. The material is photoexcited at absorption maximum for an optimized signal. A schematic for these instruments is shown in figure 3.8 with the instrument set up for (a) solution measurement and (b) film measurement. To measure photoluminescence from solution, we use dilute solution in a quartz cuvette. To measure photoluminescence for a film sample, we typically spin cast the polymer film onto a quartz substrate.

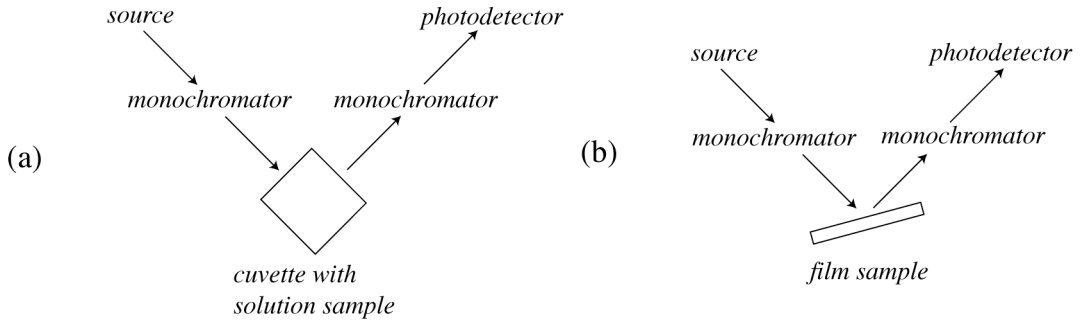

Figure 3.8 Brief schematic of the instrument used to measure the photoluminescence of (a) dilute solution and (b) film sample. The film sample is mounted such that collection of reflected light in the photodetector is minimized.

3.4 Atomic force microscopy (AFM)

The experimental technique of Atomic Force Microscopy (AFM) allows for the detailed (nm-scale) study of surface properties. In the field of polymer science, applications can range from the study of film roughness and uniformity to the measurement of a variety of local properties such as conductivity. In this work, AFM is used primarily to determine polymer film thickness.

The operating mechanism of the AFM includes a sharp probe, or tip, that is moved over the surface being studied (figure 3.9). This tip is mounted at the end of a cantilever which moves up or down in response to the force between the tip and the sample as it is moved across the sample in a raster scan. A laser is aimed at the tip and detected by a split photodiode. In this way, as the tip moves in the vertical direction in response to the surface profile, the difference in signal in the split photodiode allows for the measurement of the height of the tip. In this work, the mode used is referred to as contact mode, meaning simply that the tip remains in contact with the surface in the repulsive regime of the intermolecular force.

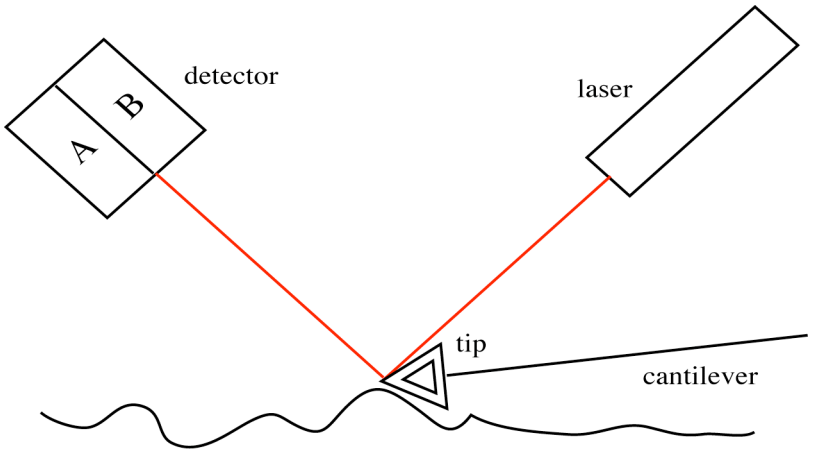

Figure 3.9 The basic operating mechanism of the atomic force microscope (AFM).

The primary use for the AFM in this work is to determine the thickness of various polymer films. To achieve this measurement, a small scratch is made in the

polymer film, and then imaged using the AFM. The profile of the scratch gives the height difference between the film surface and the substrate, and the average is used to obtain the thickness of the film (figure 3.10).

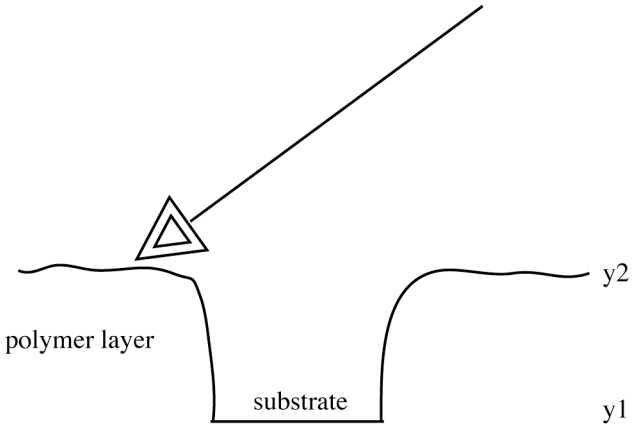

Figure 3.10 The profile of a polymer film during a thickness measurement.

3.5 Electronic characterization of devices

The electronic characterization of the devices studied in this project is achieved primarily through the measurement of the device's current-voltage dependence (IV curves). This data gives important information about charge motion through the device, including charge injection and charge mobility. When combined with radiance measurements as described in section 3.6, the current-voltage measurements can also be used to determine external quantum efficiency.

IV curves are taken with a Keithley 2400 sourcemeter in an inert nitrogen atmosphere (glovebox). Data acquisition includes stepping through applied voltages and measuring the current through the device. A LabView script controls this procedure, allowing data acquisition to begin and end at any chosen voltage. Variables include the size of voltage step and the delay between step and measurement. A typical measurement delay for an LED is ~500 ms. Because the ion mobility is so much lower than electron or hole mobility in the polymer, the response time of doping-dependent devices after a voltage step is much lower than for LED's. A delay for an LEC or ECD, therefore, is typically much longer, between 1000ms and 5000 ms depending on the device.

A typical IV curve for a polymer LED is shown in figure 3.11. At lower voltages the device is dominated by diffusion current (see section 2.1). When the applied voltage is equal to the turn-on voltage, charge injection is initiated and drift current dominates. For many devices a slight kink can be seen in the IV curve at the approximate turn-on voltage of that device. For an LED in forward bias with properly chosen contact materials, the turn-on voltage is approximately equal to the band gap of the polymer less the exciton binding energy. If the contact materials are chosen such that the work functions of the contacts lie within the band gap of the polymer, however, the turn-on voltage will be higher due to the extra energy required to inject the charge carriers into the polymer. Analysis of the portion of the IV curve

that displays space-charge limited current yields information about charge mobility in the polymer layer (see section 2.1).

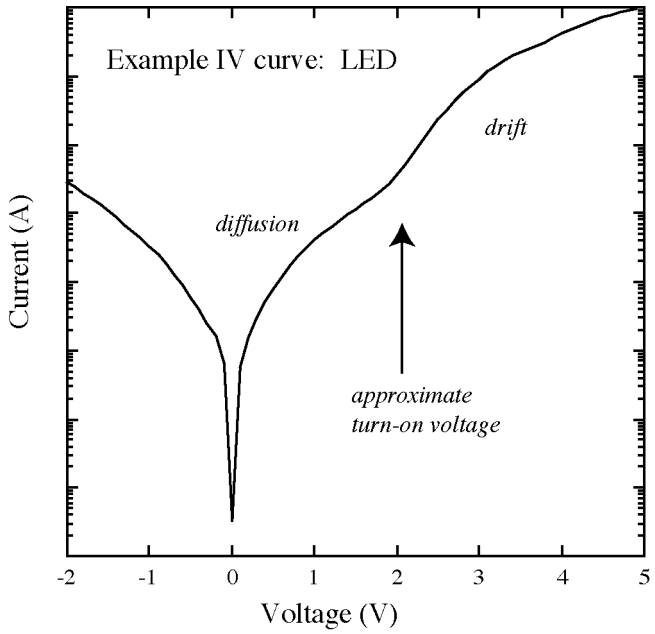

Figure 3.11 Example IV curve for a polymer LED.

An IV curve for an LEC that emits light in both forward and reverse bias is shown in figure 3.12. Despite the significant differences in the operating mechanism of polymer LED's and LEC's, the IV curves of these device types display remarkably similar features, with the exception of the reverse turn-on seen in the LEC. As mentioned previously, however, the testing of an LEC requires a much longer step-measurement delay due to the slow equilibration of the device, and frequently significant hysteresis is evident upon repeated cycles of measurement.

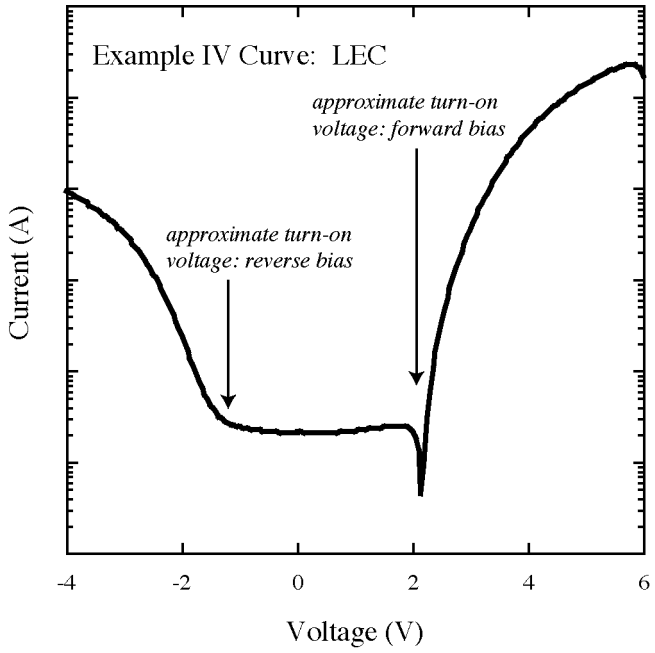

Figure 3.12 Example IV curve for a polymer LEC.

An IV curve for a typical polymer ECD is shown in figure 3.13. An ECD is essentially a solid state realization of a cyclic voltammetry experiment in the sense that we are electrochemically doping a polymer film with either cations or anions by cycling the system through a range of voltages in the presence of an electrolyte (see section 2.3). Accordingly, the features of such an IV curve correlate quite well with that of a cyclic voltammogram as described in section 3.1. ECD curves, however, do not typically display the clean peaks and clear reversibility seen in the cyclic voltammograms, due to the lowered ion mobility of the solid state.

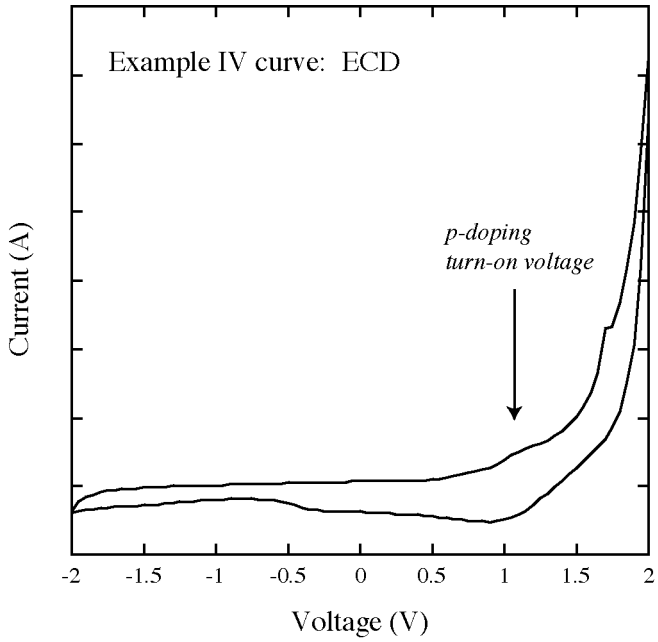

Figure 3.13 Example IV curve for a polymer ECD.

3.6 Optical characterization of devices

The optical characterization of polymer devices is of primary importance for this work and includes the measurement of the electroluminescence spectra and radiance for LED's and LEC's as well as the transmission spectra for ECD's. Subsequent analysis of this data involves the calculation of CIE coordinates, external quantum efficiency for LED's and LEC's, and Δ%T (change in optical transmittance) for ECD's.

The measurement of a device's electroluminescence (EL) spectrum is achieved using an Ocean Optics SD2000 fiber optic spectrometer. The device is held at a constant applied voltage or current using a Keithley 2400 sourcemeter, and a

LabView script is used to acquire spectral data in the form of photon counts as a function of wavelength over a set period of time. From this information, the emitted spectrum, average photon energy (eV), and radiant exitance (W/cm^2) can be directly obtained. By weighting the measured spectral power distribution with the response function of the human eye, the values of luminous efficacy (lm/W) and luminous exitance (lm/cm^2) can be calculated. In addition, this distribution is used to calculate the C.I.E. coordinates of the device (see below).

The measurement of the device radiance and external quantum efficiency is done in tandem with the measurement of the current-voltage curve (see section 3.5). The device is enclosed with pins allowing electrical contact to the device, and a Si photodetector is placed on the ITO side of the device. The voltage is stepped linearly as described in section 3.5. The light emission incident on the photodetector induces a current through the photodetector that is read by a Keithley 485 picoammeter. This data, in combination with the spectral information determined with the spectrometer, gives the information necessary to determine the device luminance (cd/cm^2) and radiance (W/cm^2).

The external quantum efficiency can also then be calculated using the measured current through the device using the following definition;

$$\text{External quantum efficiency} = \frac{\#\ \text{photons out}}{\#\ \text{electron-hole pairs in}}$$

This value is typically reported as the primary means of expressing the level of device performance for a light-emitting device. An EQE plot for a polymer LED is shown in

figure 3.14. The quantum efficiency begins to rise at the turn-on voltage of the device and eventually levels off. In theory the external quantum efficiency of a device is the product of the internal quantum efficiency with factors such as the amount of light emitted in the forward direction due to the geometry of the device and the decrease in light intensity due to interference effects (see section 1.3).

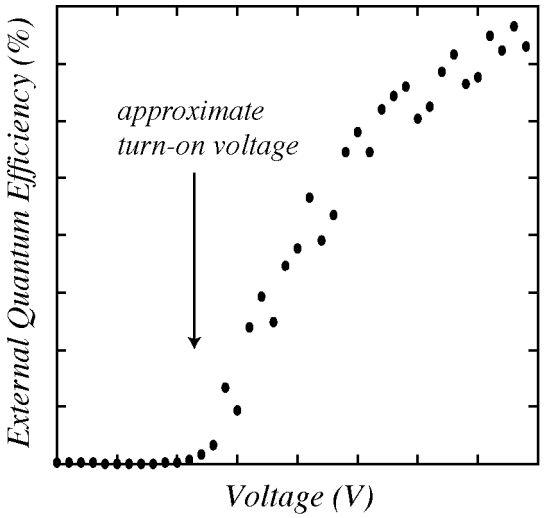

Figure 3.14 A representative plot of external quantum efficiency as a function of applied voltage for a polymer LED.

The optical characterization of electrochromic devices involves mainly the measurement of the change of the device's transmission spectrum from the initial (non-doped) state to the colored (doped) state. The measurement of a transmission spectrum is described in detail in section 3.3. Typically the transmission spectrum is taken for the non-doped state of the device, a voltage is applied to the device for a given period of time, and then the transmission spectrum is quickly taken again for

the colored state before any bleaching can occur. The change in transmission spectra is often reported as Δ%T for the wavelength within the visible that displays the maximum difference in transmission. Finally, the transmission spectra are used to determine the C.I.E. coordinates of the device as described below.

The C.I.E. chromaticity coordinates are used to map the color of an object with respect to hue and saturation onto a two-dimensional C.I.E. chromaticity diagram (figure 3.15). They are derived from either the electroluminescence spectrum for a light-emitting object or the transmission spectrum for an electrochromic device. The procedure for calculating the C.I.E. coordinates is as follows: The spectrum used is first weighted by each of three C.I.E. color-matching functions (figure 3.16). Each data column is summed to obtain the three C.I.E. tristimulus values X, Y, and Z. The values are then normalized to obtain the C.I.E. chromaticity coordinates $x=X/(X+Y+Z)$ and $y=Y/(X+Y+Z)$. This is the most common procedure for reporting color despite the limitations of the C.I.E. color system such as the loss of information about brightness and color mixing.

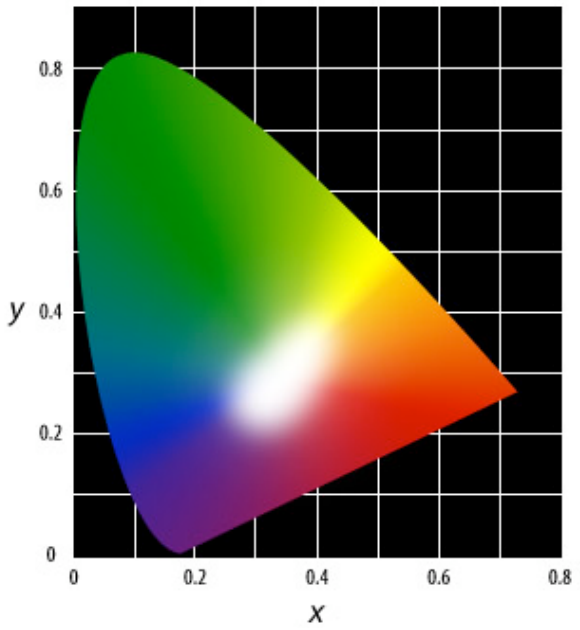

Figure 3.15 The C.I.E. chromaticity diagram.

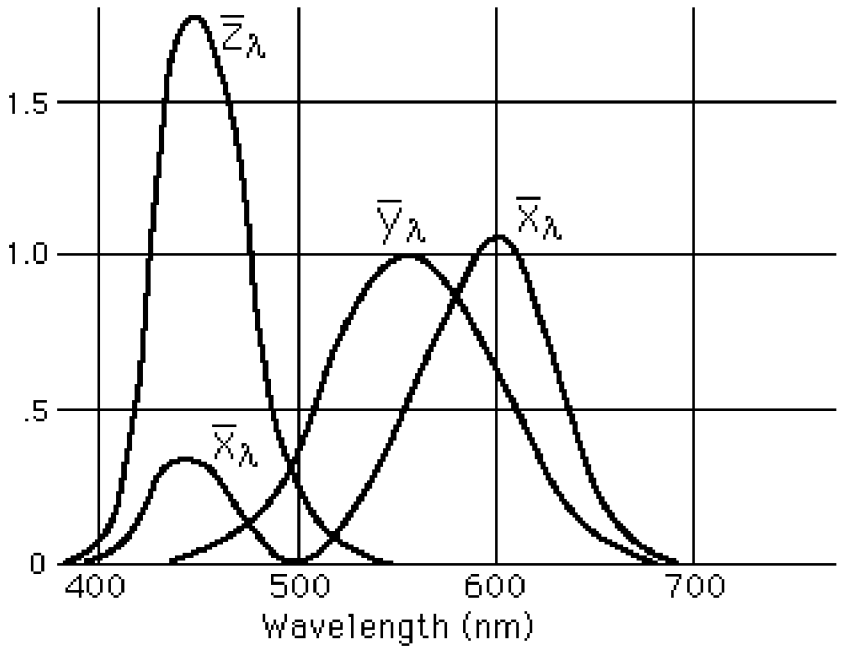

Figure 3.16 The C.I.E. color matching functions.

CHAPTER 4

THICKNESS DEPENDENCE AND INTERFERENCE EFFECTS IN POLYMER LIGHT-EMITTING DIODE STRUCTURES

4.1 Abstract

We explore the thickness dependent optical properties of single layer polymer light emitting diodes for two materials, Poly[2-methoxy-5-(2-ethylhexyloxy)-1,4-phenylene-ethenylene-2,5-dioctyloxy-1,4-phenylene-ethenylene] (MEH-DOO-PPV) and Poly(2,7-(9,9-bis(2-ethylhexyl))fluorene)-2,7-bis(4-methylphenyl)phenylamine (PF with 2% endcap). We compare experimental electroluminescence spectra and radiance values as a function of emissive layer thickness with simulations utilizing dipole methods within a transfer matrix formalism. The technique is then extended to explore how simulated results depend on the assumed location of emission within the polymer layer. We show that thickness dependent optical properties of these devices are dominated by interference effects.

4.2 Introduction

Since the discovery of semiconducting polymers in 1990 (Burroughes et. al. 1990), considerable progress has been made in understanding the electronic and optical properties of these materials in light emitting diode (LED) structures (Friend

et. al. 1999). Our understanding, however, has been complicated by the fact that these properties can vary significantly for liquid processed polymer films when the deposition conditions are varied (Braun 1991). While there have been several studies on the effect of solvent and annealing conditions on the polymer film morphology (Nguyen et. al. 1999, Ariu et. al. 2000), few systematic studies have been done on understanding changes in the optical properties when varying the thickness in single layer devices (Cimrova et. al. 1996, Bulovic et. al. 1998). This lack is surprising since modest changes in thickness in two of the more commonly studied class of materials, namely polyfluorenes and polyphenylenevinylenes, can result in substantial color shifts accompanied by order of magnitude changes in the device efficiency. Moreover, the polymer film thicknesses are frequently not reported or vary substantially, making comparisons between different experimental works difficult.

Thickness dependent changes in the optical properties can be caused by changes in the self-absorption, local film morphology in the region of light emission, and optical interference (i.e. microcavity effects). In this chapter, we explore the optical properties of single layer polymer LED's as a function of emissive layer thickness in an attempt to understand the relative importance of these effects. Devices are made with Poly[2-methoxy-5-(2-ethylhexyloxy)-1,4-phenylene-ethenylene-2,5-dioctyloxy-1,4-phenylene-ethenylene] (MEH-DOO-PPV) and with Poly(2,7-(9,9-bis(2-ethylhexyl))fluorene)-2,7-bis(4-methylphenyl)phenylamine (PF with 2% endcap), materials that both show substantial changes in the CIE coordinates

and device efficiency with thickness. We compare experimental electroluminescence spectra and radiance values as a function of emissive layer thickness with simulations that model the optical interference effects in single layer PLED structures utilizing dipole methods within a transfer matrix formalism. The technique is then extended to explore how simulated results depend on the assumed location of emission within the polymer layer. We find that optical interference is the primary factor in understanding changes in the optical properties of our devices due to varying thickness.

4.3 Experimental details and thickness-dependent results

The material synthesis and characterization of both MEH-DOO-PPV (Hörhold et. al. 2001) and PF (Nothofer) have been described previously (for chemical structures see inlays in figures 4.1(a) and 4.1(b)). Absorption and photoluminescence measurements were performed on the polymers as described in chapter 3.3, with the exception that absorption spectra for MEH-DOO-PPV were taken using a Hewlett-Packard 8452A Diode Array Spectrophotometer. Normalized absorption and photoluminescence data are presented in figure 4.1, and showed minimal dependence on layer thickness. This is expected, due to the minimal optical interference present in a multilayered structure of very low variation in reflectivity. The geometry of the experimental apparatus is such that self-absorption effects are minimized.

Devices were constructed using a single emissive layer structure with the addition of a hole transport layer. Poly(3,4,ethylenedioxythiophene)-poly(styrenesulfonate) (PEDOT-PSS, provided by Bayer corp.) of 60 nm thickness was spin-coated onto patterned ITO on glass substrates and annealed at 128°C for 1 hour under vacuum (Carter et. al. 1997). The emitting polymer layer was spin-coated from solution at various spin speeds and from solutions of varying concentrations to achieve a range of film thicknesses. The MEH-DOO-PPV film thicknesses were varied between 55 nm and 100 nm, resulting in a color shift from orange (CIE 0.577, 0.422) to reddish (CIE 0.619, 0.379) emission. PF film thicknesses were varied between 135 nm and 213 nm, resulting in a color shift in this range from blue (CIE 0.191, 0.134) to violet (CIE 0.171, 0.092) emission. The error on measured layer thickness is +/- 5 nm. The polymer layers are dried under vacuum overnight. A 25 nm layer of calcium followed by a 25 nm layer of aluminum is thermally evaporated onto the device. Devices were constructed and tested using the techniques described in chapter 3.

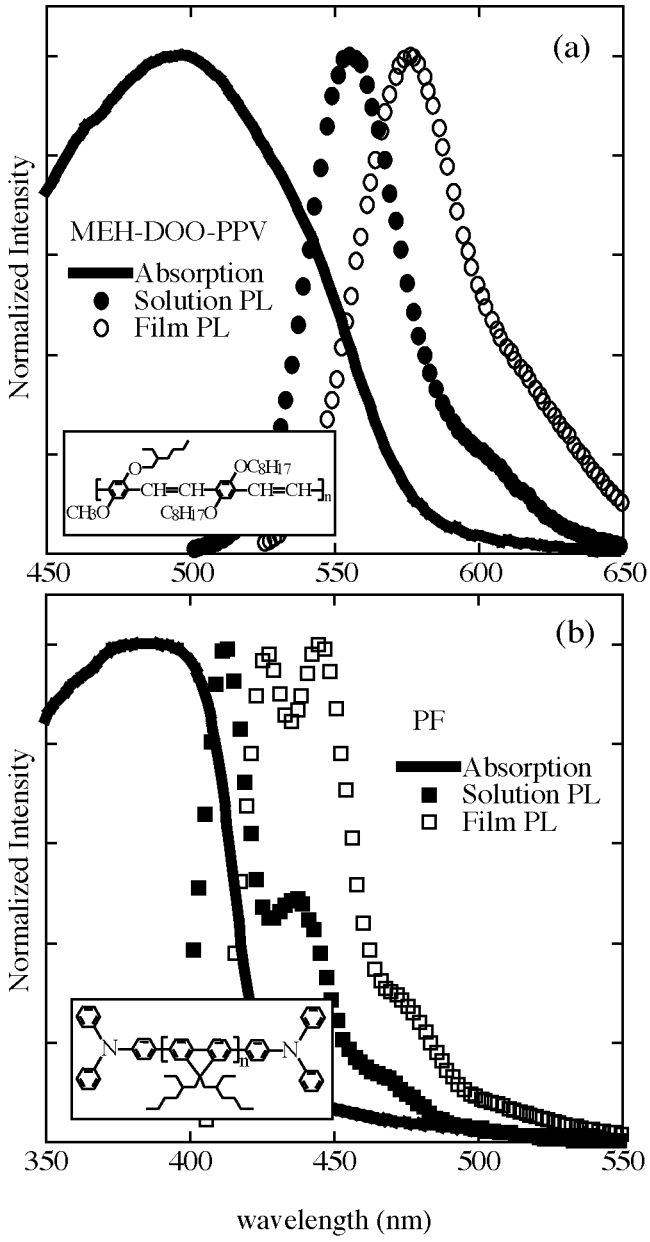

Figure 4.1 Experimental normalized film absorption, solution PL, and film PL for (a) MEH-DOO-PPV and (b) PF. Inlays show the chemical structures for each polymer.

Figure 4.2(a) shows the normalized electroluminescence spectra from polymer LED's with MEH-DOO-PPV as the emissive material. Spectra are shown for polymer layer thicknesses of 55 nm, 62 nm, 86 nm, and 100 nm. We observe a significant drop in the relative weight of the 580 nm vibrational peak and a concurrent rise in emission at lower energies as the thickness of the polymer layer is increased. The broad lower energy peak observed at ~680 nm may be attributed to aggregate emission (Jakubiak et. al. 1999). Similarly, as shown in figure 4.2(b), the normalized electroluminescence spectra from polymer LED's with PF as the emissive material also show strong thickness dependence. Here, the spectra shown have thicknesses of 135 nm, 151 nm, 186 nm, and 213 nm. Again we see a drop in the relative weight of the primary vibronic peak at 420 nm with increased emissive layer thickness.

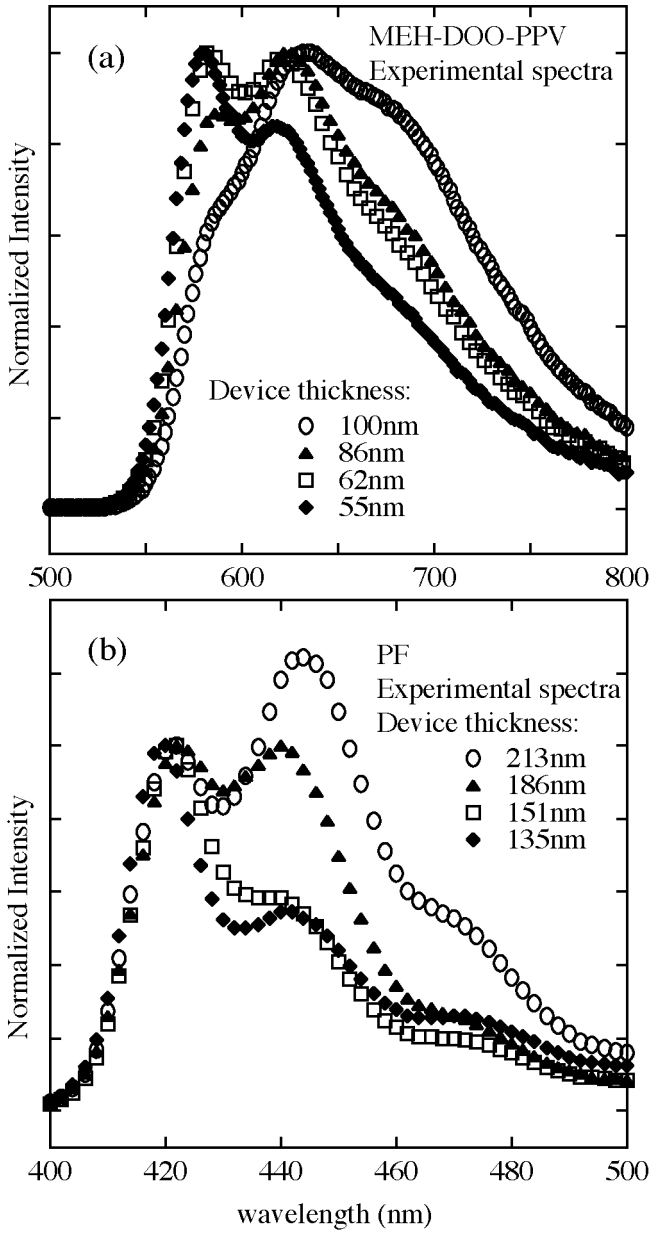

Figure 4.2 Experimental normalized EL spectra for (a) MEH-DOO-PPV, with thicknesses 55 nm, 62 nm, 86 nm, and 100 nm and (b) PF, with thicknesses 135 nm, 151 nm, 186 nm, and 213 nm.

4.4 Simulation of interference effects in PLED structures

In order to understand the effects of optical interference on the properties of polymer LED's, we did simulations which model thickness dependence in single layer polymer LED structures. Since polymer LED's consist of a multilayer thin film stack with a total thickness on the order of the emission wavelength, the emission spectra critically depend on the thicknesses and refractive indices of the individual layers. The theory underlying the simulations of interference effects used in this study are described in section 2.4.

For our investigations, we assume that the emission zone location scales with device thickness as expected if relative charge mobilities and injection rates remain unchanged. The simulation parameters thickness, refractive index and basis spectra were determined experimentally. For both the PF and the MEH-DOO-PPV, we use an experimentally determined EL spectrum as the emission spectrum of the dipole. The refractive index dispersion curves of MEH-DOO-PPV and PF were determined by spectroscopic ellipsometry (VASE by Woollam Inc.). In particular, a Cauchy dispersion model was fit to the transparent regime and subsequent extrapolation to lower wavelengths was carried out by point-to-point fits. For this fit, an isotropic model was chosen, thus ignoring birefringence in the films. The model gives a very good fit to the experimental data. Inclusion of birefringence in the model is a subject of future work. The resulting dispersion curves are shown in Figure 4.3.

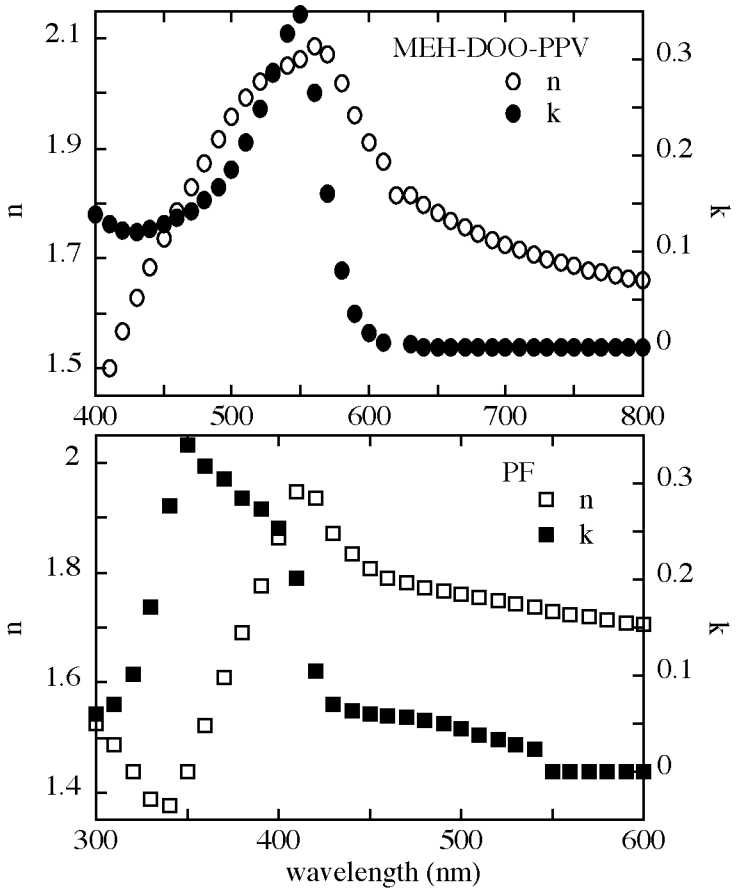

Figure 4.3 Refractive index dispersion curves for MEH-DOO-PPV and PF.

For PEDOT-PSS, a constant refractive index value of 1.53 was assumed (Pettersson et. al. 1998). The resulting simulated spectra are shown in figure 4.4(a) for the MEH-DOO-PPV emission and in figure 4.4(b) for the PF. We can see that in both the MEH-DOO-PPV and the PF simulations, for which we chose the same or similar thicknesses as our experimental devices, the simulations very closely match the experimentally determined spectra. We have shown that the simulations were

successful in modeling the changes in the relative weights of the two leading vibronic peaks of the EL spectra with changing device thickness.

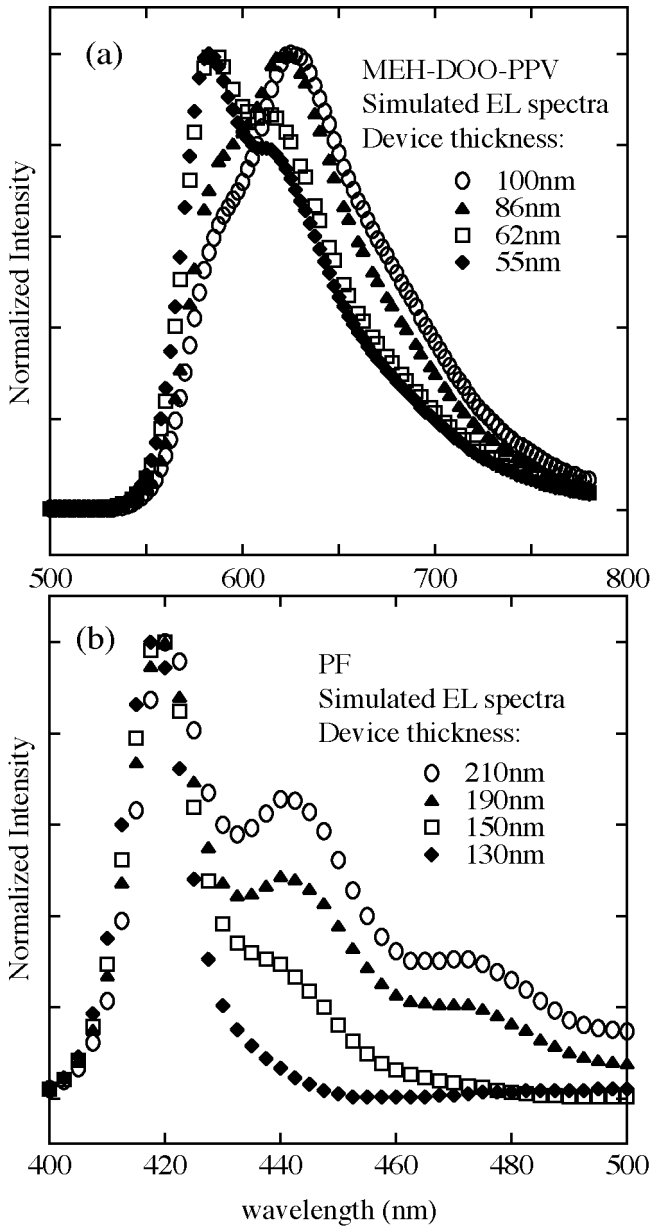

Figure 4.4 Simulated normalized EL spectra for (a) MEH-DOO-PPV, and (b) PF, with various thicknesses.

In addition to simulating the EL spectra of these devices as a function of device thickness, we looked at the radiance as a function of device thickness and compared the experimental data to the simulated results. Those results are plotted as figure 4.5(a) and 4.5(b). Experimentally determined values for radiance were measured at the same current for all devices. Values plotted in figure 4.5 were normalized to compare the relative changes in radiance with simulated results. The overall trends in relative radiance with device thickness are nicely reproduced in the simulated data.

We would expect that the trend in radiance with increased self-absorption would be a steady decrease with increasing device thickness, and so we can conclude that the observed trend in radiance is dominated by optical interference effects. In addition, self-absorption should have the effect of decreasing the relative intensity of the EL at wavelengths in the region of overlap between emission and absorption as the thickness of the polymer layer is increased. As seen in figure 4.1, this region is in both cases the leading vibronic peak in EL spectrum. Therefore the thickness dependent effects seen in the experimental EL spectra are at least partially due to self-absorption effects. However, the overlap is not large, and the difference in device thickness is not significant enough to completely explain the strong thickness dependence seen in the spectra of these devices. Again therefore, we expect that interference may play the dominant role.

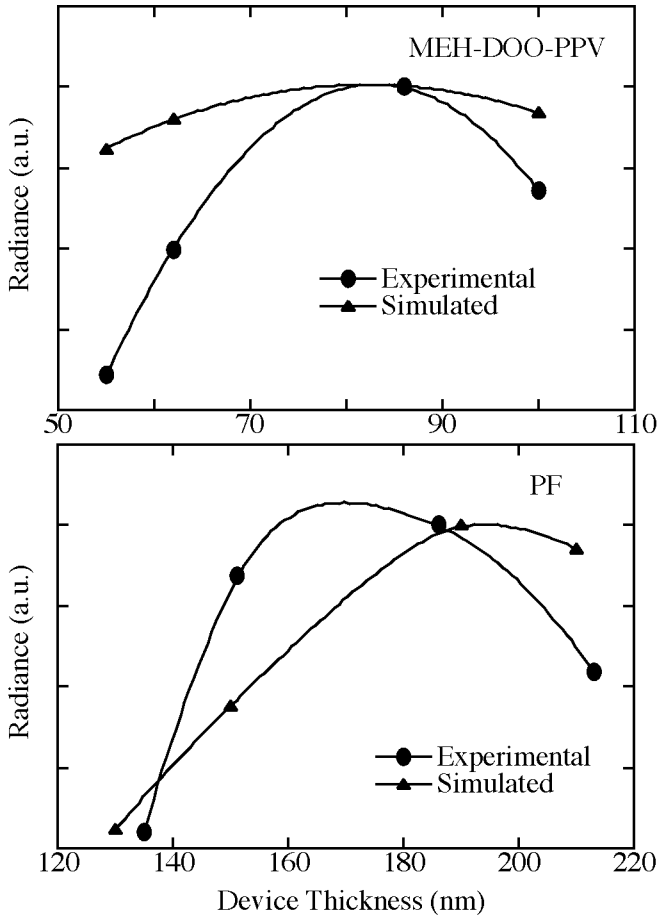

Figure 4.5 Experimental and simulated radiance curves in arbitrary units, for (a) MEH-DOO-PPV and (b) PF. For the simulated results, emission is assumed to occur 20% of device thickness away from the anode.

4.5 Simulation of emission zone location

For both the PF and the MEH-DOO-PPV thickness dependence simulations discussed above, we assumed the emission zone to be a distance 20% of the emissive layer thickness away from the anode. To come to this assumption, it was necessary to explore the dependence of the simulations on location of light emission. These

simulations are shown in figures 4.6 and 4.7. First we explore several emission zone locations for a given device thickness in figure 4.6. Figure 4.6(a) shows a simulated 100nm thick MEH-DOO-PPV device, with light emission occurring at various locations in the polymer layer. As the emission moves from the anode to the cathode, we see an increase in the first peak intensity as well as a slight blueshift in peak location. In contrast, the dependence on emission zone location for PF, shown in figure 4.6(b) for a 190 nm thick device, does not display a clear trend. We see that the emitted spectra for PF are highly sensitive to modest changes in emission zone location.

Figure 4.7 shows the thickness dependent simulations recalculated under the assumption that the emission is occurring nearer to the cathode. In figure 4.7(a), the MEH-DOO-PPV simulation is done assuming emission to be a distance 70% of the emissive layer thickness away from the anode. In this case, the thickness dependent trend seen in the experimental data is reproduced; however, the effect in simulation is less dramatic than seen in the experimental data. In figure 4.7(b), the PF simulation is done assuming emission to be a distance 80% of the emissive layer thickness away from the anode. Clearly in this case the thickness dependent trend seen in the experimental data is no longer accurately reproduced. The emission location parameter used in the simulations of thickness dependence in MEH-DOO-PPV and in PF devices were chosen such that the resulting simulated spectra and radiance trends

most closely matched those seen in our experimental results. For both materials this value is 20% of the polymer layer thickness from the anode.

Finally, we consider whether recombination near the anode is consistent with our understanding of the device architecture. For PF*, electron injection from the calcium cathode (work function ~ 2.9 eV) to the LUMO of PF (3.0 eV) is nearly Ohmic; however, a large barrier to hole injection exists from the PEDOT-PSS (5.1 eV) to the HOMO of PF (5.8 eV) (Janietz et. al. 1998). For PF without endcaps, it is thought by some that this barrier to hole injection causes electron-hole recombination to occur directly at the polymer/PEDOT-PSS interface. The endcaps appear to assist in hole injection into PF (Miteva et. al. 2001), moving recombination slightly into the bulk of the material, increasing device efficiency and decreasing aggregation peaks associated with the polymer morphology at the interface (Nakazawa et. al. 2002). It is therefore reasonable to assume in this scheme that recombination should occur near to the device anode, and light emission occurring at 20% of the polymer layer thickness from the anode would then be consistent with this assumption. However, there has been some evidence (Campbell et. al. 2002) that the lower electron mobility in PF's inhibits movement of electrons through the film toward the anode significantly enough that despite a barrier to hole injection at the interface, recombination may be occurring nearly at the cathode. In this scheme then, our assumptions are no longer accurate, and therefore our simulations do not provide a close match to experiment. In the case of PF materials, a straightforward conclusion about the location of

recombination may not be possible based on injection barrier and mobility arguments alone.

In contrast, for MEH-DOO-PPV*, both the HOMO (5.3 eV) and LUMO (3.0 eV) levels are closely matched to the electrodes (Campbell et. al. 1996), providing nearly Ohmic contacts for both electron and hole injection. As a consequence, we would expect to see emission occurring at a thickness consistent with experimentally determined relative charge mobilities in the material. Due to its similarities with MEH-PPV, the hole mobilities for MEH-DOO-PPV should be on the order of, or slightly higher than, the electron mobilities (Bozano et. al. 1999). This would suggest that recombination should occur close to the center or cathode side of the device rather than near to the anode (Malliaras et. al. 1998). However, the simulations of thickness dependence in MEH-DOO-PPV show rather low emission zone location sensitivity, and it is while it may not be the closest match to experiment, a simulation using an emission zone located closer to the cathode would still provide a reasonable simulation of MEH-DOO-PPV device thickness dependence.

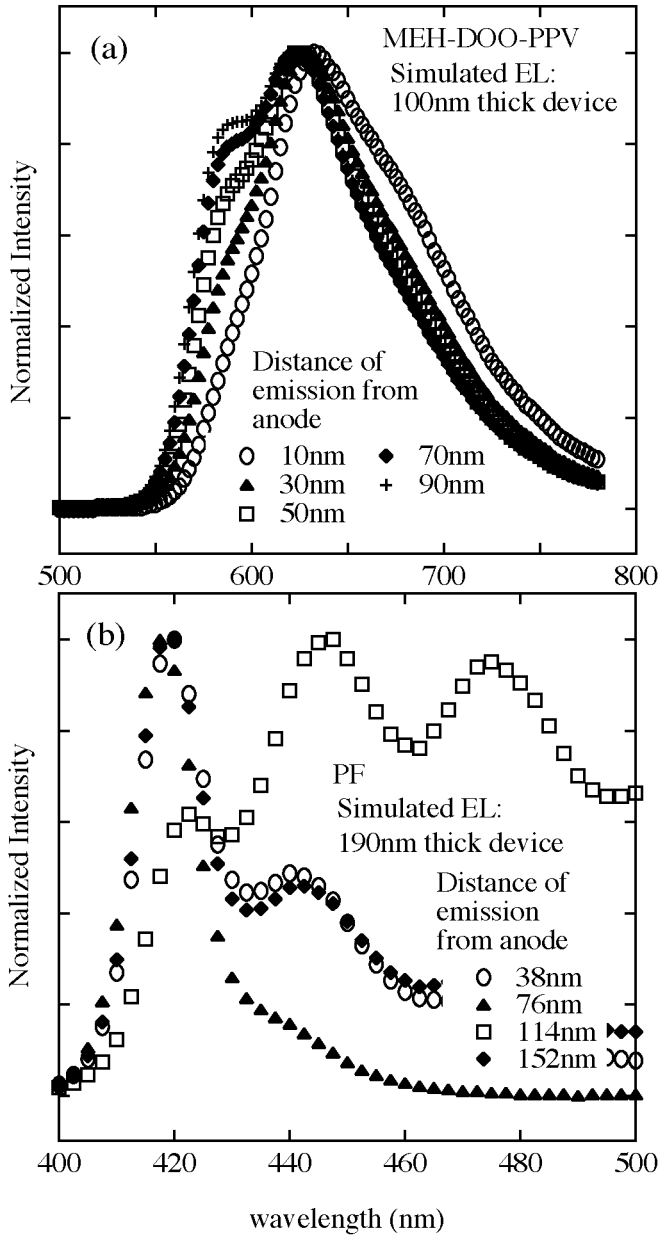

Figure 4.6 Simulated normalized EL spectra for single device thickness as a function of emission zone for (a) 100 nm MEH-DOO-PPV device, with emission occurring at 10 nm, 30 nm, 70 nm, and 90 nm from anode, and (b) 190 nm PF device, with emission occurring at 38 nm, 76 nm, 114 nm, and 152 nm from anode.

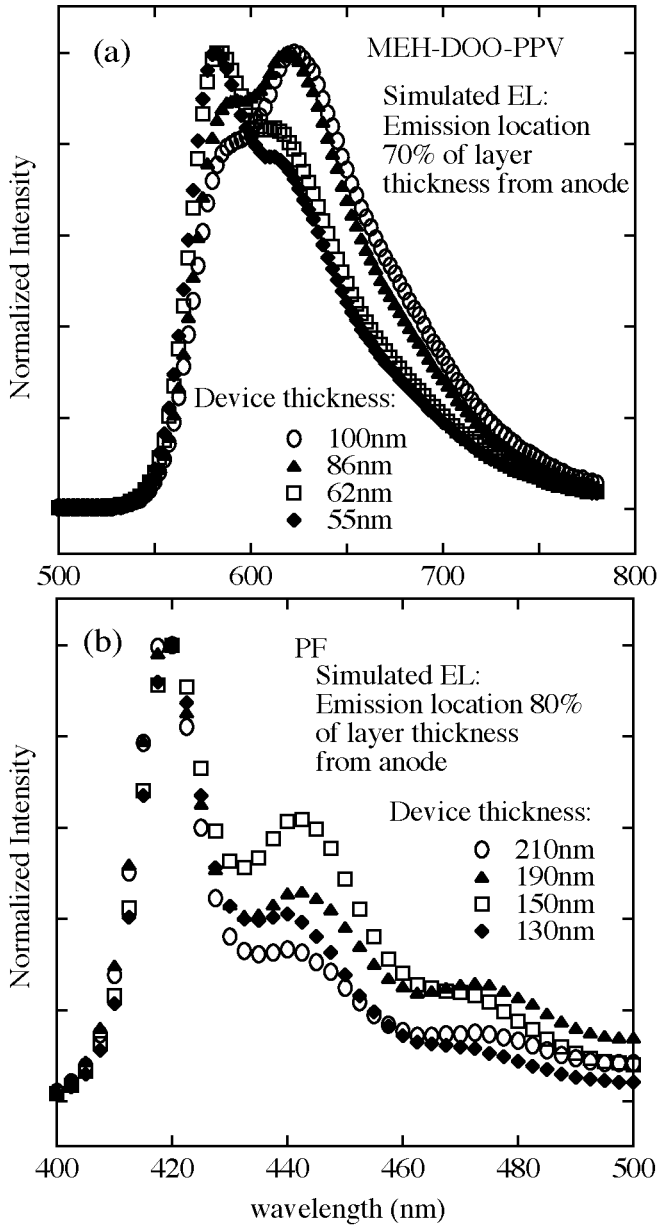

Figure 4.7 Simulated normalized EL spectra for (a) MEH-DOO-PPV, with thicknesses 55 nm, 62 nm, 86 nm, and 100 nm and emission assumed to occur 70% of device thickness away from the anode, and (b) PF, with thicknesses 130 nm, 150 nm, 190 nm, and 210 nm, and emission assumed to occur 80% of device thickness away from the anode.

4.6 Conclusions

Several aspects of the simulations make it rather difficult to exactly reproduce the experimental data. As previously mentioned, the choice of dipole emission spectrum can significantly alter the overall appearance of the simulated spectra. In addition, the simulation can be rather sensitive to parameters that are experimentally determined, such as the thickness of both the hole injection layer and the polymer layer, and are therefore subject to experimental errors in comparing with experiment. Finally, assumptions are made in the calculations concerning the nature of charge recombination, exciton diffusion, and emission zone location which are not fully understood but which can change the final simulated thickness dependent effects. We note that in polymer LED's as discussed here, the emission zone may extend over a few tens of nanometers. Thus the above model with an exact dipole location is an approximation (Wan et. al. 2000). However, the simulations are able to illustrate that the changes in the optical properties of polymer LED's seen as a function of device thickness can be well accounted for by simulation of optical interference effects.

*Values given for HOMO/LUMO energy levels are those corresponding to the closely related materials PFO and MEH-PPV. We expect the true values to be very similar to those reported.

CHAPTER 5

RECOMBINATION PROFILES IN MEH-PPV LIGHT-EMITTING ELECTROCHEMICAL CELLS

5.1 Abstract

We present a study on the optical and electronic properties of light-emitting electrochemical cells (LECs) based on poly[2-methoxy-5-(2-ethylhexyloxy)-1,4-phenylenevinylene] (MEH-PPV) with the goal of understanding the emission profiles in vertical device structures and characterizing their salt and electrode dependence. Photoluminescence and electroluminescence profiles of planar LECs were directly imaged as they varied with applied voltage, and simulations of interference effects in multilayered device structures were performed in order to gain insight into emission profiles in vertical structure LECs. While our results are consistent with oxidative doping, they imply a lack of reductive doping in LECs under normal operating conditions. We observe that trends in emission profiles for vertical structure LECs follow those reported in planar structures and are independent of thickness, salt and electrode type. In addition, device I-V and radiance characteristics were measured as a function of salt and electrode type. Al electrodes resulted in variations in the I-V characteristics and turn-on voltage due to oxidation of aluminum contacts as compared to devices with Au contacts. Device performance was mainly independent

of anion selection; however, substantial changes in rectification were observed for different cations. Finally, we discuss the implications of our findings on the operating mechanism of LECs.

5.2 Introduction

Polymer light-emitting electrochemical cells (LECs) were first introduced by Pei et. al. in 1995 (Pei et. al. 1995). In an LEC, a thin film of light-emitting polymer admixed with an ionic conductor (typically polyethylene oxide, or PEO) and a salt, is sandwiched between two electrodes. According to the initial proposed operating mechanism, an applied voltage leads to electrochemical doping of the polymer, p-type near the anode and n-type near the cathode, leading to the *in situ* creation of a light-emitting pn-junction (Pei et. al. 1995, Pei et. al. 1996). Charge injection is then facilitated through the creation of Ohmic contacts between the electrodes and the highly conductive doped states of the polymer. The LEC was shown to operate in both forward and reverse bias, effectively independent of electrode work function, at voltages just above the polymer bandgap, consistent with the properties expected from a dynamically reversible pn-junction (Pei et. al. 1995, Pei et. al. 1996, Li et. al. 1999, Smith 1997, Riess and Cahen 1997).

In 1998, deMello et. al. proposed an alternate theory also capable of explaining these observed properties of the LEC (deMello et. al. 1998). They claimed that the accumulation of ions at the electrode-polymer interfaces introduces large

electric fields that reduce the barriers to charge injection (deMello et. al. 1998, deMello et. al. 2000). Thus electrochemical doping is not responsible for charge injection in the LEC. Further, they claim that any electrochemical doping present in an LEC under normal operation is unlikely (deMello et. al. 1998). Subsequent studies reporting direct photoluminescence (PL) and electroluminescence (EL) imaging in planar LEC structures, however, show a region of quenched PL that clearly indicates the presence of doped polymer (Pei et. al. 1996, Dick et. al. 1996, Gao and Dane 2003, Gao and Dane 2004). These results would seem to suggest that the model presented by Pei et. al. is the more likely picture; however, direct evidence that this model is accurate and complete is still lacking.

Recently, we have presented an in-depth study of electrochemical doping in MEH-PPV (Holt et. al., submitted), one of the most commonly used light-emitting polymers for LEC studies. We have shown that while p-doping of this material is highly reversible, efficient, and effectively independent of anion type, n-doping in MEH-PPV is characterized by low efficiency in most cases and inherent instability in all cases. Further, it has been shown that lithium salts are effectively incapable of n-doping MEH-PPV using acetonitrile at room temperature (Holt et. al., submitted), an observation supported by the observation that n-doping with alkali salts in polythiophenes and polyacetylene is not possible except when the ionic radius is increased with judicious solvent selection (Mastragostino and Soddu 1990, Zotti et. al. 1995). Lithium triflate is the primary salt used in studies of polymer LECs. It is

thus highly doubtful that n-doping is strictly necessary for the operation of typical MEH-PPV LECs, such as those presented in many previous works. Indeed, convincing evidence of n-doping in an LEC or pLEC structure at room temperature has yet to be presented. Clearly, further clarification concerning the fundamental operating mechanism is necessary for a full understanding of the polymer light-emitting electrochemical cell.

Surprisingly, light-emitting electrochemical cells have been little explored systematically, considering their potential for use in air-stable displays and the controversy surrounding their operating mechanism. Experimental results have been limited primarily to a single structure (ITO/polymer:PEO:Li salt/Al). In particular, there have been no systematic studies done on the effects of different salts and electrode materials on the electrical and optical properties of the LEC. Finally, planar structures have been well studied but the results obtained for these structures have not been correlated to trends in vertical structure LECs to allow the generalization of these important results.

In this work, we built both vertical and planar geometry LECs using MEH-PPV as the emissive material. Devices were varied by salt type, salt concentration, operating voltage, and electrode type. For the planar devices, *in situ* photoluminescence and electroluminescence profiles were directly imaged using a confocal microscope and CCD camera. For the vertical geometry devices, EL spectra are measured in both forward and reverse bias, in addition to typical current-voltage

and radiance-voltage characterization. We use simulations of interference effects in multilayered device structures using parameters obtained by observing emission profiles in pLECs to predict emission profiles and compare with experimental results. Finally, we discuss implications regarding the underlying operating mechanism of the LEC.

5.3 Experimental details

Both planar and vertical geometry LECs were constructed using MEH-PPV provided by American Dye Source as the emissive material. All polymer solutions consisted of MEH-PPV and PEO in a 9:4 ratio, and salt in varying amounts, in chlorobenzene. Salts used include lithium trifluoromethanesulfonate (triflate), tetrabutylammonium (TBA) tetrafluoroborate (BF_4), TBA hexafluorophosphate (PF_6), and TBA-triflate. Planar geometry LECs used a lower molecular weight (~100,000) PEO to minimize phase separation while the vertical geometry LECs used higher molecular weight (~5,000,000) PEO to achieve thicker films. After spin-casting, films were annealed at 80ºC for 3 minutes in an inert atmosphere, and placed under vacuum (~10^{-7} Torr) overnight. Film thicknesses were measured on a Park Scientific Autoprobe CP Atomic Force Microscope (AFM) and showed a variation of +/- 15 nm.

Planar geometry LECs were fabricated by evaporating gold strips onto glass substrates after prior masking with a 15 μm fine wire. Carefully removing the wire

resulted in a clean gap of ~20 μm thickness as determined by AFM. A polymer solution was then spin-cast onto the substrate, annealed at 80ºC for 3 minutes in an inert atmosphere, and placed under vacuum (~10^{-7} Torr) overnight. Prior to testing, the devices were encapsulated under inert atmosphere under a glass slide using Addison Clear Wave AC A1425 UV curable epoxy. Contact to the electrodes was made using copper tape with conducting adhesive. Images of PL and EL were obtained using a 40x oil immersion lens on a Technical Instruments K2 SBIO confocal microscope with a QImaging micropublisher CCD camera. The photoluminescence source was an Osram HBO-100 W/2 mercury short arc photo optic lamp with a rhodamine filter.

The vertical geometry LEC devices were prepared by spin-casting polymer solution to a thickness of ~350 nm onto pre-patterned ITO glass substrates. Top electrodes were deposited by thermal evaporation. All device testing took place in a dry nitrogen glove box using a Keithley 2400 Sourcemeter, a picoammeter, and a calibrated silicon photodetector. Electroluminescence spectra were also taken in an inert nitrogen atmosphere with an Ocean Optics fiber optic spectrometer.

5.4 Planar geometry LECs

Planar geometry LECs were constructed as shown in figure 5.1 using various salt types and with an average width of ~20 μm. Images of the device photoluminescence and electroluminescence profiles were captured using a confocal

microscope and CCD camera as described above. We found that the salt type made little difference in the general results despite significant differences in the type and size of the anions (triflate$^-$ vs BF_4^-) and cations (Li^+ vs TBA^+). The 0 V photoluminescence, 3 V bias photoluminescence, and electroluminescence at 10 V of a representative device are shown in figure 5.2.

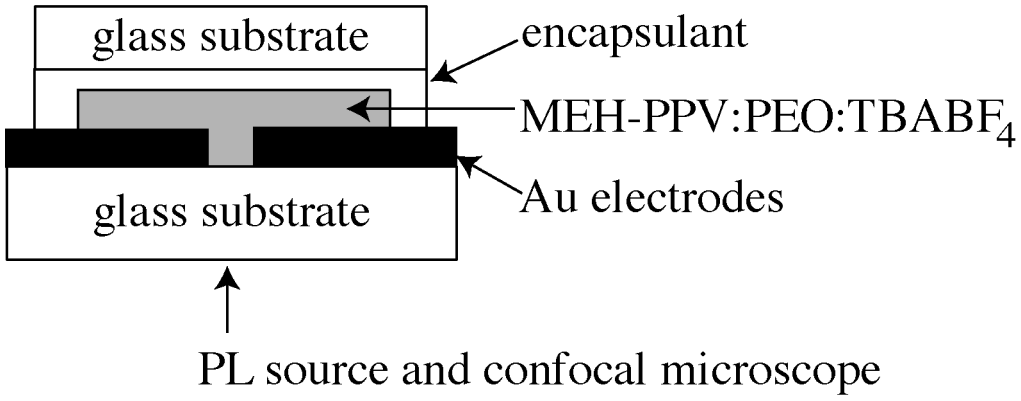

Figure 5.1 Device structure of a planar geometry light-emitting electrochemical cell.

As the applied voltage is increased, PL quenching can be observed at the anode beginning as low as 1 V, indicating oxidative doping. Edman et. al. show that the onset of p-type doping at voltages well below the bandgap of the material in planar LEC structures is due to the location of the gold work function relative to the HOMO/LUMO levels of the polymer (Edman et. al. 2004). Of particular interest is the observation that no evidence of PL quenching occurs at the cathode, suggesting a

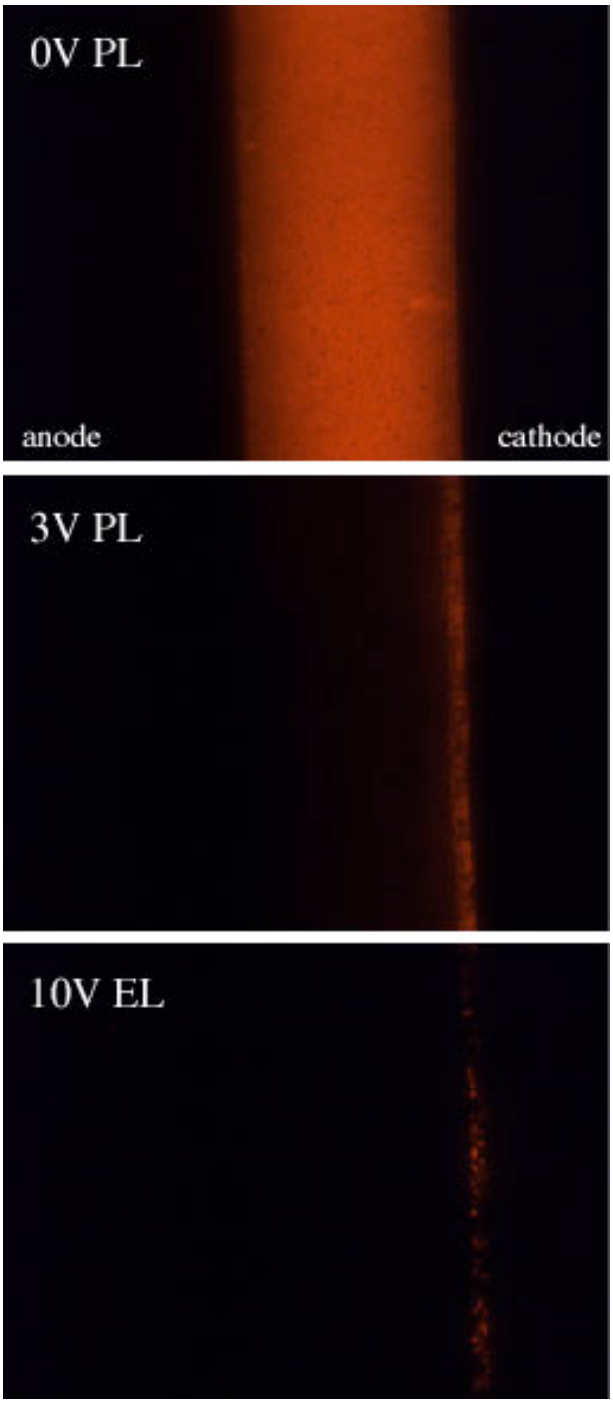

Figure 5.2 The 0 V photoluminescence, 3 V photoluminescence, and 10 V electroluminescence of a planar LEC with $TBABF_4$ salt.

lack of reductive doping in the device under normal operation. Previous groups have suggested that the lack of distinct PL quenching at the cathode is due rather to low concentrations of doped material or that PL quenching may be less efficient in n-doped than in p-doped polymer, although a clear argument is not given in either case (Pei et. al. 1996, Gao and Dane 2003).

At 3 V, the PL is highly quenched to within ~10% of the polymer layer thickness from the cathode. As the bias is increased, the quenched region moves toward the cathode as noted by other groups. The precise location of the quenched/unquenched interface varied significantly from device to device but occurred typically between 10%-40% of the device width away from the cathode. It is possible that this location is highly sensitive to variations in salt concentration. In our findings, the region of EL always occurred on the anode-side edge of the unquenched region with a characteristic width of ~ 1/14 – 1/16 of the device thickness. This could be due to the creation of a pn-junction within the device, or could suggest that charge recombination may be limited by hole injection from the p-doped polymer into the undoped region.

The ability to directly image the photoluminescence and electroluminescence profiles of planar LEC structures has provided very important information that may help to understand the operating mechanism of LECs. It is reasonable to assume that in general the devices in planar and vertical geometry operate under the same basic principles (Wenzl et. al. 2002); however, observations of planar devices are limited in

several important respects. First, the planar devices necessarily are restricted to using the same material for both electrodes, disallowing the study of device operation in the presence of a built-in electric field. Second, the imaging of these devices takes place outside of inert atmosphere. This requires some kind of encapsulation and exposure to air, both of which may affect device operation and prevents the successful study of devices with electrodes, which are oxygen sensitive such as Al or Ag.

Finally, the construction of devices with such drastically different geometries may result in a very different electric field profile within the device. In order to make conclusions from the observations of planar LECs we desire some evidence that the basic observed properties of the planar devices are duplicated in the vertical devices, and then extend the study to include devices with variations in thickness and electrode work functions. Unfortunately the vertical geometry prevents the direct observation of emission and photoluminescence profiles, requiring the study of these properties via a less direct approach.

5.5 Simulating interference effects in vertical geometry LECs

In order to investigate emission profiles in vertical geometry LECs, we did simulations which model interference effects in single layer polymer light-emitting device structures (ETFOS Emissive Thin Film Optics Simulator provided by B. Ruhstaller). Since polymer LECs consist of a multilayer thin film stack with a total thickness on the order of the emission wavelength, the emission spectra critically

depend on the charge recombination profile within the polymer layer, in addition to the layer thicknesses and refractive indices of the individual layers. In the previous chapter, we used simulations of interference effects to investigate the dependence of polymer light-emitting diodes on polymer layer thickness (Leger et. al. 2003). The simulation technique is based on a transfer matrix formalism with an oscillating point dipole source and is described in further detail there.

The simulation parameters thickness, basis spectra, refractive index, and emission profile were determined experimentally. In particular, the layer thicknesses of our experimental devices were measured with AFM and the resulting values used in simulation. We use the EL spectrum of a very thin (30 nm) MEH-PPV LED as the emission spectrum of the dipole. The spectral features of such a thin device were found to be effectively independent of interference effects as determined via simulation and thus suitable as a basis spectrum for this application. The refractive index dispersion curves of MEH-PPV:PEO were measured by spectroscopic ellipsometry (VASE by Woollam Inc.) and are shown in figure 5.3.

For the emission profile, we use a gaussian distribution of dipole locations with a characteristic width of 1/15 of the polymer layer thickness. This value was obtained by observing the typical width of the EL emission in our planar LEC devices. We make the assumption that the width of the emission profile scales with device thickness as observed by others (Gao and Dane 2003). After defining the parameters within the simulation software to match those measured for the

experimental device, spectra were generated assuming a dipole location specified as a percentage of the polymer layer thickness relative to the interface with the evaporated top electrode.

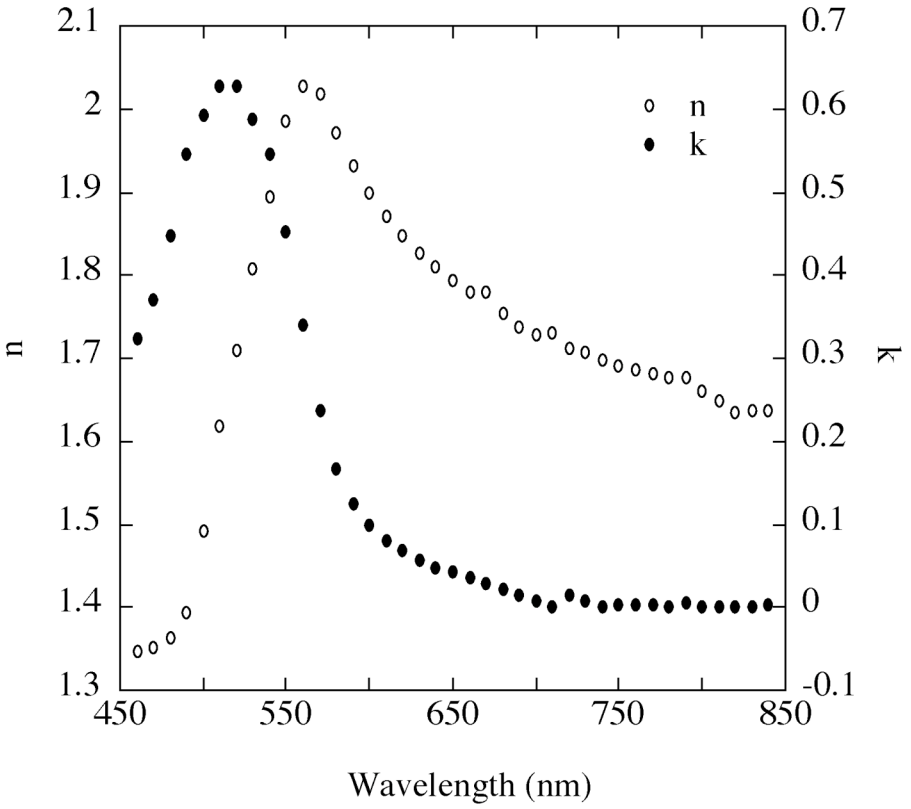

Figure 5.3 Optical constants n and k of a thin film of MEH-PPV:PEO.

5.6 Comparison of simulation and experiment: EL spectra of MEH-PPV LECs

The experimental and most closely matched simulated EL spectra for three different devices and various operating voltages are shown in figures 5.4 through 5.7. Figure 5.4 compares spectra for a 500 nm device with Au top electrodes and figure 5.5 shows similar results for a 300 nm device with Al top electrodes. In both cases, the best simulation results were obtained by assuming the location of light emission to be approximately 30% of the device thickness away from the cathode for both forward and reverse bias. It should be noted that, as with the planar LECs, no noticeable dependence of the emission profiles were observed for variations in salt type.

Figures 5.6 and 5.7 compare experimental and simulated EL spectra for a 250nm thick device with Au top electrodes. Figure 5.6 shows forward and reverse bias while figure 5.7 shows spectra for high and low reverse bias voltages. For this device, emission occurs symmetrically at approximately 10% of the layer thickness away from the electrodes and shifts toward the cathode by about 4% of the polymer layer thickness upon increasing the applied voltage from –4 V to –8 V.

The precise location of the symmetric light emission as a fraction of the polymer layer with respect to the electrodes varies a significant amount for each simulated device but typically fell in the range of 10% to 30%. This number clearly

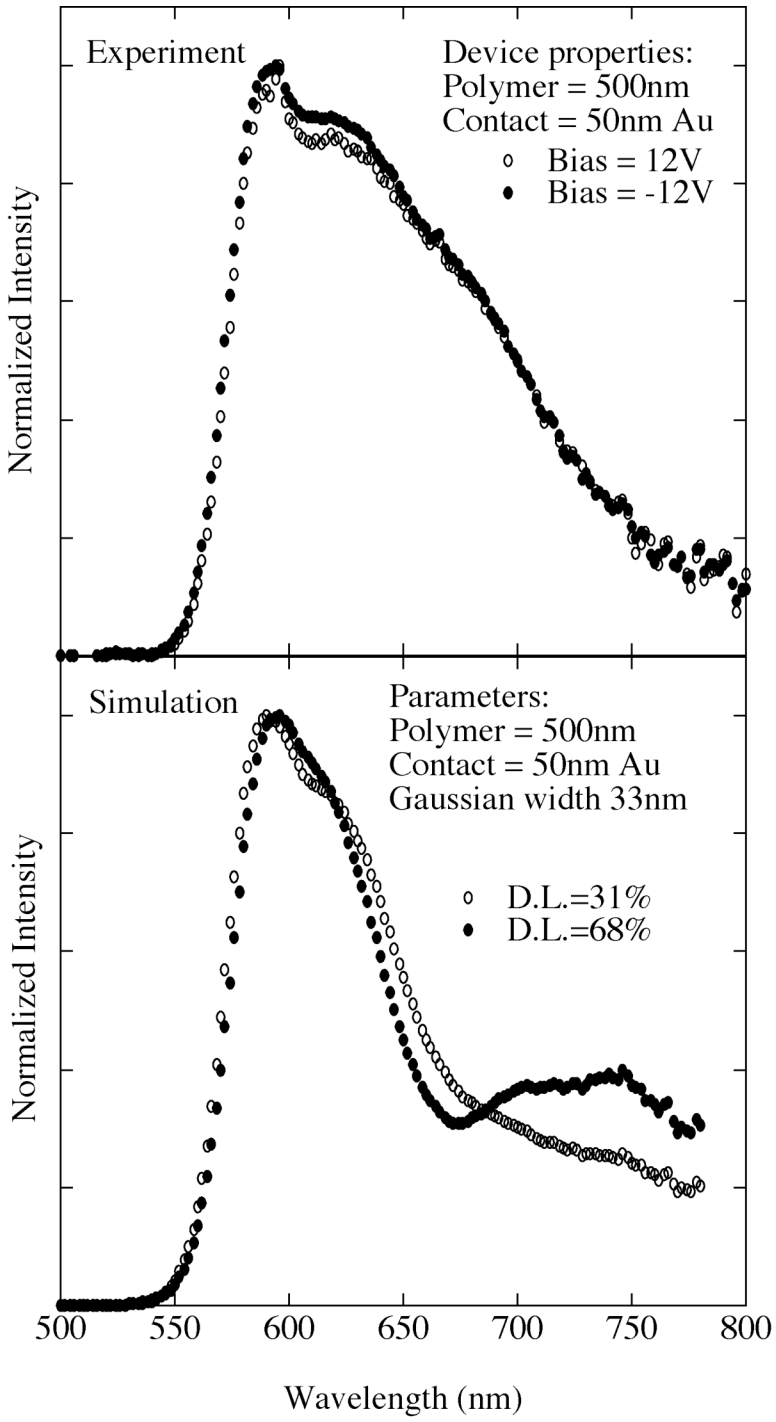

Figure 5.4 Experimental and simulated EL spectra of a 500 nm device with Au top electrodes in forward and reverse bias. D.L. = Emissive dipole location as a function of layer thickness relative to the top electrode.

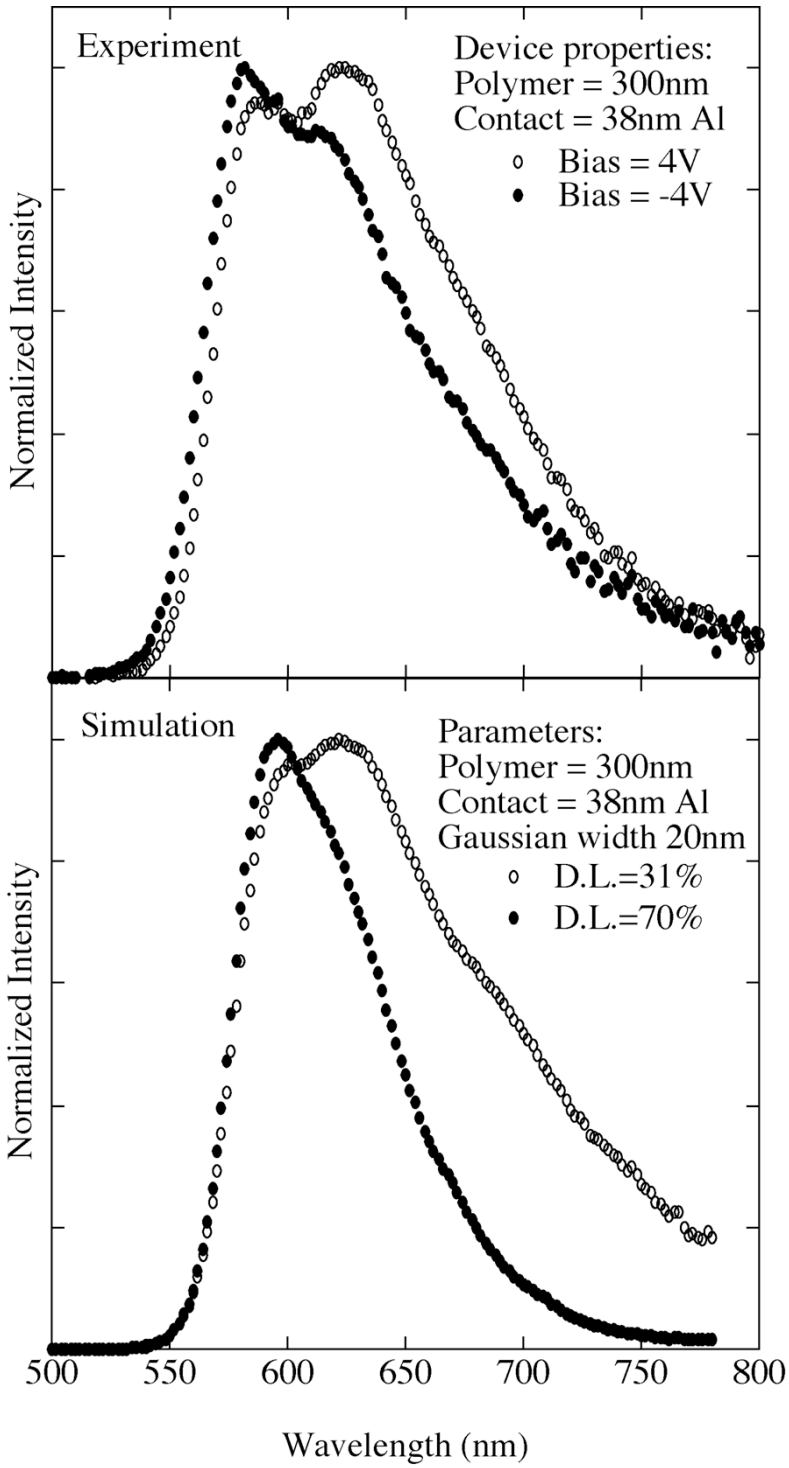

Figure 5.5 Experimental and simulated EL spectra of a 300 nm device with Al top electrodes in forward and reverse bias.

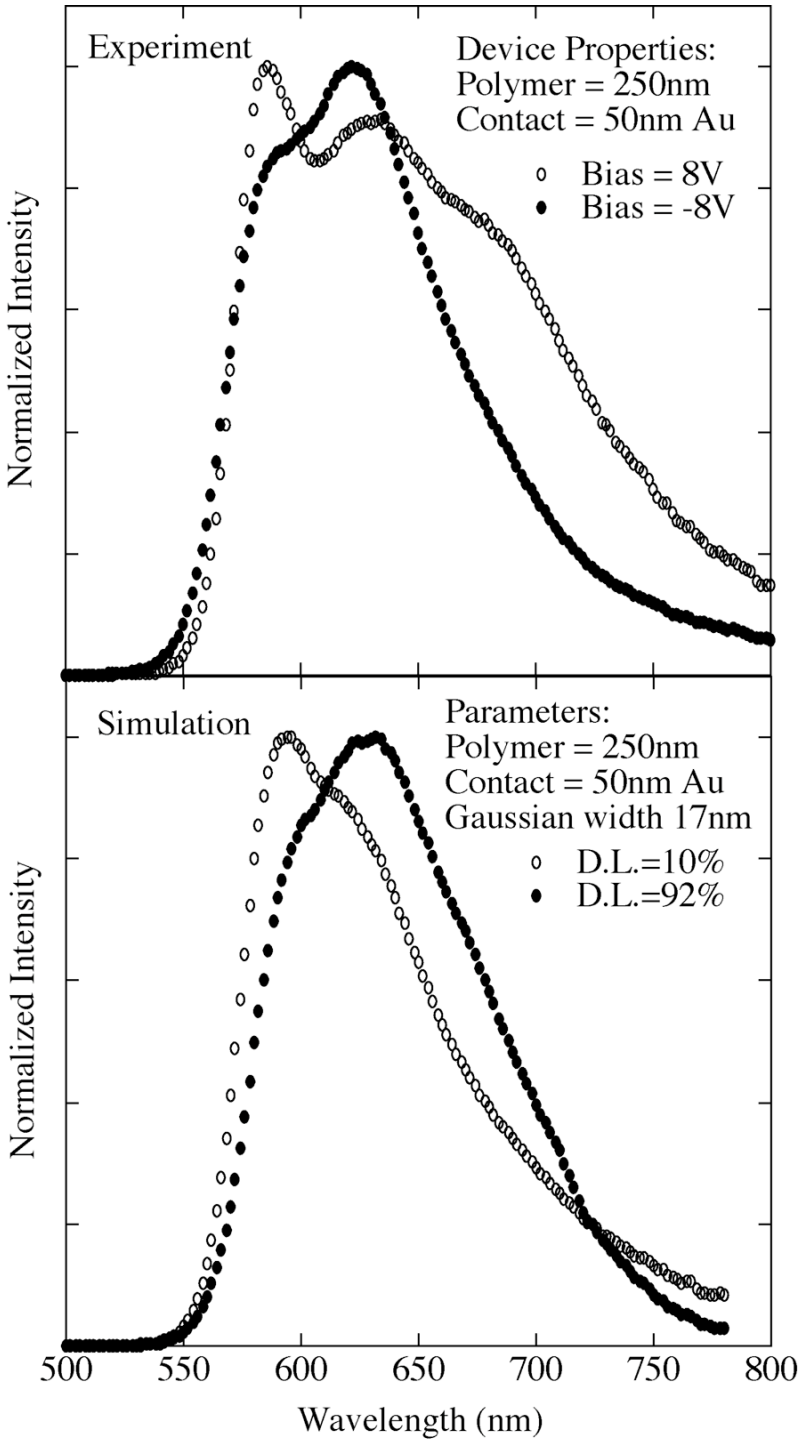

Figure 5.6 Experimental and simulated EL spectra of a 250 nm device with Au top electrodes in forward and reverse bias.

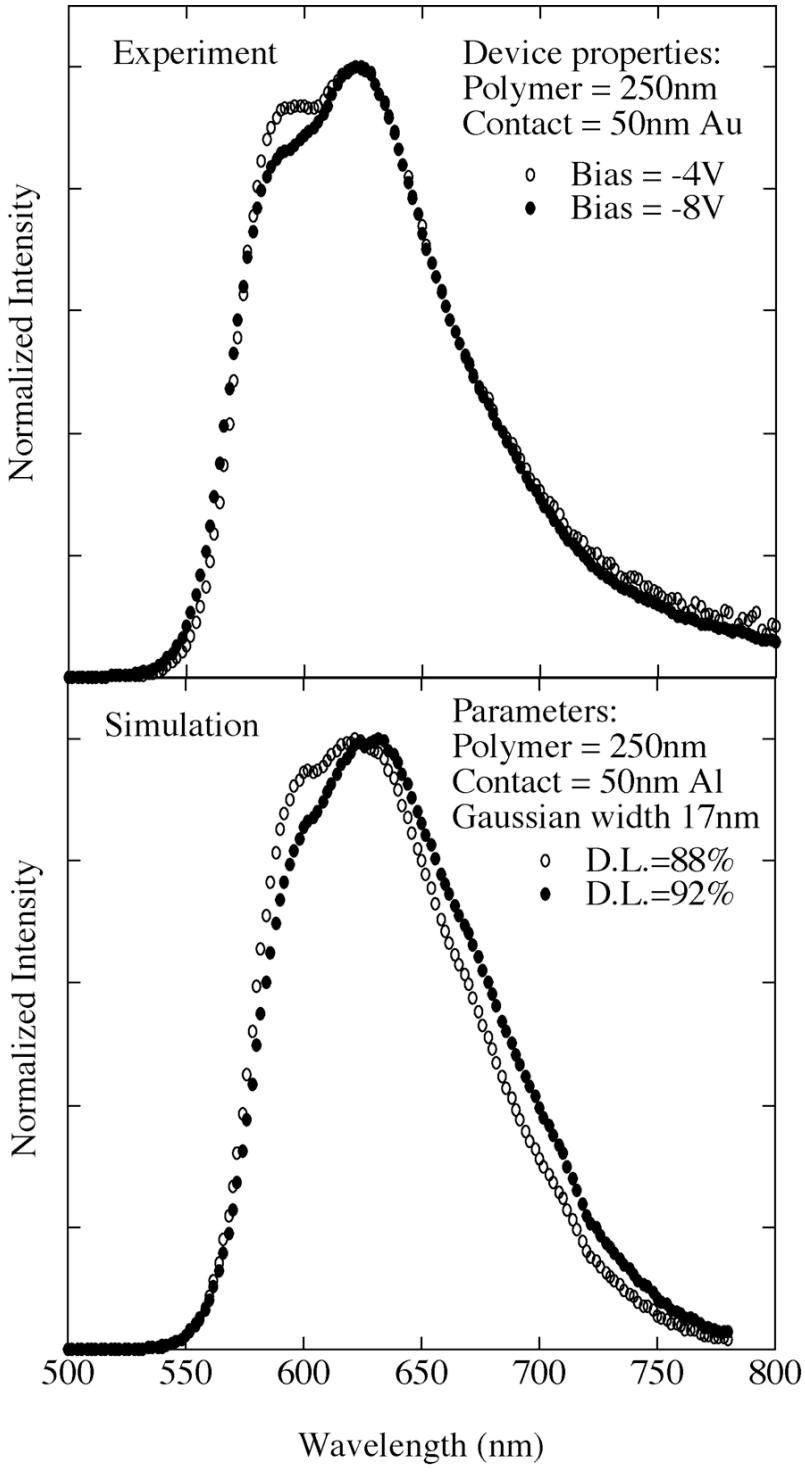

Figure 5.7 Experimental and simulated EL spectra of a 250 nm device with Au top electrodes in high and low reverse bias.

varied with the applied voltages at which the spectra were obtained, but also varied significantly from device to device, suggesting that the location of light emission in a given device is highly sensitive to slight changes in the device preparation. It should be noted that the variation in emission location for the vertical structure LECs as determined by simulation is of a similar range as the variation seen for the planar structures. For reference, figure 5.8 shows simulated EL spectra for a 300 nm device with an Al top electrode as a function of dipole location within the device. The variation is quite dramatic and in nearly all cases the match to the experimental spectra for a given voltage was unique to one specific emission location. We can therefore assume that the predicted emission locations are correct.

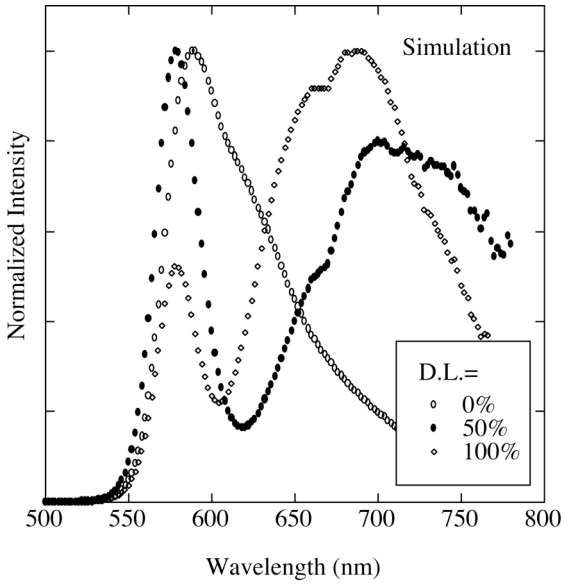

Figure 5.8 Simulated EL spectra of a 300 nm device with Al top electrodes as a function of emission location throughout the polymer layer.

In general, the comparison between the experimental voltage-dependent EL spectra and simulations of these spectra show excellent correlation when we assume a gaussian dipole emission with a characteristic width of about 1/15 of the polymer layer thickness centered an approximately equal distance from the cathode and anode in forward and reverse bias respectively. These results therefore successfully reproduce the trends in emission profile as determined experimentally for the planar devices for each device. Further, they indicate that the voltage-dependent trends in emission profiles are general with respect to polymer layer thickness and top electrode work function. The simulation of optical interference effects in vertical geometry polymer light-emitting electrochemical cells therefore show remarkably strong evidence that the various results demonstrated for planar structure LECs can be generalized to vertical structure devices.

5.7 Electrical and optical characterization of vertical geometry LECs

In order to further characterize our vertical geometry LECs with respect to top electrode and salt type, we took current-voltage and radiance curves for several devices. The devices were held at the maximum range of positive or negative voltages until fully charged and stable light output was achieved prior to scanning. A 1.5 second delay between voltage step and current-radiance measurement was introduced to compensate for the slow device response. Typical I-V curves for a

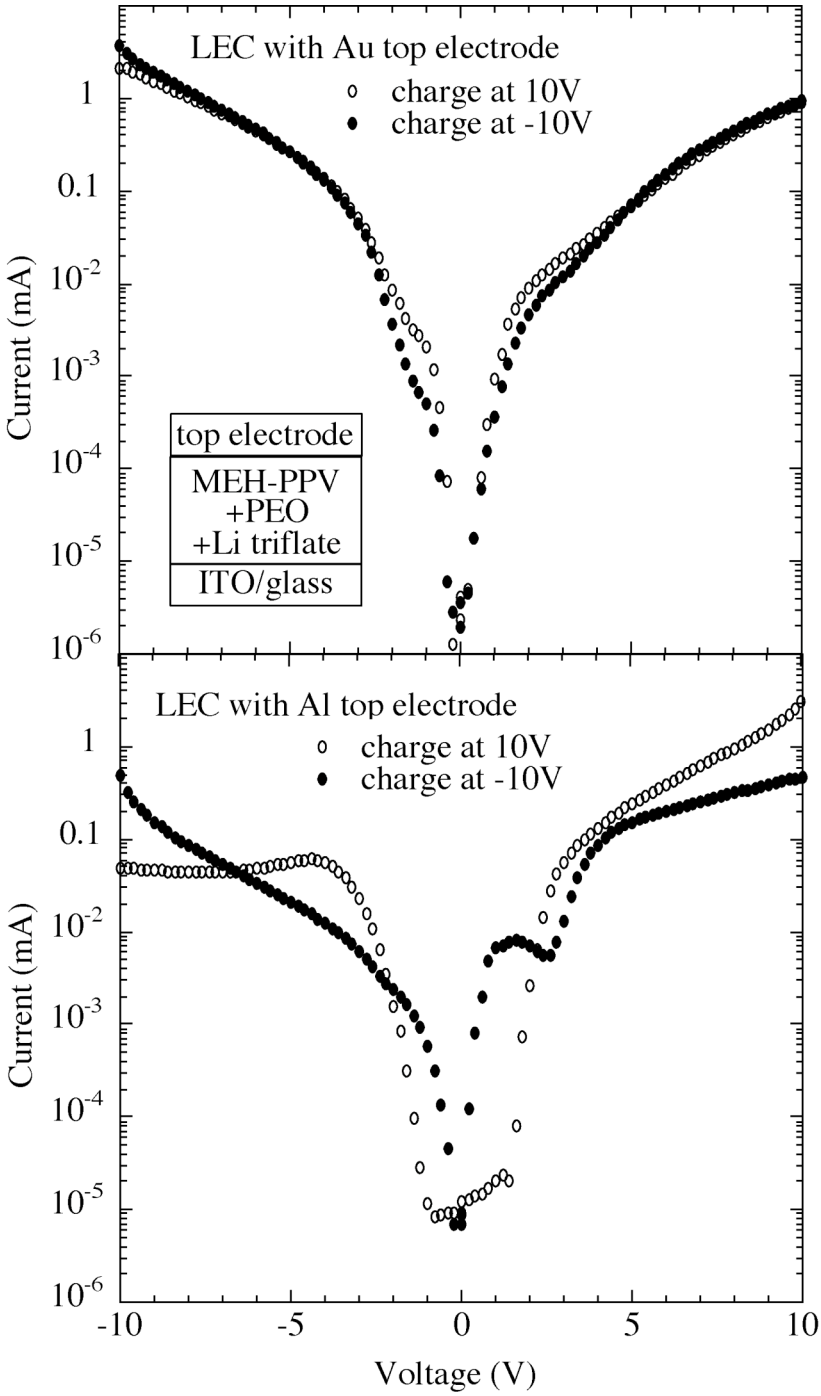

Figure 5.9 Current-voltage curves for LECs using Li triflate and both Au and Al top electrodes. Devices were first charged at high positive or negative voltages prior to voltage sweep.

vertical structure LEC with Au and Al top electrodes are shown in figure 5.9. Using an Au top electrode, the devices display remarkably symmetric diode-like I-V characteristics that are fairly independent of charging voltage. For the device with Al top electrode, however, the I-V curves show much stronger dependence on charging voltage.

In chapter 6, we show that the reversibility of oxidation in MEH-PPV depended strongly on the tendency of the electrode on which the doping took place to oxidize. Specifically, the reversibility of p-doping in MEH-PPV films on Al substrates in an oxygen reduced, but not inert, atmosphere was very low. When charging in forward bias, the oxidation takes place at the ITO interface. As the scan reaches high negative potentials, the current decreases, possibly due to some oxidation occurring of the Al electrode. When charging at negative voltages, oxidation occurs at the Al interface. Presumably the low oxygen levels present in the inert atmosphere result in only a limited oxide layer on the Al and thus in steady state reverse bias the device current is uncompromised. As the device is scanned to positive voltages a feature appears in the I-V curve that may be attributed to the reversal of the oxidation in the Al electrode that results in a temporary decrease in device current.

Figure 5.10 shows radiance-voltage curves for two LEC devices with Au and Al top electrodes. The device with Au top electrode showed lower turn-on voltages in reverse bias than the device with Al top electrode, also indicating a possible

process such as oxidation of our top electrode in reverse bias, occurring for Al but not for Au. Although the devices were placed in high vacuum overnight and tested in an inert nitrogen atmosphere, evidence suggests the presence of some minor oxide formation of the Al contacts in both the I-V and radiance data. If the differences in these devices were due simply to the difference in electrode work functions, we would expect to see more straightforward differences in the I-V and radiance characterization such as similar shapes but shifted turn-on voltages in both directions. This sensitivity of the device behavior to the presence of minor amounts of oxygen has implications for the light-emitting displays constructed with air-stable top electrodes such as Al or Ag.

Figure 5.11 shows the radiance curves for LECs with various salts. The device made using Li triflate shows much lower turn-on voltages in reverse bias than those with TBA cations after charging at high positive voltages. It is possible that the tendency of the TBA cation to reduce ITO at voltages lower than those necessary to reduce MEH-PPV or a reduced mobility of the TBA cation could be affecting the device turn-on in reverse bias.

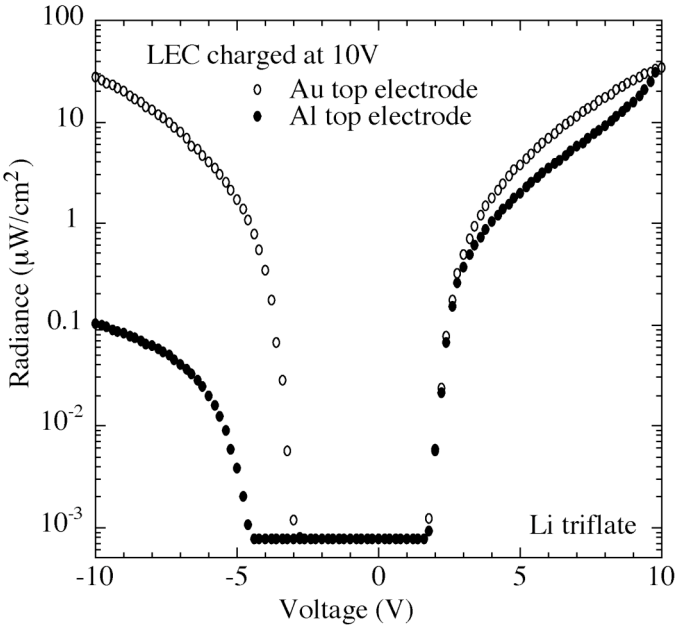

Figure 5.10 Radiance-voltage curves for devices using Li triflate and Au or Al top electrodes.

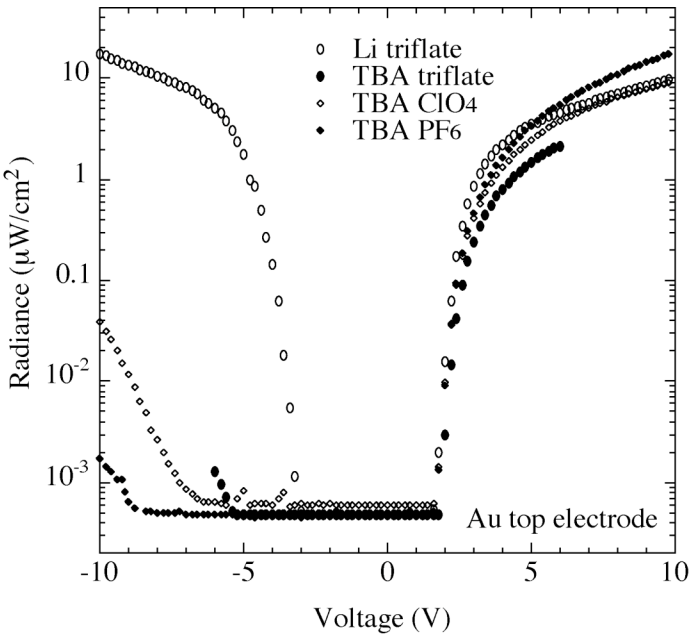

Figure 5.11 Radiance-voltage curves for devices using various salts and Au top electrodes.

5.8 Discussion and Conclusions

We have reported a study on MEH-PPV based light-emitting electrochemical cells that includes a study of the emission profiles in both planar and vertical structure LECs and systematically explores device performance in LECs with various salt types and top electrode metals. Planar geometry LECs were constructed and their photoluminescence and electroluminescence profiles were directly imaged. Our results confirm previously reported studies that p-doping occurs at voltages well below the polymer bandgap (Edman et. al. 2004), that EL occurs with a characteristic width at the edge of the region with unquenched PL and shifts toward the cathode with increased voltages, and that no clear evidence of n-doping is seen under normal operating conditions, even with TBA salts which have been shown to be effective in n-doping MEH-PPV.

We performed simulations of optical interference effects in multilayered device structures to predict emission profiles in vertical structure LECs and found that the results correlated surprisingly well with those results presented for planar devices. We showed further that these results are general with respect to polymer layer thickness, top electrode choice, and salt type.

Finally, we characterized the optical and electronic properties of LECs and found that the I-V characteristics and light emission depend strongly on the choice of top electrode and salt cation. In particular, devices with Au top electrodes and Li salts show highly symmetric diode-like I-V curves and symmetric turn-on behavior.

Devices with Al top electrodes show sensitivity to oxidation of the top contact even when tested in inert atmosphere which affects the I-V curves and causes delayed emission in reverse bias. Devices using TBA salts also show delayed and reduced emission in reverse bias.

Recent results in the study of the electrochemical doping process in MEH-PPV have highlighted the need to revisit the issue of the operating mechanism of the LEC for which electrochemical doping is thought to be central to the operation of the device. The results of studies on planar LECs under normal operating conditions in combination with studies showing that Li triflate, a commonly used salt in LEC applications, does not n-dope MEH-PPV in most cases, suggest that n-doping is not strictly necessary for the operation of the LEC. The simulation results allow us to generalize these results to vertical LECs with a variety of salts and electrodes. We strongly suspect that the inclusion of dipole effects at the polymer-cathode interface are in fact necessary to fully explain the efficient electron injection seen in these devices and successfully model the LEC operating mechanism.

CHAPTER 6

ELECTROCHEMICAL AND OPTICAL CHARACTERIZATION OF p- AND n-DOPED MEH-PPV

6.1 Abstract

We study electrochemical p- and n-type doping in the well-known light-emitting polymer MEH-PPV (poly [2-methoxy-5-(2-ethylhexyloxy)-1,4-phenylenevinylene)]). Doping reactions are characterized using cyclic voltammetry. Optical measurements including photoluminescence and UV/Vis/NIR transmission were performed on doped samples. We find that oxidation in MEH-PPV is a highly reversible reaction resulting in stable free-standing doped films, while the reduced form is unstable and the reaction irreversible. We discuss the dependence of doping reactions on scan rate, film thickness, salt type and concentration, and working electrode type. We observe the development of two additional broad absorption bands in both lightly and heavily doped films accompanied by a slight blue-shift in the primary optical transition suggesting bipolaron band formation. Finally we find that doping results in extremely sensitive photoluminescence quenching. We propose a physical model for understanding electrochemical doping in MEH-PPV and the implications this has on the development of such technologies as polymer light-emitting electrochemical cells, electrochromic devices, actuators and sensors.

6.2 Introduction

The soluble derivatives of poly(phenylene vinylene) PPV are useful for studying the mechanical and electrical characteristics of luminescent, conducting polymers. One of the most well studied soluble PPV derivatives is MEH-PPV (poly [2-methoxy-5-(2-ethylhexyloxy)-1,4-phenylenevinylene)]). Commended for its ease of use, reproducibility and versatility, MEH-PPV is widely used in the study of many applications such as organic polymer photovoltaics (Yu et. al. 1994), light emitting diodes (Friend et. al. 1990, Braun and Heeger 1992, Parker 1994), and LECs (Yang and Pei 1996, Santos et. al. 2001), as well as a water soluble version in biosensors application (Chen et. al. 1999). In the work presented in chapter 7, MEH-PPV was the material of choice for a solid-state electrochromic device because of the sharp contrast in color between doped and undoped states (Holt et. al. 2005).

Understanding the factors affecting doping reactions and the effects that doping have on the characteristics of the polymers are essential to the improvement of existing technologies in which doping is a critical component of the operating mechanism such as light emitting electrochemical cells (LECs) (Pei et. al. 1995, Pei et. al. 1996), piezoelectric devices (Fukada 2000), and electrochromic devices (Monk et. al. 1995, Mortimer 1999). That knowledge is equally valuable for application to the development of novel technologies such as in biosensors, and integrated sensors and displays.

The doping process in conducting polymers as currently understood introduces

deformations called solitons, polarons and bipolarons into the polymer system causing new levels to form in the bandgap, increasing the amount of possible energy transitions (Bredas and Street 1985, Baeriswyl et. al. 1992). Because polymers are inherently disordered, it is difficult to characterize the fundamental roles of these quasi-particles in the doping process. Many optical spectroscopic techniques are used to explore doping in conducting polymers. We can better understand the dopant deformations by utilizing these experimental techniques as well as studying theoretical models.

There have been many studies on the electrochemistry of PPV and on the optical properties of doped PPV using Raman spectroscopy (Baitoul et. al. 1997, Baitoul et. al. 2000, Obrzut and Karasz 1987), UV absorption and infrared absorption (Sakamoto et. al. 1994) as well as many studies on the electronic and electrochemical properties of PPV and is derivatives (Voss et. al. 1991, Eckhard et. al. 1989, Cervini et. al. 1997, Orion et. al. 1998). Despite the importance of MEH-PPV in devices, studies on the electrochemical and optical characteristics of doped MEH-PPV (Santos et. al. 1992) have been fairly limited in scope.

In this chapter, we present an electrochemical study of the p and n-doping processes in MEH-PPV, and its affect on the absorption and photoluminescence spectra of the polymer. Different methods were used to analyze the doping process of MEH-PPV. Cyclic voltammetry is used to characterize and study redox reactions at an electrode with regard to such properties as reversibility, stability and doping onset

values. UV/VIS/NIR transmission spectra and photoluminescence spectra were obtained in order to examine the changes in optical transitions associated with p- and n- type doping in MEH-PPV. This information is vital for example to the development of optical sensors in which photoluminescence quenching is the determining factor.

6.3 Experimental details

The polymer studied was MEH-PPV provided by American Dye Source. MEH-PPV is an orangish-red colored, luminescent polymer easily solvable in common organic solvents that exhibits a color change to greenish-brown when electrochemically doped. Figure 6.1 shows the structure, absorption and photoluminescence spectra of MEH-PPV.

Cyclic voltammetry experiments were performed using a non-aqueous silver/silver ion reference electrode (Ag/Ag^+, 0.3 V vs. SCE), a platinum counter electrode and most often, a MEH-PPV/ITO working electrode. Other working electrodes tested were MEH-PPV/gold, aluminum, and titanium nitride (TiN). Substrates consisted of ITO glass substrates, provided by Thin Film Devices, TiN substrates, and metals, gold, aluminum and silver, thermally deposited up to 50 nm on glass. A polymer solution of MEH-PPV and chlorobenzene was then spun-cast on the metal to the desired thickness. Following polymer deposition, all substrates were annealed at 120 °C for one hour under vacuum and dried in a vacuum chamber

overnight. The electrolyte consisted of salts lithium trifluoromethanesulfonate (Li triflate), tetrabutylammonium tetrafluoroborate (TBA BF_4) or TBA triflate in acetonitrile at 0.01 M and were purged with nitrogen prior to testing in order to reduce oxygen contamination. Data was obtained on an EG&G Princeton Applied Research Model 362 Scanning potentiostat and two 2010 Keithley mulitmeters. Film thicknesses measurements were taken using a Thermomicroscope Autoprobe CP atomic force microscope and typically have a variation of ~ 15 %.

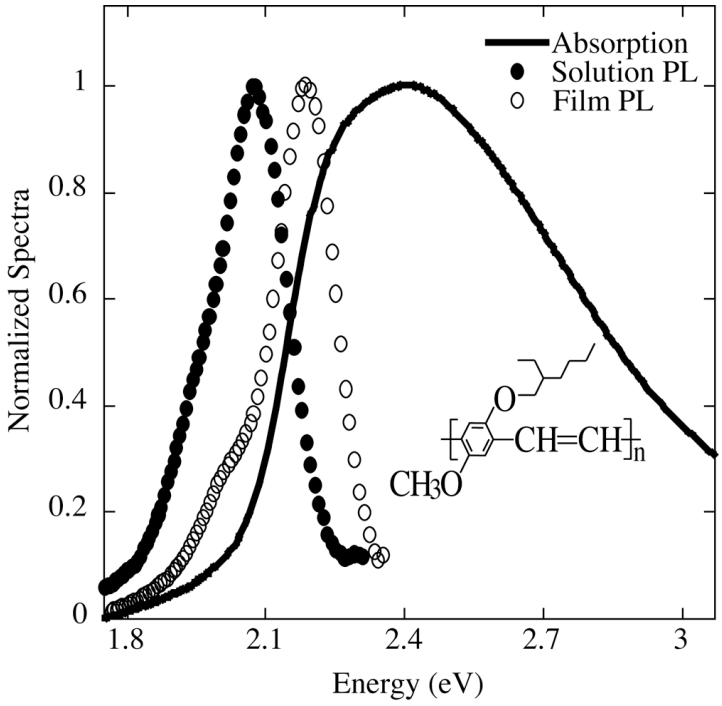

Figure 6.1 MEH-PPV chemical structure, absorbtance spectra, and photoluminescence spectra for film and solution.

Transmission spectra for p-doped films were taken on three machines each with a different wavelength range to study the material from the visible region past the near infra-red region. For wavelengths from 380 nm to 1200 nm, transmission spectra were taken with a Perkin Elmer UV/Vis/NIR Spectrometer Lambda 9 and for the *in situ* n-doped films, with a Varian Cary 3 spectrophotometer. A Perkin Elmer Spectrum One Spectrometer was used for the range from 1100 nm to 3000 nm. Although the data from each machine matched fairly well, to neatly plot the full wavelength range for the p-doped films, the data from the Spectrum One was shifted uniformly by no more than 6% of total absorption to match that from the Lambda 9 in their overlapping region. The Photoluminescence spectra were acquired only on the p-doped films using a Perkin Elmer Luminescence Spectrometer LS 45. The material was excited at 505 nm, the undoped MEH-PPV absorption maximum. Solid-state devices for photoluminescence and absorption experiments were constructed as described in chapter 7 (Holt et. al. 2005).

For optical studies of p-doped MEH-PPV, removing films from the electrolyte solution at the desired doping voltage produced films of different doping levels. The p-doped films retained their characteristics indefinitely. However, optical spectra of n-doped MEH-PPV films were more difficult to acquire as n-doped films are highly unstable. They must be kept under constant potential and cannot be removed from the electrolyte. Thus, *in situ* experiments were performed solely on one instrument in a wavelength range from 380 to 900 nm.

6.4 Cyclic voltammetry results

Cyclic Voltammetry was the primary tool used to characterize doping in MEH-PPV and was also used to produce doped films for transmission and photoluminescence studies. In the redox reactions of an MEH-PPV film, counter ions from the electrolyte diffuse into the material and allow the p and n doping of the material. MEH-PPV is capable of being both p and n-doped and exhibits a color change from orangish-red to greenish-brown (Santos et. al. 2002). With p-doping, the anodic peak occurs at about 0.8 V (vs. Ag/Ag^{+}) and the cathodic peak at about 0.4 V. For voltages higher that 1 V, increases in the current indicate the onset of an overoxidation peak that occurs around 1.3 V and results in the degregation of the polymer. We performed experiments exploring the effects that the salt type and salt concentration in the electrolyte have on the doping process as well as how the doping of the material is affected by the working electrode type, the scan rate, and the film thickness.

Anions tested in the p doping process were triflate^{-}, tetrafluoroborate (BF_4^-), hexafluorophosphate(PF_6^-), and sulfonate(SO_4^-). When examining optical contrasts in solid-state devices, we observed that organic anions were slightly more effective at p-doping than inorganic ones. In the cyclic voltammetry experiment however, no systematic differences were observed for different salts. This could be due to larger errors in the cyclic voltammetry experimental setup or due to varying mobilities of ions in the solid electrolyte of the solid-state devices.

Cations tested in the n-doping process were Li^+ and TBA^+. It has been demonstrated that alkaline cations cannot effectively electrochemically n-dope polythiophene or polyacetylene in certain solvents such as acetonitrile and propylene carbonate due to their small effective ionic radius (Zotti et. al. 1995, Mastrogostino and Soddu 1990). The cyclic voltammogram in figure 6.2 shows that there is no redox reaction in the negative voltage range, suggesting that Li^+ is unable to n-dope MEH-PPV. Only slightly reversible n-doping accompanied by color change occurs with the organic cation TBA^+. It is understood that most polymers are electrochemically unstable when n-doped due to redox reactions with water and oxygen (deLeeuw et. al. 1997). An indication of the instability of n-doped MEH-PPV was its inability to retain a change in color outside of the electrolyte.

Under a carefully monitored experimental setup, the highest occupied molecular orbital (HOMO), and the lowest unoccupied molecular orbital (LUMO) energy levels, of a conductive polymer can be approximated by the p and n-doping onset potentials (Li et. al. 1999). We performed detailed studies on whether the electrodes, ITO, Au, Ag, Al, and TiN onto which the polymer is deposited affect the onset potentials. As expected, the onset potentials for n and p-doping, determined from the intercept of a line tangent to half the largest slope value, for most of the electrodes varied no more that 0.05 eV and suggest an electrochemical band gap of about 2.4 eV, corresponding well with previous studies of single-particle energy gaps at 2.45 eV (Campbell et. al. 1996). The values of the onset potentials for electrodes Al and TiN, though are quite

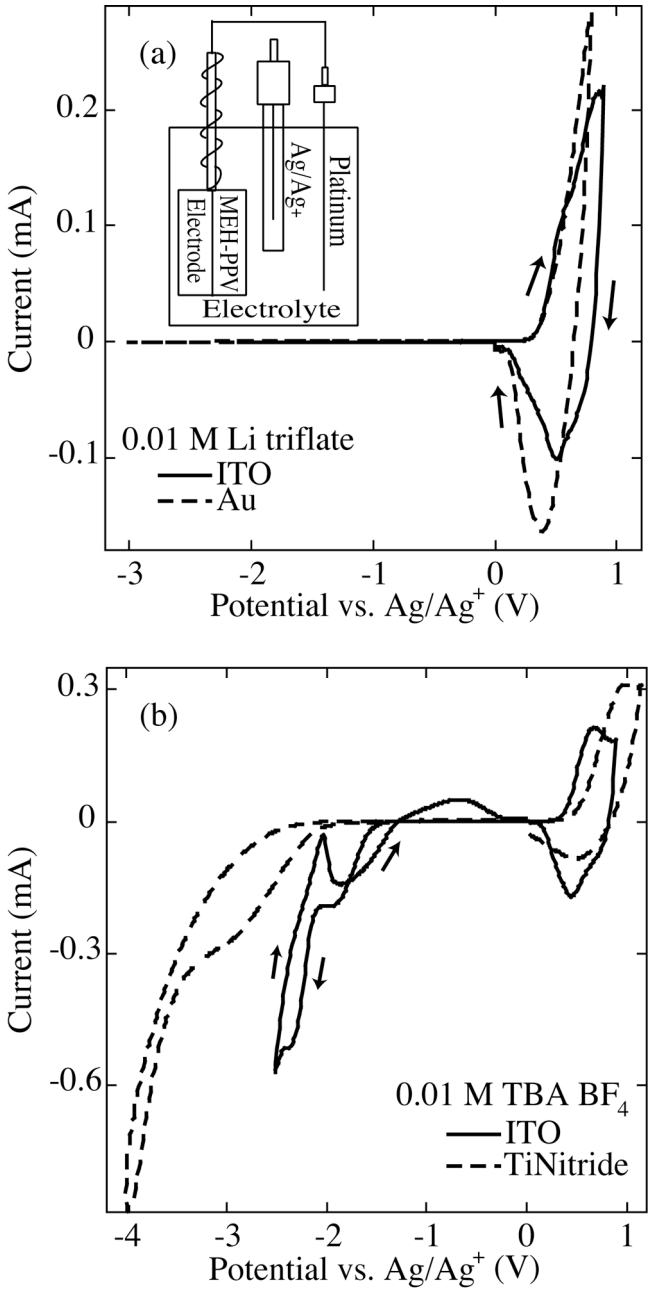

Figure 6.2 Cyclic voltammetry setup and cyclic voltammagrams for various MEH-PPV working electrodes with a) 0.01 M Li triflate and b) 0.01 M TBA BF_4 electrolyte.

different possibly due to prior oxidation of the material. Using the methods employed by Li et al. 1999 to calculate the HOMO and LUMO levels for MEH-PPV, the average level for the HOMO was about -5.1 eV and for the LUMO, -2.7 eV. These values, listed in Table 6.1 for various electrode materials, are similar to those calculated by Y. Li et al. 1999 and R. Cervini et al. 1997.

Electrode	p onset (V)[a]	n onset (V)[a]	HOMO (eV)[b]	LUMO (eV)[b]	Electrochemical bandgap (eV)[c]	reversiblity[d]
ITO	0.32	-2.10	-5.02	-2.60	2.42	n and p
Au	0.34	-2.00	-5.04	-2.70	2.34	n and p
TiN	0.49	-2.00	-5.19	-2.70	2.49	slightly in n
Ag	0.31	-2.00	-5.01	-2.70	2.31	n only
Al	0.60	-2.66	-5.30	-2.04	3.26	slightly in n

[a] $V_{error} \pm 0.05V$, [b] $eV_{error} = \pm 0.05eV$, [c] $eV_{error} = \pm 0.1eV$, [d] *as defined by visible color change*

Table 6.1 Doping onset potentials, calculated HOMO/LUMO levels, electrochemical bandgap, and qualitative reversibility for MEH-PPV on various electrodes.

In a general, for a Nerstian system, a reversible redox reaction meets the criteria that the peak potentials are independent of the sweep rate with a difference of 54 mV between them and that the ratio of the current values at the peak potentials is unity. The redox reaction of MEH-PPV is a quasi-reversible one. This is illustrated in Figure 6.3 which shows that for higher scan rates, the anodic peak occurs at a higher

potential and the current increases. The increase in current for faster scan rates is a result of charge conservation while the increase in anodic peak potential indicates that the rate of reaction is comparable to the scan rate.

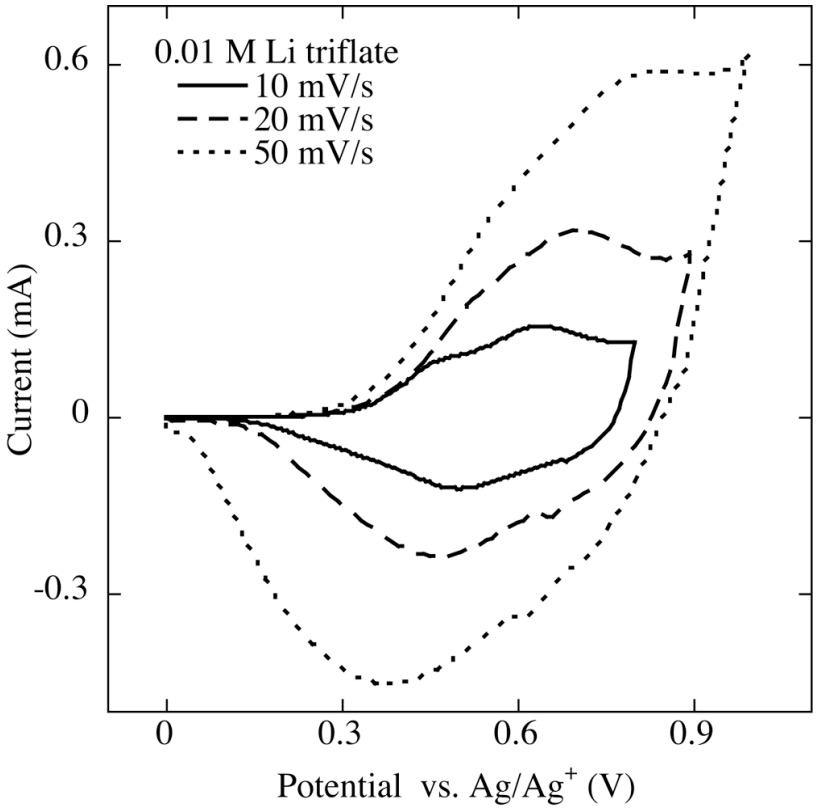

Figure 6.3 Cyclic Voltammogram for MEH-PPV at varied scan rates in 0.01 M Li triflate electrolyte.

The reversibility of MEH-PPV depends on which type of metal is used for the electrode. As depicted in figure 6.2, for p-doping using TiN, the cathodic peak has a much lower current value than the anodic peak in contrast to ITO and Au which both have more comparable peak heights. When n-doping, reversibility is higher for the

ITO electrode than TiN which has no anodic peak. We assign the second peak at -2.5 V for ITO as the cathodic peak for n-doping of MEH-PPV and assign the first peak to reduction of ITO.

The difference in reversibility for the various electrodes may be due to the oxidation of Al and Ag resulting in non-uniform color change of the film. No anodic peaks were observed with p-doping for Ag and Al, only overoxidation onset and they exhibited a color change reaction with small increasing fully doped regions that afterwards, failed to return to their original color. It is possible that an oxide layer formed on the metal prevents the uniform doping of the polymer material. The n-doping reactions however, were slightly more reversible but showed similar features.

Although the doping onset potentials should not be affected by the experimental setup, the position of the doping current peaks are affected by salt concentration in the electrolyte and film thicknesses. Increasing salt concentration in the electrolyte increases the reaction rate and occurs until the effects of ion pairing in the concentrated electrolyte slow the reaction rate down (Holt et. al. 2005). This affects the anodic and cathodic peak potentials and is the opposite effect to that of increasing the film thickness. Due to reduced ion mobility, a thicker film exhibits a slower reaction rate. Figure 6.4 exhibits the effects that film thickness and salt concentration have on the anodic and cathodic peak positions. It should be noted that the onset potentials, however, remain constant.

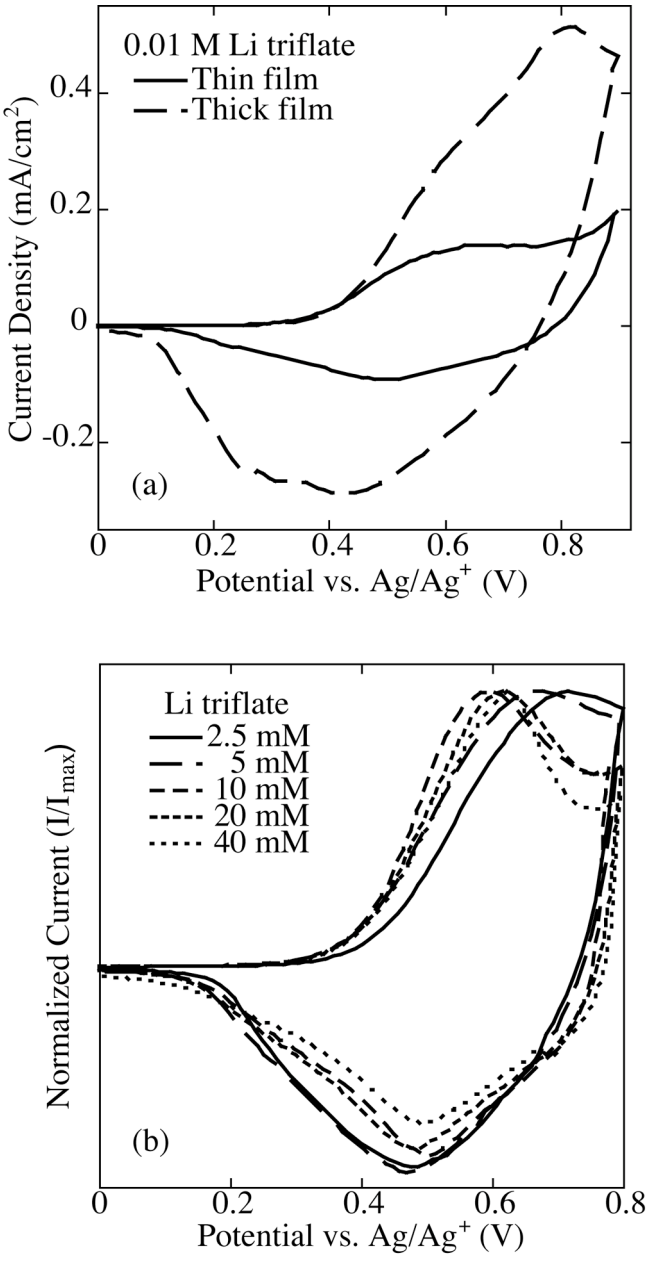

Figure 6.4 Cyclic Voltammograms for MEH-PPV for a) different film thicknesses and b) varied salt concentration.

6.5 Absorption spectra at progressive doping levels

Upon oxidation, an electron is removed from the pi-system of the polymer backbone leaving a positive spinless charge and a free radical. This spin ½ combination, called a polaron, creates two energy levels inside the band gap, one singly occupied, symmetrically placed around the center of the gap, as described in Chapter 1. That single electron can also be removed creating a spinless bipolaron with localized energy states farther from the band edges than the polaron states because of the stronger lattice relaxation. Figure 6.5 displays the energy levels of these quasi-particles as well as the possible energetic transitions. Within the continuum electron-phonon-coupled model utilized by Fesser, Biship, and Campbell (FBC model), w_1 and w_2 are the dominant transitions for the polaron and ω_1' for the bipolaron (Fesser et. al. 1983).

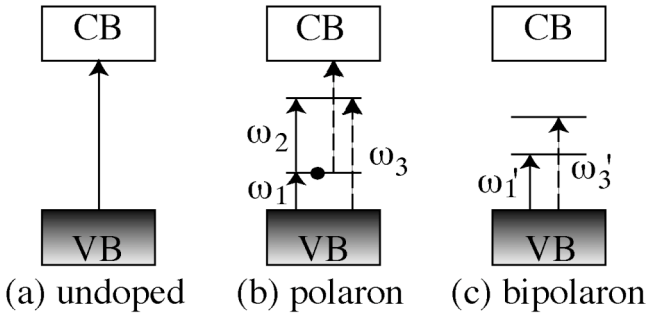

Figure 6.5 Illustration of the energy transitions for a) an undoped polymer, b) a positive polaron and c) and positive bipolaron.

Theories and past experiments suggest that polarons are present in systems at low doping levels while bipolarons are more favorable at higher doping levels (Patil et. al. 1997). As shown in figure 6.6, we examine the absorption spectra of MEH-PPV and observe two mid-gap transitions at high doping voltages, at about 1.74 and 0.67 eV, consistent with the theory of bipolaron formation. Figure 6.7 depicts these transitions with w_1' = 0.67 eV and w_3'= 1.74 eV which sum up to approximately equal the band gap which peaks at about 2.45 eV. We observe a shift in spectral weight from the band gap transition to the ω_1' and ω_3' bipolaron transitions as expected. We also observe a blue shift of about 0.11 eV in the interband absorption peak that accompanies the extremely broad low energy transition indicating the formation of bipolaron bands within the gap that occurs with heavy doping (Bredas and Street 1985).

Within the FBC model, the absorption coefficient and confinement parameter are both functions of the ratio ω_0/Δ_0 where $\omega_0 = (\omega_3' - \omega_1')/2$ for bipolarons and $\Delta_0 = E_g/2$. For MEH-PPV, the ratio $w_0/D_0 = 0.44$ and is consistent with previous measurements (Voss et. al. 1991). However, the ratio of the intensities of the two peaks $I(w_1')/I(w_3') = I(0.67\text{ eV})/I(1.74\text{ eV}) = 1$ does not agree with $I(w_1)'/I(w_3') \approx 12$ as predicted by the FBC model. This "intensity anomaly" has been frequently discussed. Proposed explanations include theoretical drawbacks within the FBC model or misallocated observed transitions.

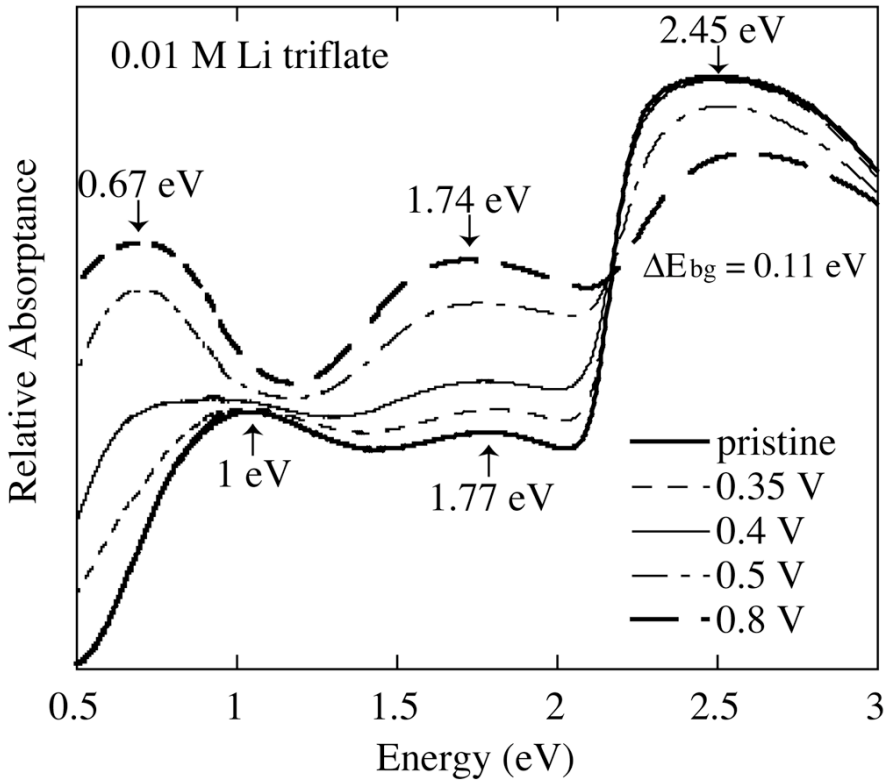

Figure 6.6 Absorptance spectra for an MEH-PPV film at progressive doping levels.

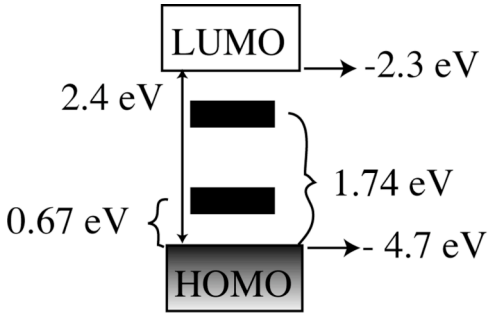

Figure 6.7 Illustration of bipolaron energy levels in MEH-PPV.

Also inconsistent with the polaron/bipolaron picture is the observation of only two transitions in addition to the primary transition at low doping levels. As the doping level increases, the lower energy transition at 1 eV disappears while the higher energy one at 1.77 eV appears to either red shift 0.03 eV or be replaced by a different optical transition at 1.74 eV. Since both transitions appear in the pristine spectra as well as at lower doping levels, there may be other reasons for their appearance. The 1 eV transition is likely caused by a doping reaction between ITO and the MEH-PPV film as it is not present when spectra are obtained on quartz while the higher energy transition tends to be more prominent in thinner films and is likely due to aggregation in the polymer film.

The issue of what is the most favorable defect (polaron vs. bipolaron) with doping in conjugated polymers and their absorption signature is currently in debate. The literature forming the main body of this debate is reviewed in Chapter 1, section 3. Our data suggests primarily bipolaron and bipolaron band formation because of the values of the energy levels. It is a possibility that we are observing the coexistence of polarons and bipolarons at heavy doping because of the inability to distinguish several specific transitions within the broad low energy transition peak. In that case, vibrational spectroscopy would be needed to distinguish the two.

We also performed limited range *in situ* absorption experiments in order to obtain spectra for n-doped MEH-PPV films. Using MEH-PPV/ITO as the working

electrode, we observe reversible n-doping reactions. Figure 6.8 shows the spectral progression and a color change is evident. There is a decrease in the intensity of the interband transition peak accompanied by an increase in intensity of absorption at lower energies for doping voltage values up to –2.4 V. Larger negative voltages applied across the material resulted in n-doped films of greater instability and the data acquired provided no new information. We see an additional peak forming with a higher spectral weight at 2.9 eV likely caused by changes in the absorption spectra of n-doped ITO. There also appears to be a peak forming between 1 and 1.5 eV. However, this is not certain due to the limited energy range.

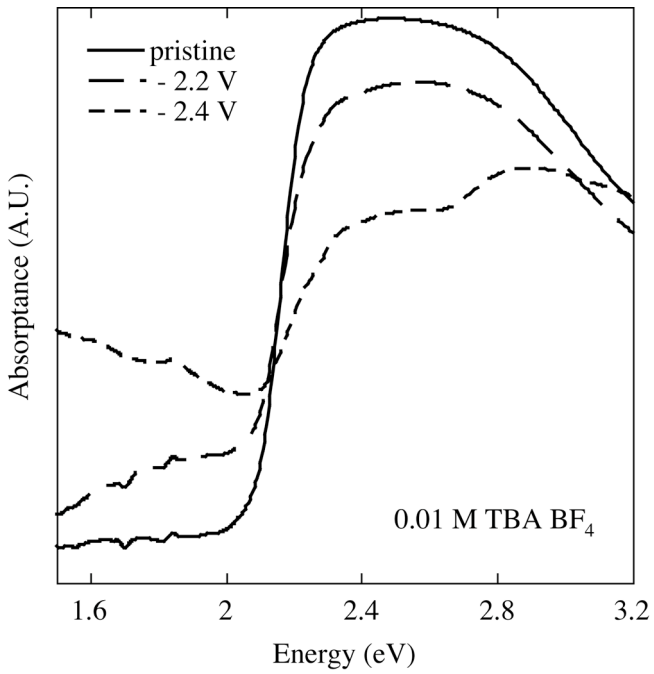

Figure 6.8 *In situ* obtained absorbtance spectra of n-doped MEH-PPV film.

6.6 Photoluminescence quenching

As MEH-PPV is doped, color change is preceded by a quenching affect in the photoluminescence of the material. Figures 6.9 and 6.10 show that the photoluminescence is sensitively quenched with doping level. For oxidative doping, full quenching occurs at 0.35 V while visually, color change typically occurs at about 0.5 V. For reductive doping, PL quenching measurements were taken *in situ* due to the unstable nature of the reduced films. For this data, full PL quenching is seen by around -2.2V vs Ag/Ag+. Similar degrees of photoluminescence quenching with doping occur in the solid state devices as well and the photoluminescence is fully recovered upon dedoping. Photoluminescence quenching is expected for doped MEH-PPV because as the material becomes more metallic, there are more states available to which an exiton can non-radiatively decay. Photoluminescence quenching due to electrochemical doping has been observed in polythiophene films (Hayashi et. al. 1987) and similar effects due to photo-oxidation have been observed in PPV films (Yan et. al. 1994) and MEH-PPV solution (Xiong et. al. 2004). The sensitivity of the photoluminescence spectra to doping level is likely explained by the observation that the effective size of the defect is much larger than its actual size for trapping exitons and one defect is able to quench an entire polymer chain (VandenBout et. al. 1997).

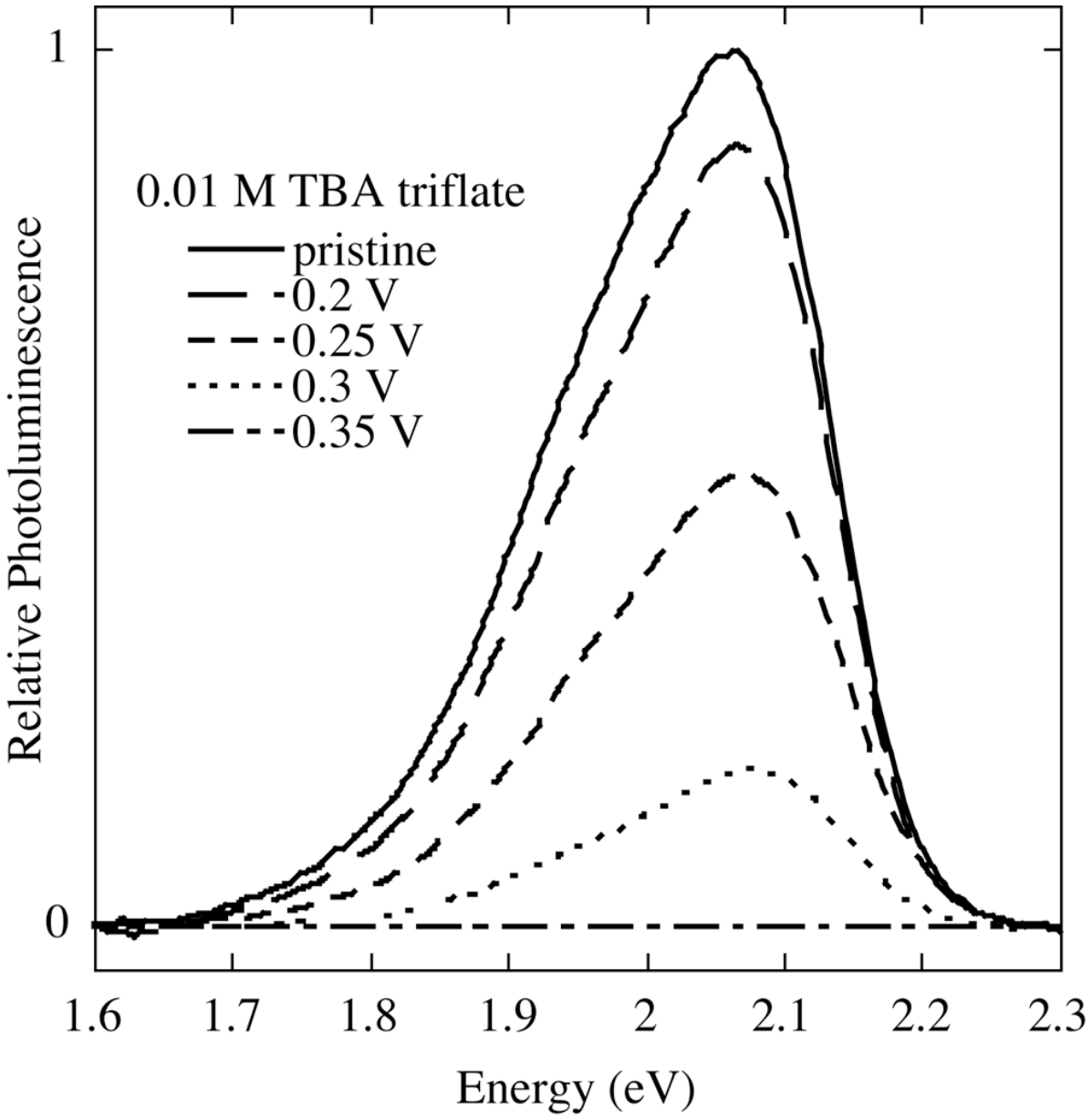

Figure 9 Photoluminescence spectra for MEH-PPV film at progressive oxidative doping levels.

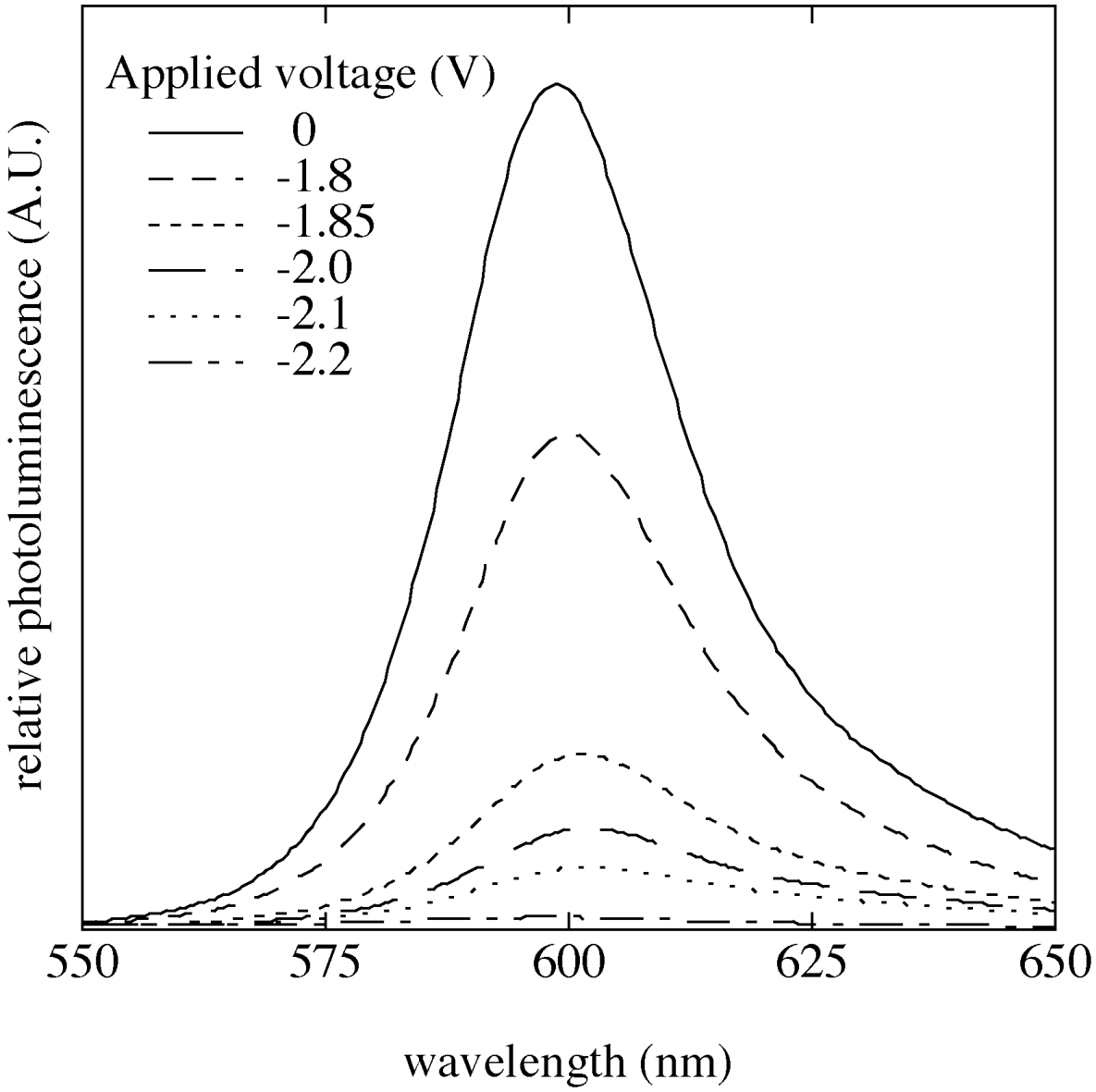

Figure 6.10 Photoluminescence spectra for MEH-PPV film at progressive reductive doping levels.

An interesting effect occurs when attempting to n-dope the solid-state devices. When using Li triflate, the photoluminescence of the material increases by up to 50% with increasingly negative voltages down to -3 V. Hence it is possible that prior to testing, there are already defect sites in the polymer film from reactions with ITO, as studied by Werner et al. 1998, and compensated by charged ions. The application of a voltage across the pristine device aids in the removal of these impurities from the material thereby increasing its ability to photoluminescence. At higher doping voltages, no resulting n-doping occurred as expected for Li triflate. On the other hand, when using TBA triflate, initially the photoluminescence increases as with Li triflate but thereafter proceeds to decrease slowly indicating the occurrence of moderate n-doping in the polymer layer.

6.7 Conclusions

The electrochemical properties and doping processes of MEH-PPV, a useful light-emitting soluble derivative of PPV, were extensively studied and the results of the cyclic voltammetry experiments, absorption studies, and photoluminescence studies were presented. Cyclic voltammetry curves of MEH-PPV illustrate the dependence of the doping process on salt type, salt concentration, film thickness and electrode type. Although the type of salt used has little effect on the process, the quasi-reversible doping reaction of MEH-PPV is susceptible to changes in salt concentration and film thickness which affect the speed of the reaction.

Theoretically, electrode type should not effect the doping onset potentials as they reflect the HOMO and LUMO levels of the polymer and was observed for the most part in agreement with other experimental studies. However, oxygen sensitivity does affect the onset potentials for electrodes Al and TiN.

Throughout the doping process, transmission and photoluminescence spectra were taken. The absorption spectra indicate the formation of bipolarons with heavy doping. Other transitions observed at low doping levels were attributed to aggregation and reactions with substrate ITO. *In situ* transmission and photoluminescence data was obtained for n-doped MEH-PPV films which has not before been published or studied. Photoluminescence in MEH-PPV was much more sensitive to doping level than the absorption and was observed to be almost entirely quenched prior to visible color change in agreement with observations that one defect is able to create a quenching site the size of an entire chain.

CHAPTER 7

SOLID-STATE ELECTROCHROMIC DEVICES BASED ON PPV POLYMERS

7.1 Abstract

We present a solid-state electrochromic device structure employing a PPV-based light-emitting polymer and explore device performance as a function of salt type, salt concentration, and polymer layer thickness. Devices display high reversibility, dramatic optical contrasts, and low operating voltages comparable to state of the art conducting polymer electrochromic devices. Salts employing organic anions display slightly improved optical contrasts. Thicker devices, higher voltages, and higher salt concentrations produce higher optical contrasts at the cost of slowed switching speeds. Understanding the factors affecting doping in PPV-based polymers is crucial for the development of applications such as polymer LECs, actuators, and sensors.

7.2 Introduction

Soluble light-emitting polymers based on poly (phenylene vinylene) (PPV) have been extensively studied for their use in applications such as light-emitting diodes (Burroughs et. al. 1990, Friend et. al. 1999) and photovoltaic cells (Tang 1986, Brabec et. al. 2001); however, understanding doping effects in these materials have

largely been limited to light emitting electrochemical cells (Pei et. al. 1995. Pei et. al. 1996). This is surprising since doping can be used for controlling a wide variety of other interesting properties, including electrochromic (Monk et. al. 1995, Mortimer 1999) and piezoelectric effects (Fukada 2000). In particular, the ability to control electrochromism in electroluminescent polymers opens up wide range of potential technologies for novel integrated sensors and displays.

We discuss the construction of a solid-state electrochromic device employing a PPV-based light-emitting polymer as the color-changing material. We show that the color changes observed for PPV-based materials have properties comparable to the best and most widely studied polymer electrochromic materials, such as polypyrrole and polythiophene (Lu et. al. 2002, DePaoli et. al. 1990, Garnier et. al. 1983). By studying changes in the electrochromic properties as a function of doping concentration and type and device thickness, we propose a model for understanding and optimizing the effect of doping on the absorption in PPV-based materials.

7.3 Construction and characterization of MEH-PPV ECDs

Solid-state electrochromic devices were constructed using the sandwich structure ITO/PPV polymer/gel-electrolyte/ITO. The polymer layer contained a blend of PPV-based polymer and poly(ethylene oxide) in chlorobenzene. For the PPV polymer, several materials were studied; for clarity, we focus our results on the most reproducible material, MEH-PPV (poly [2-methoxy-5-(2 -ethylhexyloxy)-1,4-

phenylenevinylene), although large bandgap materials resulted in more striking color changes. Other PPV materials tested showed similar color changes. The gel electrolyte consisted of salt, poly(methyl methacrylate), propylene carbonate, ethylene carbonate, and acetonitrile at 1:2.4:4:4.9 respectively. A variety of salt concentrations and types were tested, including Li Triflate, Tetrabutylammonium (TBA) Triflate, TBA PF_6, TBA BF_4, and TBA p-Toluene Sulfonate. The devices were constructed by spin-casting the polymer solution to a thickness of 200 nm onto a glass/ITO substrate, annealing at 120° C for one hour, and drying in a vacuum chamber overnight. The gel electrolyte was then spin-cast onto a second ITO glass substrate, exposing to dry nitrogen for twenty minutes, and finally sandwiching with the other polymer/ITO substrate to form the layered device. All device fabrication was performed in an inert atmosphere glove box to minimize exposure to water and oxygen.

The transmission spectra of the solid-state devices were taken with a Varian Cary 3 spectrophotometer in their pristine (non-doped) forms and then again after each device had been held at the given voltage for 2 minutes with a 2400 Keithley sourcemeter. The solution-based electrochemical experiments were performed using a non-aqueous silver/silver ion reference electrode, a platinum counter electrode and a MEH-PPV/ITO working electrode. Data was obtained on an EG&G Princeton Applied Research Model 362 Scanning potentiostat and two 2010 Keithley multimeters as the potential was scanned at 20 mV/s. Film thickness measurements

(±15 nm) were taken using a Thermomicroscopes Autoprobe CP atomic force microscope. MEH-PPV was provided by American Dye Source and the ITO substrates were provided by Thin Film Devices.

In a polymer electrochromic device (ECD) operating in forward bias, the anions (namely Triflate, PF_6, BF_4 and p-Toluene Sulfonate) diffuse into the polymer layer resulting in oxidation, or p-doping, of the polymer layer at the contact. For MEH-PPV, this results in a visible color change from orange-red to greenish-brown (Santos et. al. 2002) beginning at approximately 1.5 V. The device may be operated in reverse bias resulting in reduction, or n-doping, of the polymer layer by the salt cation.

The pristine and oxidized absorption spectra, device structure and material structure for the MEH-PPV/gel electrolyte ECD are shown in figure 7.1. The color change is due to doping within the band-gap of the polymer, as has been observed previously (Thompson et. al. 2000). Optimal devices exhibited switching speeds of about 5 seconds, had large optical contrasts in the visible region (30-50%) and were reversible during several days of testing. The performance of the devices thereafter depended heavily on their exposure to air. The devices with Li Triflate and TBA Triflate showed the highest optical contrast and were more reversible than those with TBA PF_6, TBA BF_4, or TBA p-Toluene Sulfonate at comparable concentrations. However, because Li Triflate is highly hydroscopic, these devices were more susceptible to water contamination thereby shortening their lifetimes.

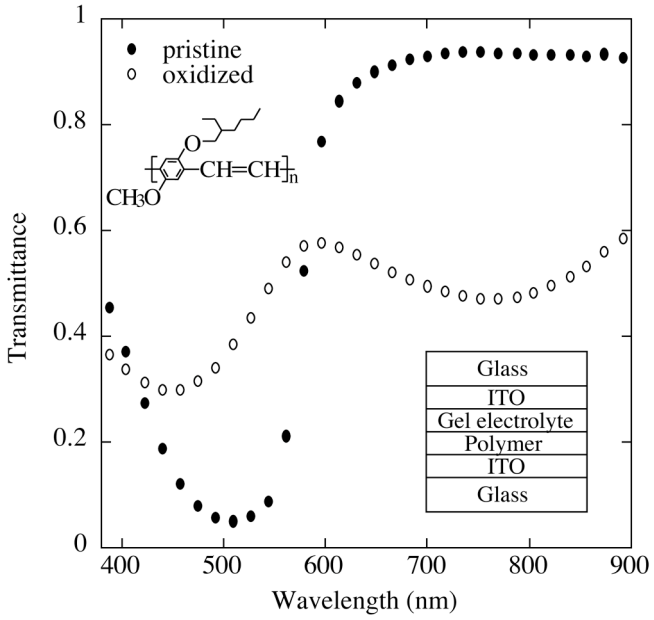

Figure 7.1 ECD structure, MEH-PPV chemical structure, and the absorbance spectra for an undoped device (0 Volts) in comparison with that of a fully doped device (2 Volts). The salt is Li triflate at a concentration of 1.8%.

7.4 Physical models for factors affecting device performance

Experiments were performed in order to understand the dependence of the electrochromic material on polymer layer thickness, salt type, and salt concentration. Figure 7.2a demonstrates the dependence of the optical contrast (Δ%transmission) of our devices on the thickness of the polymer film. At low applied voltages, thicker devices exhibit a slight decrease in optical contrast; however, at higher voltages, the optical contrast increases with increasing film thickness. We interpret the thickness dependence as being due to the amount of the film that is doped for a given operating voltage. For low voltage, the film is only partially doped. Therefore in thicker films

the lower field strength for the same operating voltage results in lower volume of doped material, and thus lower optical contrast. For higher voltage, however, the films are fully doped and thus the thicker films display higher optical contrast.

Figure 7.2b demonstrates the dependence of the optical contrast on the type of salt in the gel electrolyte. The data show that the optical contrast is approximately the same for Li Triflate and TBA Triflate and also for TBA PF_6 and TBA BF_4. The optical contrast of the two triflates, however, is slightly higher than that of TBA PF_6 and TBA BF_4. As expected the oxidation of the polymer film does not depend on the cation of the salt. Differences in doping with salts with different anions though may be expected. The organic anions may be more effective at doping the polymer film than the inorganic salts, possibly due to greater solubility of the organic salt in the polymer matrix.

The dependence on salt concentration in electrolyte was examined with both solid-state devices and cyclic voltammetry. Figure 7.2c shows the dependence of the optical contrast of the solid-state devices on the salt concentration in the gel electrolyte for sufficient voltage application periods to achieve complete doping. At lower voltages, up to 1.4 V, the devices with lower salt concentrations have higher optical contrasts, but at applied voltages of 1.8 V and higher, the devices with a larger salt concentration have higher optical contrasts. Experiments performed with higher salt concentrations showed similar results with higher average optical contrasts but slower switching speeds. For a 5 second voltage application period, we observed a

maximum in optical contrast of nearly 50% for Li Triflate at a concentration of 8% and 2.4 V.

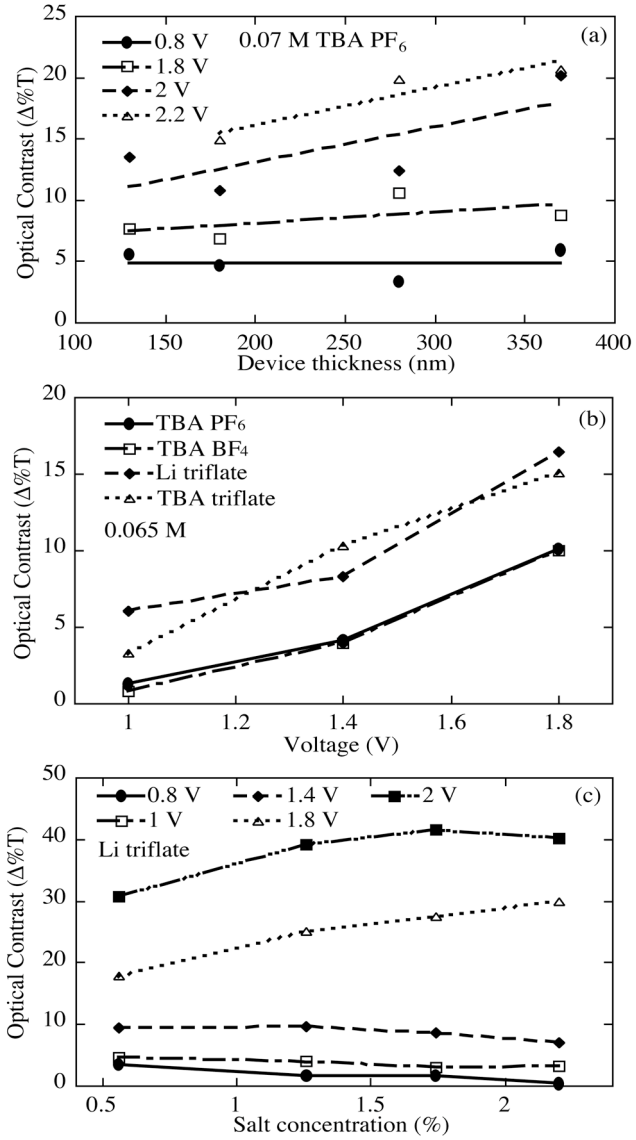

Figure 7.2 The dependence of the optical contrast of a solid state device at 700 nm on a) device thickness with a concentration of 0.07 M of TBA PF_6, b) salt type each at 0.65 M, and c) salt concentration measured in weight percentage of Li triflate.

Figure 7.3 displays cyclic voltammograms for MEH-PPV films for a variety of electrolyte concentrations. As the concentration of salt is increased from 2.5 mM to 10 mM, the anodic peak moves to lower voltages. As the salt concentration is further increased from 10 mM to 40 mM, the anodic peaks shifts back to higher voltages. These results can be interpreted as being due to the dependence of the conductivity of the electrolyte on salt concentration. Previous results have observed a maximum in the conductivity of salt electrolytes occurring with salt concentration (Kim et. al. 2001, Kucharski et. al. 2004). Increasing the number of ions past this optimal concentration lowers the conductivity because of a rise in the viscosity of the solution due to ion pairing and other electro-dynamical effects. In the CV results, increasing the salt concentration up to 10 mM increases the rate of doping reaction indicating that more ions are present in the material. Past a 10 mM concentration, the reaction is slowed due to a decrease in ion mobility and aggregation of ions in the electrolyte affects the doping of the material.

Similarly, in the solid state devices, lower voltages are less able to break apart or move the aggregates naturally present in the electrolyte that increase with increasing concentration. Thus, we observe a decrease in the optical contrast. For higher salt concentrations and higher voltages, the optical contrast depends largely on the doping time intervals. Therefore, when the voltage application period is small, we observe a peak in the optical contrast indicating an optimal salt concentration.

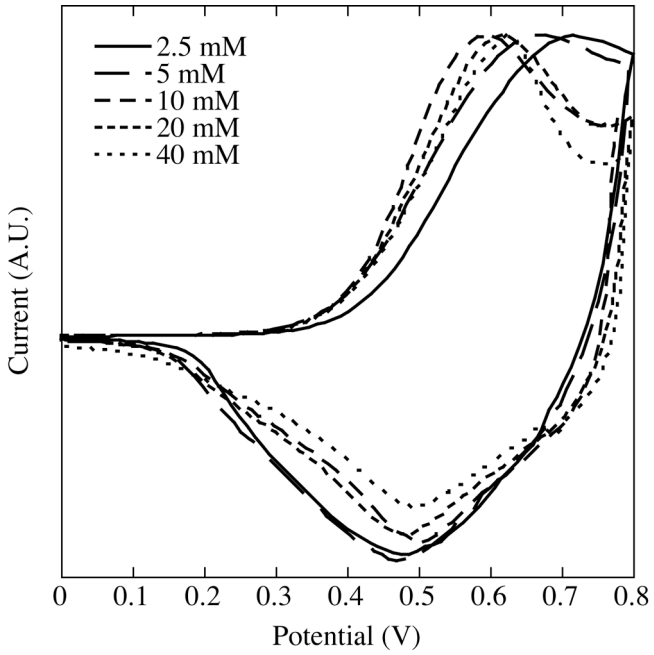

Figure 7.3 Cyclic voltammograms normalized at the anodic peak taken at 20 mV/s for varying salt concentrations from 2.5 mM to 40 mM.

7.5 Conclusions

In conclusion, an ECD was constructed from light-emitting polymer MEH-PPV that exhibited visible change in color and reversible characteristics. The degree of the voltage-dependent color change is dependent on polymer layer thickness, anion type, and salt concentration. Visible color change begins at about 1.5V, but a voltage of about 1.8V is necessary to fully dope the polymer film. Preliminary results suggest that organic anions result in higher optical contrasts and that the limiting factor in the dependence of optical contrast on salt concentration is related to the time interval in which the doping reaction is allowed to take place. These results have implications for controlling doping in PPV-based polymer LECs, actuators, and sensors.

CHAPTER 8

REVERSIBLE THERMOCHROMIC EFFECTS IN MEH-PPV

8.1 Abstract

We study the thermochromic response of MEH-PPV thin films. MEH-PPV undergoes a reversible, continuous color change from red to yellow in the practically relevant temperature range of 25 °C – 100 °C. We show that the absorption of MEH-PPV continuously decreases and blue-shifts as the temperature is increased. The shift in HOMO/LUMO levels responsible for the widening of the bandgap was investigated using temperature dependent cyclic voltammetry. We find that both the HOMO and LUMO levels increase with heating. Understanding the changes in the energetic structure of this widely used, versatile material at elevated temperatures is important in controlling the operation of such devices as polymer photovoltaics.

8.2 Introduction

Thermochromic materials, or materials that change their color depending on temperature, have been known for some time (Granqvist 1990). The applications for such materials include smart windows, temperature sensors, color filters, and displays. The typical organic thermochromic materials achieve color change with increased temperature through a change in crystal structure (Crano and Guglielmetti 1999). The discovery that conjugated polymers, which are naturally disordered in the

solid state, can also undergo temperature-dependent color changes occurred in 1988 using substituted polythiophenes (Yoshino et. al. 1989). Polymers of this type form the bulk of the literature on thermochromic effects in conjugated polymers. A few polyphenylenevinylene (PPV) derivatives that display thermochromic properties have been reported (Gelinck et. al. 1996, Chen et. al. 1998, Onoda et. al. 2003). However, these materials suffer from low contrast at practical temperature ranges, low reversibility, or phase changes that accompany the color change, rendering them impractical for many applications.

We report a study on the thermochromic effects in the widely used light-emitting polymer MEH-PPV. Thin gel films of MEH-PPV were formed that exhibited a striking color change from red to yellow when heated from room temperature to 100C. The color change was rapid, reversible, and was not accompanied by any phase or volume changes. We measured the temperature-dependent absorption spectra of these films and showed that a temperature increase results in a continuous blue-shift and decrease in spectral weight of the polymer absorption spectra. We performed temperature-dependent cyclic voltammetry experiments in order to understand how the HOMO and LUMO levels were shifting to produce an overall blue-shift in the polymer bandgap. Our results are consistent with conformational changes in the polymer backbone induced by heating.

8.3 Experimental details

The primary thermochromic species studied was MEH-PPV, provided by American Dye Source. MEH-PPV is an orange-red colored, luminescent polymer easily solvable in common organic solvents. Thermochromic MEH-PPV gel films were prepared from a solution of 0.8% MEH-PPV in a mixture of chlorobenzene and dibutyl sebacate at a typical ratio of 5:1. Similar thermochromic effects were observed with pure MEH-PPV films but the effects appeared to be slower and slightly less reversible. The solution is spin-cast on quartz substrates and dried under vacuum (10^{-6} Torr) overnight prior to testing. For typical purposes, temperature is controlled by placing the film on a hot-plate.

Transmission spectra for thermochromic films were taken on an n&k Varian Cary 3 spectrophotometer. Samples were heated *in situ* by securing a nichrome wire against the outer edge of the film with a conductive tape and passing current through the wire. Heating of the film occurred through conduction and therefore suffered a minor level of non-uniformity. Temperatures were tested immediately prior to the scan at the film center. The high-temperature limit of such a setup appeared to be the breakdown of the tape adhesive occurring at around 80 °C.

Cyclic voltammetry experiments were performed using a non-aqueous silver/silver ion reference electrode (Ag/Ag^+, 0.3 V vs. SCE), a platinum counter electrode and a spin-cast MEH-PPV/ITO working electrode. Solutions were 1% MEH-PPV in chlorobenzene. Following polymer deposition, all substrates were

annealed at 120 C for 30 minutes under vacuum, and dried in a vacuum chamber (~10^{-6} torr) overnight. The electrolyte consisted of 0.01 M tetrabutylammonium tetrafluoroborate (TBA BF_4) in acetonitrile and was purged with nitrogen prior to testing in order to reduce air contamination. Data was obtained on an EG&G Princeton Applied Research Model 362 Scanning potentiostat and two 2010 Keithley mulitmeters. The entire cell was placed on a hot plate and the temperature monitored by thermometer. Electrolyte was allowed to reach equilibrium temperature prior to scanning.

8.4 Results and discussion

Figure 8.1 shows photographs of the MEH-PPV films at 25 °C, 62 °C, 80 °C, and 100 °C. In this temperature range, the film undergoes a transition from a slightly orange-red to yellow. After placing the film on the hot-plate, the color change occurred in less than one second. After removing the film from the heat source its original color returned immediately upon cooling of the film. This color change appeared to be completely reversible and no volume change or melting of the polymer film was observed.

To understand more qualitatively the observed color change, temperature-dependent absorption spectra were obtained. The film absorption for 25 °C, 54 °C, 62 °C, and 80 °C are shown in figure 8.2. Clearly as temperature is increased the film undergoes a continuous blue-shift and decrease in overall absorption. These results

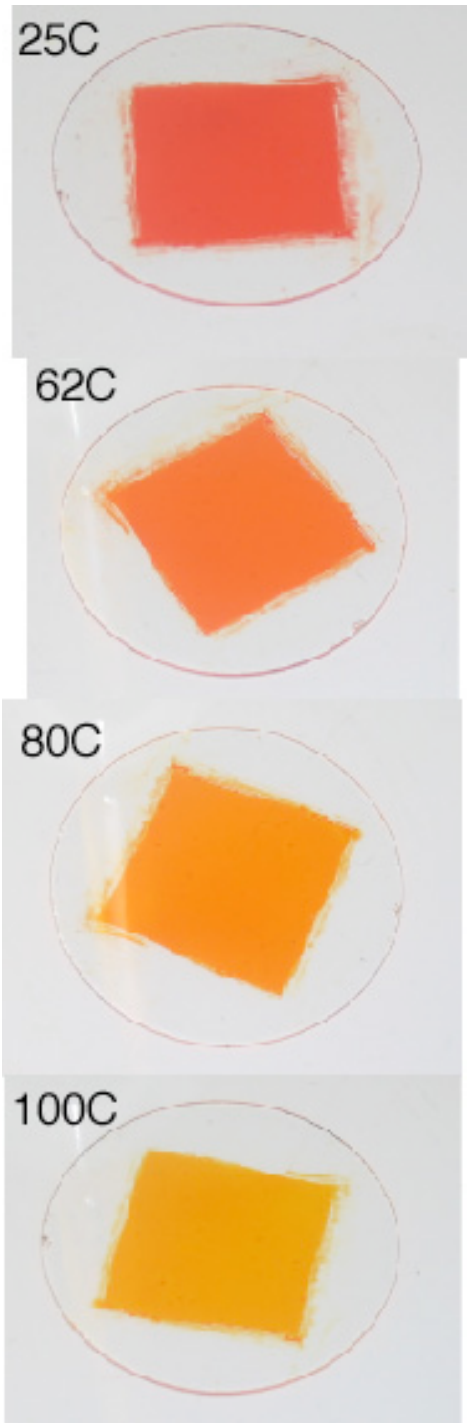

Figure 8.1 MEH-PPV gel films at increasing temperatures.

are consistent with the well understood proposed mechanism for thermochromic effects in conjugated polymers first proposed in 1989 (Yoshino 1989). In this model, the polymer sidechains become bulkier with heating. Stearic hinderance between in-plane sidechains forces twisting to occur in the polymer backbone. It is this conformational change in the polymer backbone that shortens the conjugation length and thus blue-shifts the material absorption (Yoshino et. al. 1989, Garreau et. al. 2003).

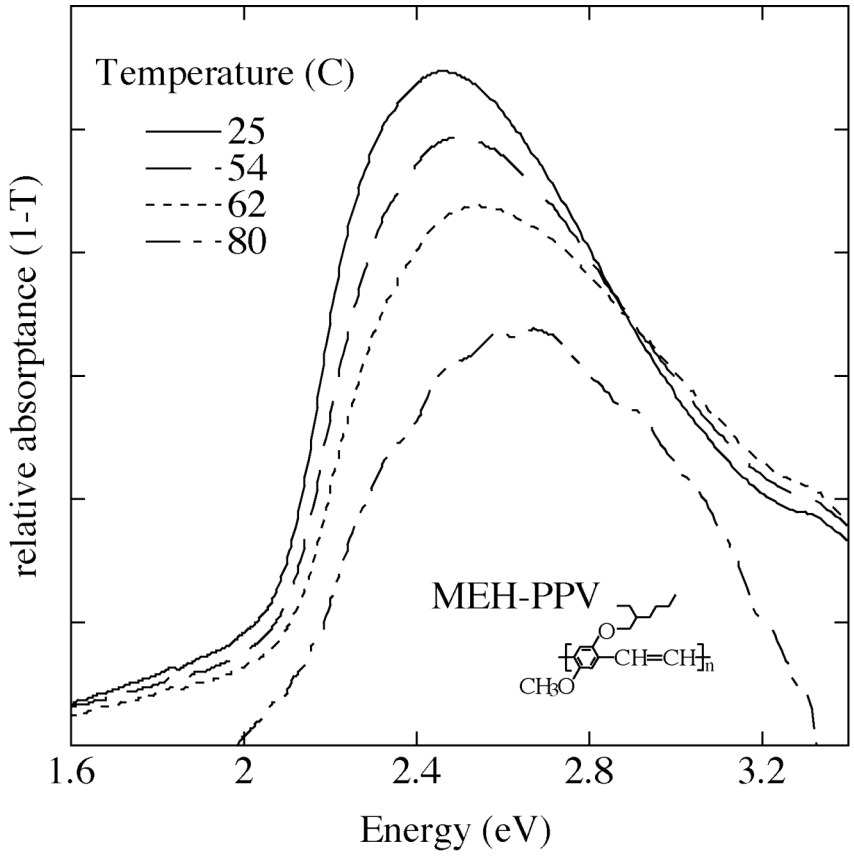

Figure 8.2 Temperature-dependent absorption spectra for MEH-PPV.

Along with an increase in the polymer effective bandgap, we expect to see shifting of HOMO/LUMO energy levels. We therefore performed temperature dependent cyclic voltammetry experiments in the range 25 °C to 40 °C as described above. HOMO and LUMO levels were extracted from the p and n onset potentials as described in chapter 6 (Holt et. al. submitted). Figure 8.3 shows the effect of increased temperature on the HOMO/LUMO levels of MEH-PPV. Both the HOMO and LUMO levels are increased as the sample is heated, but the LUMO shifts more dramatically resulting in an overall increase in the bandgap, consistent with the results obtained for similar PPVs (Onoda et. al. 2003).

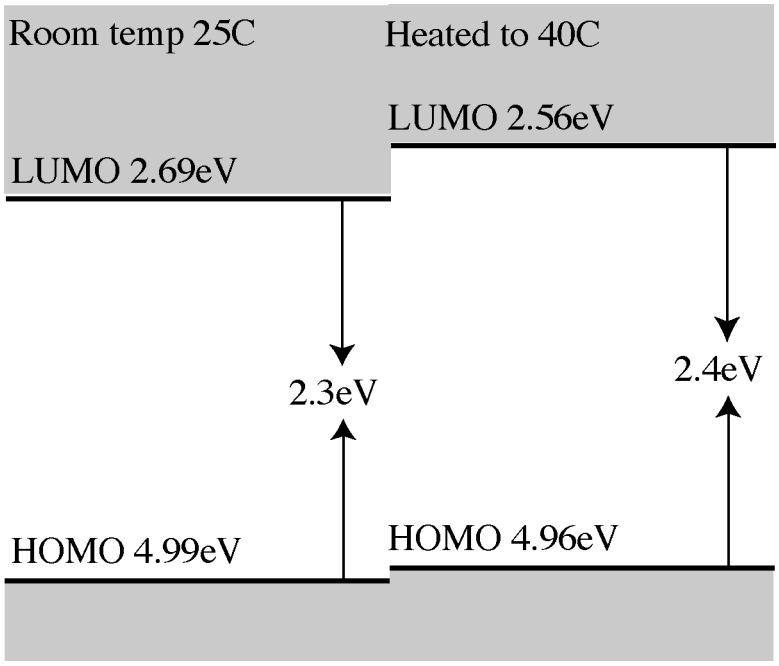

Figure 8.3 Temperature dependence of HOMO/LUMO energy levels in MEH-PPV.

8.5 Conclusions

We have studied the thermochromic effects in films of the light-emitting polymer MEH-PPV. Films exhibited a striking color change from red to yellow when heated from room temperature to 100 °C. We showed that these films show promising thermochromic characteristics such as a rapid and reversible color change in a practical temperature range, and that the color change was not accompanied by any phase or volume changes. We showed that heating results in a continuous blue-shift and overall decrease in the polymer absorption spectra. We showed that both the HOMO and LUMO levels are shifting up with increased temperature at different rates to affect an overall increase in bandgap energy.

MEH-PPV is widely used in such applications as LEDs (Friend et. al. 1990, Braun and Heeger 1992) and photovoltaics (Yu et. al. 1994), and has been shown to be promising also in ECDs (Holt et. al. 2005) as well as some sensing applications (Chen et. al. 1999). The demonstration of promising thermochromic properties in such a versatile, robust material introduces the possibility of realizing novel multifunctional device structures, particularly sensors. Further, an understanding of how the energetic structure of such materials change with increasing temperature is crucial for the development of applications such as polymer solar cells, which can be sensitive to changes in HOMO/LUMO levels and which may require operation at varying elevated temperatures.

BIBLIOGRAPHY

J.J. Apperloo, J. van Haare and R. Janssen, "Transparent highly-oxidized conjugated polymer films from solution", Synt. Met. **101**, 417 (1999).

M. Ariu, D. G. Lidzey and D. D. C. Bradley, "Influence of film morphology on the vibrational spectra of dioctyl substituted polyfluorene (PFO)", Synthetic Metals **607**, 111 (2000).

V. I. Arkhipov, P. Heremans, E. V. Emelianova, G. J. Adriaenssens, and H. Bässler, "Charge carrier mobility in doped semiconducting polymers", App. Phys. Lett. **82**, 3245 (2003).

Ashcroft and Mermin, "Solid state physics", Saunders College Publishing, (1976).

P.W. Atkins, "Physical chemistry" 4th ed., Oxford University Press (1990).

D. Baeriswyl, D. Campbell and S. Mazumdar, "Conjugated Conducting Polymers", edited by H. Kiess (Springer-Verlag, Berlin, 1992), pp. 36-46; H.G. Kiess and G. Harbeke, ibid., pp. 191-195.

M. Baitoul, J.P. Buisson, S. Lefrant, B. Dulier, J. Wery, and M. Lapkowski, "Spectroelectrochemical and structural studies of p-doped poly(p-phenylene vinylene)", Synt. Met. **84**, 623 (1997).

M. Baitoul, J. Wery, J.P. Buisson, G. Arbuckle, H. Shah, S. Lefrant, and M Hamdoume, "In situ resonant raman and optical investigations of p-doped poly (p-phenylene vinylene)", Polymer **44**, 6955 (2000).

Bard and Faulkner, "Electrochemical Methods: Fundamentals and Applications", Wiley (1980).

F. G. K. Baucke, "Electrochromic mirrors with variable reflectance", Sol. Energy Mat. **16** (1987) 67.

G. Björk, S. Machida, Y. Yamamoto, and K. Igeta, "Modification of spontaneous emission rate in planar dielectric microcavity structures", Phys. Rev. A **44**, 669 (1991).

P. W. M. Blom, M. J. M. de Jong, C. T. H. F. Liedenbaum, and J. J. M. Vleggaar, "Device characteristics of polymer light-emitting diodes", Synth. Met. **85**, 1287 (1997).

P. W. M. Blom and M. J. M. de Jong, "Device operation of polymer light-emitting diodes", Philips J. Res. **51**, 479 (1998).

L. Bozano, S. A. Carter, J. C. Scott, G. G. Malliaras, and P. J. Brock, "Temperature- and field-dependent electron and hole mobilities in polymer light-emitting diodes", Appl. Phys. Lett. **74**, 1132 (1999).

C.J. Brabec, N.S. Sariciftci, and J.C. Hummelen, "Plastic solar cells", Adv. Funct. Mater. **11**, 15 (2001).

D. D. C. Bradley, G. P. Evans, and R. H. Friend, "Characterisation of poly(phenylenevinylene) by infrared and optical absorption", Synth. Met. **17**, 651 (1987).

D. Braun and A. J. Heeger, "Visible light emission from semiconducting polymer diodes", Appl. Phys. Lett. **58**, 1982 (1991).

D. Braun and A.J. Heeger, "Electroluminescence from light-emitting diodes fabricated from conducting polymers", Thin Solid Films **216**, 96 (1992).

J.L. Bredas, J.C. Scott, K. Yakushi, and G.B. Street, "Polarons and bipolarons in polypyrrole: Evolution of the band structure and optical spectrum upon doping", Phys. Rev. B **30**, 1023 (1984).

J.L. Bredas and G.B. Street, "Polarons, bipolarons, and solitons in conducting polymers", Acc. Chem. Res. **18**, 309 (1985).

V. Bulovic, V. B. Khalfin, G. Gu, and P. E. Burrows, "Weak microcavity effects in organic light-emitting devices", Phys. Rev. B **58**, 3730 (1998).

S. E. Burns, N. C. Greenham, and R. H. Friend, "Modelling of optical interference effects in conjugated polymer films and devices", Synth. Met. **76**, 205 (1996).

J.H. Burroughes, C.A. Jones, and R.H. Friend, "New semiconductor device physics in polymer diodes and transistors", Nature **335**, 137 (1988).

J. H. Burroughes, D. D. C. Bradley, A. R. Brown, R. N. Marks, K. Mackay, R. H. Friend, P. L. Burns, and A. B. Holmes, Light-emitting diodes based on conjugated polymers", Nature **347**, 539 (1990).

A. J. Campbell, H. Antoniadis, T. Virgili, D. G. Lidzey, X. Wang, and D. D. C. Bradley, "Balancing electron and hole currents in single layer poly(9,9-dioctylfluorene) light emitting diodes", Proceedings of SPIE Vol. 4464 (2002).

H. Campbell, T. W. Hagler, D. L. Smith, and J. P. Ferraris, "Direct Measurement of conjugated polymer electronic excitation energies using metal/polymer/metal structures", Phys. Rev. Lett. **76**, 1900 (1996).

Y. Cao, G. Yu, A. J. Heeger, and C. Y. Yang, "Efficient, fast response light-emitting electrochemical cells: Electroluminescent and solid electrolyte polymers with interpenetrating network morphology", Appl. Phys. Lett. **68**, 3218 (1996).

S. A. Carter, M. Angelopoulos, S. Karg, P. J. Brock, and J. C. Scott, "Polymeric anodes for improved polymer light-emitting diode performance", Appl. Phys. Lett. **70**, 2067 (1997).

R. Cervini, X.C. Li, G.W.C. Spencer, A.B. Holmes, S.C. Moratti and R.H. Friend, "Electrochemical and optical studies of PPV derivatives and poly(aromatic oxadiazoles)", Synt. Met. 84, 359 (1997).

V. Cimrova and D. Neher, "Microcavity effects in single-layer light-emitting devices based on poly(p-phenylene vinylene)", J. Appl. Phys. **79**, 3299 (1996).

L. Chen, D.W. McBranch, H. Wang, R. Helgeson, F. Wudl and D. Whitten, "Highly sensitive biological and chemical sensors based on reversible fluorescence quenching in a conjugated polymer", PNAS **96**, 12287 (1999).

S.A. Chen and E.C. Chang, "Structure and properties of cyano-substituted Poly(2,5-dialkoxy-p-phenylene vinylenes)", Macromolecules **31**, 4899 (1998).

J.C. Crano and R.J. Gugliemetti, "Organic photochromic and thermochromic compounds", New York: Plenum Press V.2 1999.

O. H. Crawford, "Radiation from oscillating dipoles embedded in a layered system", J. Chem. Phys. **89**, 6017 (1988).

P. S. Davids, I. H. Campbell, and D. L. Smith, "Device model for single carrier organic diodes", J. Appl. Phys. **82**, 6319 (1997).

D.M. deLeeuw, M.M.J. Simenon, A.R. Brown, and R.E.F. Einerhand, "Stability of n-type doped conducting polymers and consequences for polymeric miroelectronic devices", Synt, Met. **87**, 53 (1997).

J. C. deMello, N. Tessler, S. C. Graham, and R. H. Friend, "Ionic space-charge effects in polymer light-emitting diodes", Phys. Rev. B **57**, 12951 (1998).

J.C. deMello, J.J.M. Halls, S.C. Graham, N. Tessler, and R.H. Friend, "Electric field distribution in polymer light-emitting electrochemical cells", Phys. Rev. Lett. **85**, 421 (2000).

M.A. DePaoli, S.Panero, P.Prosperi, and B. Scrosati, "Study of the electrochromism of polypyrrole/dodecylsulfate in aqueous solutions", Electrochimica Acta **35**, 1145 (1990).

D.J. Dick, A.J. Heeger, Y. Yang, and Q. Pei, "Imaging the structure of the p-n junction in polymer light-emitting electrochemical cells", Adv. Mat. **8**, 985 (1996).

H. Eckhardt, L. W. Shacklette, K. Y. Jen, and R. L. Elsenbaumer, "The electronic and electrochemical properties of poly(phenylene vinylenes) and poly(thienelyne vinylenes): An experimental and theoretical study", J. Chem. Phys. **91**, 1303 (1989).

L. Edman, M.A. Summers, S.K. Burratto, and A.J. Heeger, "Polymer light-emitting electrochemical cells: Doping, luminescence, and mobility", Phys. Rev. B **70** (2004).

A. J. Epstein, "Electrically conducting polymers: Science and Technology", MRS Bulletin, 16 (1997).

K. Fesser, A.R. Bishop, and D.K. Campbell, "Optical Absorption from polarons in a model of polyacetylene", Phys. Rev. B **27**, 4804 (1983).

S.R Forrest, "The path to ubiquitous and low-cost organic electronic appliances on plastic", Nature **428**, 911 (2004).

R. H. Fowler and L. Nordheim, "Electron emission in intense electric fields", Proc. Roy. Soc., London, A119, 173 (1928).

R. H. Friend, R. W. Gymer, A. B. Holmes, J. H. Burroughes, R. N. Marks, C. Taliani, D. D. C. Bradley, D. A. Dos Santos, J. L. Bredas, M. Logdlund and W. R. Salaneck, "Electroluminescence in conjugated polymers", Nature **397**, 121 (1999).

E. Fukada, “History and recent progress on piezoelectric polymers”, IEEE Transactions on Ultrasonics, Ferroelectrics, and Frequency Control **47**, 1277 (2000).

Y. Furukawa, “Electronic Absorption and Vibrational Spectroscopies of Conjugated Conducting Polymers”, J. Phys. Chem. **100**, 15644 (1996).

J. Gao and J. Dane, “Planar light-emitting electrochemical cells with extremely large interelectrode spacing”, Appl. Phys. Lett. **83**, 3027 (2003).

J. Gao and J. Dane, “Visualization of electrochemical doping and light-emitting junction formation in conjugated polymer films”, Appl. Phys. Lett. **84**, 2778 (2004).

F. Garnier, G. Tourillon, M. Gazard, and J. C. Dubois, “Organic conducting polymers derived from substituted thiophenes as electrochromic material”, J. Electroanal. Chem. **148** (1983) 299.

S. Garreau, M. Leclerc, N. Errien, and G. Louarn, “Planar-to-nonplanar conformational transition in thermochromic polythiophenes: A spectroscopic study”, Macromolecules **36**, 692 (2003).

G.H. Gelinck, J.M. Warman, and E.G.J. Staring, “Polaron pair formation, migration, and decay on photoexcited poly(phenylenevinylene) chains”, J. Phys. Chem. **100**, 5485 (1996).

C.G. Granqvist, “Chromogenic materials for transmittance control of large-area windows”, Critical Reviews in Solid State and Materials Sciences **16**, 291 (1990).

S. Hayashi, K. Kaneto and K. Yoshino, “Quenching of photoluminescence in poly(thiophene) films by electrochemical doping”, Solid State Commun. **61**, 249 (1987).

W. Helfrich and W.G. Schneider, “Transients of volume-controlled current and of recombination radiation in anthracene”. J. Chem. Phys. **44**, 2902 (1966).

A.L. Holt, J.M. Leger, and S.A. Carter, “Solid-State electrochromic devices based on PPV polymers”, APL **86**, (2005).

A.L. Holt, J.M. Leger, and S.A. Carter, “Electrochemical and optical characterization of p- and n-doped MEH-PPV”, (submitted).

H. -H. Hörhold, H. Tillmann, C. Bader, R. Stockmann, J. Nowotny, E. Klemm, W. Holzer, and A. Penzkofer, "MEH-PPV and dialkoxy phenylene vinylene copolymers. Synthesis and lasing characterization", Synth. Met. **119**, 199 (2001).

A.L. Holt, J.M. Leger and S.A. Carter, "Solid-state electrochromic devices based on poly(phenylenevinylene polymers", Appl. Phys. Lett. **68**, (2005).

D.M. Ivory, G.G. Miller, J.M. Sowa, L.W. Shacklette, R.R. Chance, and R.H. Baughman, "Highly conducting charge-transfer complexes of poly(p-phenylene)", J. Chem. Phys. **71**, 1506 (1979).

R. Jakubiak, C. J. Collison, W. C. Wan, L. J. Rothberg, and B. R. Hsieh, "Reduction of photoluminescence quantum yield by interchain interactions in conjugated polymer films", J. Chem. Phys. A **103**, 2394 (1999).

S. Janietz, D. D. C. Bradley, M. Grell, C. Giebeler, M. Inbasekran, and E. P. Woo, "Electrochemical determination of the ionization potential and electron affinity of poly(9,9-dioctylfluorene)", Appl. Phys. Lett. **73**, 2453 (1998).

S.A. Jenekhe and J.A. Osaheni, "Excimers aned exciplexes of conjugated polymers", Science **265**, 765 (1994).

J. Kagan, "Organic photochemistry: Principles and applications", Academic Press (1993).

J. -S. Kim, P. K. H. Ho, N. C. Greenham, and R. H. Friend, "Electroluminescence emission pattern of organic light-emitting diodes: Implications for device efficiency calculations", J. Appl. Phys. **88**, 1073 (2000).

S. H. Kim, J. K. Choi, and Y. C. Bae, "Mechanical properties and ionic conductivity of gel polymer electrolyte based on poly(vinylidene-fluoride-co-hexafluoropropylene)", J. App. Polymer Science **81**, 948 (2001).

T. Kobayashi, H. Yoneyama, and H. Tamura, "Polyanaline film-coated electrodes as electrochromic display devices", J. Electroanal. Chem. **161** (1984) 419.

M. Kucharski, T. Lukazewicz, and P. Morozek, Opto-Electron. Rev., **12**, 175 (2004).

P. Langevin, Annals of Chemical Physics **28**, 229 (1903).

T. Lee, H. Lee, and O. Park, "High-efficiency polymer light-emitting devices using organic salts: A multilayer structure to improve light-emitting electrochemical cells", App. Phys. Lett. **81**, 214 (2002).

S. Lefrant, E. Perrin, J. P. Buisson, H. Eckhardt, and C. C. Han, “Vibrational studies of polyparaphenylene-vinylene (PPV)”, Synth. Met. **29**, E91 (1989).

J. Lekner, "Theory of Reflection", Dodrecht, Nijhoff, 1987.

J.M. Leger, B. Ruhstaller, H.G. Nothofer, U. Scherf, H. Tillman, H.H. Horhold, and S.A. Carter, “Thickness-dependent changes in the optical properties of PPV- and PF-based polymer light emitting diodes”, Phys. Rev. B **68**, (2003).

J.M. Leger, B. Ruhstaller, and S.A. Carter, “Recomination profiles in MEH-PPV light-emitting electrochemical cells”, submitted (2005).

S. Li, F. Xiong, H. Zhang, X. Lu, L Yi, and G. Yang, “Fluorescence Quenching of Poly[2-methoxy-5-(2'-ethylhexoxy)-p-phenylene vinylene] (MEH-PPV) in Solutions”, Chinese J. Chem. **22**, 80 (2004).

Y. Li, Y. Cao, J. Gao, D. Wang, G. Yu, and A. J. Heeger, “Electrochemical properties of luminescent polymers and polymer light-emitting electrochemical cells”, Synth. Met. **99**, 243 (1999).

W. Lu, A.G. Fadeev, B. Qi, E. Smela, B.R. Mattes, J. Ding, G.M. Spinks, J. Mazurkiewicz, D. Zhou, G.G. Wallace, D.R. MacFarlane, S.A. Forsyth, and M. Forsyth, “Use of ionic liquids for π-conjugated polymer electrochemical devices”, Science **297**, 983 (2002).

W. Lukosz, “Light emission by multiple sources in thin layers”, J. Opt. Soc. Am. **71**, 744 (1981).

A.G. MacDiarmid and W. Zheng, “Electrochemistry of conjugated polymers and electrochemical applications”, MRS Bulletin June 1997.

G. G. Malliaras and J. C. Scott, “The roles of injection and mobility in organic light emitting diodes”, J. Appl. Phys. **83**, 5399 (1998).

M. Mastrogostino and L. Soddu, “Electrochemical characterization of ‘n’ doped polyheterocyclic conducting polymers – I. Polybithiophene”, Electrochim. Acta **35**, 463 (1990).

T. Miteva, A. Meisel, W. Knoll, H. G. Nothofer, U. Scherf, D. C. Müller, K. Meerholz, A. Yasuda, and D. Neher, “Improving the performance of polyfluorene-based organic light-emitting diodes via end-capping”, Adv. Mat. **13**, 565 (2001).

P.M.S. Monk, R.J. Mortimer, D.R. Rosseinsky, "Electrochromism: Fundamentals and Applications", (VCH Inc, Weinheim, 1995).

D. Monroe, "Hopping in exponential band tails", Phys. Rev. Lett. **54**, 146 (1985).

R. J. Mortimer, "Organic electrochromic materials", Electrochimica Acta **44**, 2971 (1999).

Y. K. Nakazawa, S. A. Carter, H. -G. Nothofer, U. Scherf, V. Y. Lee, R. D. Miller, and J. C. Scott, "Effects of polymer side-branching in double and single-layer polyfluorene light-emitting diodes", Appl. Phys. Lett. **80**, 3832 (2002).

K. A. Neyts, "Simulation of light emission from thin-film microcavities", J. Opt. Soc. Am. A **15**, 962 (1998).

T.-Q. Nguyen, V. Doan, and B. J. Schwartz, "Conjugated polymer aggregates in solution: Control of interchain interactions", J. Chem. Phys. **110**, 4068 (1999).

P.J. Nigrey, A.G. MacDiarmid, and A.J. Heeger, "Electrochemistry of polyacetylene, $(CH)_x$: Electrochemical doping of $(CH)_x$ films to the metallic state", JCS Chem. Comm. 594 (1979).

H. G. Nothofer, Ph.D. Thesis, University of Potsdam, Potsdam, Germany.

J. Obrzut and F.E. Karasz, "Defects in the electronic structure of poly (*p*-phenylene vinylene): Electronic spectra, electrochemical behavior, and molecular orbital calculations", J. Chem. Phys. **87**, 6178 (1987).

M. Onoda and K. Tada, "A consideration of thermochromic behavior in poly(p-phenylene vinylene derivatives", Thin Solid Films **438**, 187 (2003).

I. Orion, J. P. Buisson, and S. Lefrant, "Spectroscopic studies of polaronic and bipolaronic species in n-doped poly(paraphenylenevinylene)", Phys. Rev. B **57**, 7050 (1998).

D. Parker, "Carrier tunneling and device characteristics in polymer light-emitting diodes", J. Appl. Phys. **75**, 1656 (1994).

A.O. Patil, A.J. Heeger, and F. Wudl, "Optical properties of conducting polymers", Chem. Rev. **88**, 183 (1988).

Q. Pei, Y. Yang, G. Yu, C. Zhang, and A. J. Heeger, "Polymer light-emitting electrochemical cells: In situ formation of a light-emitting p-n junction", J. Am. Chem. Soc. **118**, 3922 (1996).

Q. Pei, G. Yu, C. Zhang, Y. Yang, and A. J. Heeger, "Polymer light-emitting electrochemical cells", Science **269**, 1086 (1995).

L. A. A. Pettersson, F. Carlsson, O. Inganas and H. Arwin, "Spectroscopic ellipsometry studies of the optical properties of doped poly(3,4-ethelynedioxythiophene): an anisotropic metal", Thin Solid Films **313**, 356 (1998).

J. R. Platt, "Electrochromism, a possible change of color producible in dyes by an electric field", J. Chem. Phys. **34** (1961) 862.

I. Riess and D. Cahen, "Analysis of light emitting polymer electrochemical cells", J. Appl. Phys. **82**, 3147 (1997).

M. Reufer, M.J. Walter, P.G. Lagoudakis, A.B. Hummel, J.S. Kolb, H.G. Roskos, U. Scherf, and J.M. Lupton, "Spin-conserving carrier recombination in conjugated polymers", Nature Materials **4**, 340 (2005).

K.K. Rohatgi-Mukherjee, "Fundamentals of Photochemistry", Wiley Eastern Limited (1978).

S. Roth, "One-dimensional metals: Conjugated polymers, organic crystals, carbon nanotubes", Wiley-VCH (1995).

N.S. Sariciftci, "Primary photoexcitations in conjugated polymers: Molecular excitation versus semiconductor band model", World Scientific (1997).

A. Sakamoto, Y. Furukawa, and M. Tasumi, "Resonance Raman and Ultraviolet to Infrared Absorption Studies of Positive Polarons and Bipolarons in Sulfuric-Acid-Treated Poly(p-phenylenevinylene)", J. Phys. Chem. **98**, 4635 (1994).

L.F. Santos, L.M. Carvalho, F.E.G. Guimaraes, D. Goncalves and R.M. Faria, "Electrical and optical properties of light emitting electrochemical cells using MEH-PPV/PEO:lithium-salt blends", Synth. Met. **121**, 1697 (2001).

L. F. W. Santos, L. Gaffo, L. M. De Carvalho, D. Goncalves, and R. M. Faria, "Reversible electrochromical response of thin MEH-PPV films", Mol. Liq. Crys. **374**, 469 (2002).

Y. Shimoi and S. Abe, "Competition between polarons and bipolarons in nondegenerate conjugated polymers", Phys. Rev. B **50**, 14781 (1994).

H. Shirakawa, E.J. Louis, A.G. Macdiarmid, C.K. Chiang, and A.J. Heeger, "Synthesis of electrically conducting organic polymers: Halogen derivatives of polyacetylene, $(CH)_x$", JCS Chem. Comm. 578 (1977).

D. L. Smith, "Steady state model for polymer light-emitting electrochemical cells", J. Appl. Phys. **81**, 2869 (1997).

W.P. Su, J.R. Schrieffer, and A.J. Heeger, "Solitons in polyacetylene", Phys. Rev. Lett. **42**, 1698 (1979).

W.P. Su, J.R. Schrieffer, and A.J. Heeger, "Soliton excitations in polyacetylene", Phys. Rev. B **22**, 2209 (1980).

C.W. Tang, "Two-layer organic photovoltaic cell", Appl. Phys. Lett. **48**, 184 (1986).

B. Tian, G. Zerbi, and K. Müllen, "Electronic and structural properties of polyparaphenylenevinylene from the vibrational spectra", J. Chem. Phys. **95**, 3198 (1991).

B. Thompson, P. Schottland, K. Zong, and J Reynolds, "In situ colorimetric analysis of electrochromic polymers and devices", Chem. Mater. **12**, 1563 (2000).

M. Tzolov, V. P. Koch, W. Bruetting, and M. Schwoerer, "Optical characterization of chemically doped thin films of poly(p-phenylene vinylene)", Synt. Met. **109**, 85 (2000).

D. Vanden Bout, W. Yip, D. Hu, D. Fu, T. Swager and P. Barbara, "Discrete intensity jumps and intramolecular electronic energy transfer in the spectroscopy of single conjugated polymer molecules", Science **277**, 1074 (1997).

K.F. Voss, C.M. Foster, L. Smilowitz, D. Mihailovic, S. Askari, G. Srdanov, Z. Ni, S. Shi, A. J. Heeger, and F. Wudl, "Substitution effects on bipolarons in alkoxy derivatives of poly(1,4-phenylene-vinylene)", Phys. Rev. B, **43**, 5109 (1991).

W. M. V. Wan, N. C. Greenham, and R. H. Friend, "Interference effects in anisotropic optoelectronic devices", J. Appl. Phys. **87**, 2542 (2000).

F. P. Wenzl, P. Pachler, E. J. W. List, D. Somitsch, P. Knoll, S. Patil, R. Guentner, U. Scherf, and G. Leising, "Self-absorption effects in a LEC with low Stokes shift", Physica E **13**, 1251 (2002).

E. Werner, M. Meier, J. Gmeiner, M. Herold, W. Brutting, and M. Schwoerer, "Doping and trap states in PPV light-emitting devices", Optical Mater. **9**, 109 (1998).

M. Yan, L.J. Rothberg, F. Papadimitrakopoulos, M.E. Galvin, and T.M. Miller, "Defect Quenching of Conjugated Polymer Luminescence", Phys. Rev. Lett. **73**, 744 (1994).

Y. Yang and Q. Pei, "Voltage controlled two color light-emitting electrochemical cells", Appl. Phys. Lett. **68**, 2708 (1996).

K. Yoshino, S. Nakajima, D.H. Park, and R. Sugimoto, "Thermochromism, photochromism and anomalous temperature-dependence of luminescence in poly (3-alkylthiophene) film" , Japanese Journal of Applied Physics **27**, L716 (1988).

K. Yoshino, Y. Manda, K. Sawada, M. Onoda, and R. Sugimoto, "Anomalous dependence of luminescence of poly(3-alkylthiophene) on temperature and alkyl chain length", Solid State Commun. **69**, 143 (1989).

G. Yu, K. Pakbaz, and A.J. Heeger, "Semiconducting polymer diodes: Large size, low cost photodetectors with excellent visible-ultraviolet sensitivity", Appl. Phys. Lett. **64**, 3422 (1994).

G. Yu, C. Zhang, and A.J. Heeger, "Dual-function semiconducting polymer devices: Light-emitting and photodetecting diodes", Appl. Phys. Lett. **64**, 1540 (1994).

G. Zotti, G. Schiavon and S. Zecchin, "Irreversible processes in the electrochemical reduction of polythiophenes. Chemical modifications of the polymer and charge-trapping phenomena", Synt. Met. **72**, 275 (1995).